University of Pécs
Doctoral School of Chemistry

The impact of mass transfer on efficiency in reversed phase liquid chromatography

PhD thesis

Nándor Csaba Lambert

Supervisor:
Dr. Attila Felinger
professor of chemistry

PÉCS 2018

Abstract

The aim of the study was to characterize the mass-transfer properties that can be determinant during the separation of either small or macromolecules in different types of packed columns. This study covers the examination of the effect of frictional-heating in columns packed with fine particles, the comparison of the efficiency of novel fast liquid chromatographic columns regarding the efficiency loss at the column ends, highlights the role of intraparticle diffusion of macromolecules and makes comparison in the mass-transfer properties between supercritical fluid chromatography (SFC) and reversed phase liquid chromatography (RPLC).

The contribution of frictionalheating to the efficiency loss, which appears in columns packed with sub 2 μm particles at elevated flow rates was characterised. For this, the mass-transfer properties of a superficially-porous packing material, with 1.6 μm particle diameter, and of a fully porous packing material with 1.7 μm particle diameter were investigated and compared to the thermostating and the adiabatic insulation of the columns. It has been shown that the contribution of frictional heating at elevated flow-rates is in similar extent as the sum of the intraparticle mass-transfer and the external mass-transfer resistance in the examined columns.

The kinetic performance of five chromatographic columns designed for fast liquid chromatography including fully porous, core-shell and monolithic packings with identical column dimensions (2.1×50 mm) were tested. The effect of the presence of the frits and the bed heterogeneity of the columns near the frits were characterized by a flow-reversal method. Significant difference was found between the two ends of the packed columns, while the monolithic column shows rather similar performance at either column end.

The mass-transfer properties of three superficially-porous packing materials – one with 2.6 μm particle and 1.9 μm inner core diameter and two packings provided with the same 3.6 μm particle diameter but different 2.6, and 3.2 μm inner core diameters –, were investigated and compared with those of fully porous packings with similar particle properties by injecting insulin sample onto the columns at various mobile phase velocities. The contribution of the intraparticle diffusion was analyzed and identified as the sum of the surface and pore diffusions. The separate determination of the pore diffusion and the surface diffusion coefficients shows that the latter has a crucial role in the intraparticle movement of the macromolecules.

The chromatographic behavior of the homologous series of alkylbenzenes (from octylbenzene to octadecylbenzene) on the same C_{18} reversed-phase column was investigated in supercritical fluid chromatography and liquid chromatography at various experimental conditions, such as different eluent compositions, flow-rates, and mobile phase densities. The results indicate the broader variation of mass-transfer properties in SFC compared to liquid chromatography. As expected, the optimum mobile phase velocity is higher in SFC, but there is no real difference in the obtainable efficiency.

List of abbreviations

A : A-term of the van Deemter equation
A_s : ratio of the stationary phase surface to the geometrical column volume
A_z : column cross-section area
B : B-term of the van Deemter equation
C : C-term of the van Deemter equation
C_e : sample concentration in the bulk mobile phase
C_i : sample concentration in the stationary phase
$C(t)$: chromatographic band profile
D_e : intraparticle diffusion
D_{eff} : effective diffusion coefficient
D_m : molecular diffusion coefficient
D_L : axial dispersion coefficient
D_s : surface diffusion coefficient
d_p : particle diameter
d_i : inner core diameter
D_p : pore diffusion coefficient
D_s : surface diffusion coefficient
E_s : activation energy
$F(\lambda_m)$: hindrance factor
F : phase ratio
F_v : volumetric flow rate
H : plate height
h : reduced plate height
j_s : density of the mass flux
k : retention factor
K : equilibrium constant
k_{ext} : external mass-transfer resistance
L : column length
l : migration distance
M_w : molecular weight of the analyte n : average number of the adsorption events
P_f : frictional power $[W/m]$
Pe : Péclet number Q_{st} : isosteric heat of adsorption
Re : Reynolds number
r_c : column radius
r_i : radius of the inner core (core-shell particle)
r_p : radius of the stationary phase particles
R_s : characteristic radius of the cylindrical particles
Sc : Schmidt number
T : absolute temperature
t_R : retention time
t_0 : void time

t_e : elution time of an unretained marker that is excluded from the stationary phase pores
t_p : parking time during the PP experiments
u_0 : mobile phase linear velocity
u_h : interstitial velocity of the mobile phase
u_z : linear velocity of the sample band
V_a : molar volume of the solute
V_b : molar volume of the solvent
V_0 : void volume of the column
V_e : interstitial volume of the mobile phase
V_{ext} : extra column volume
V_g : geometrical column volume
V_R : retention volume
V_t : total volume of the mobile phase (equal to V_0)
ABPR : ambient back pressure regulator
EMG : exponentially modified Gaussian curve
HETP : height equivalent to a theoretical plate
HPLC : high performance liquid chromatography
RPLC : reversed phase liquid chromatography
SFC : supercritical fluid chromatography
TPB : Total Pore Blocking method
UHPLC : ultra-high performance liquid chromatography
vHPLC : fast liquid chromatography

α : empirical parameter of the Knox equation
γ_e : external obstruction factor
γ_p : internal obstruction factor
ΔE : internal energy change
ΔH : enthalpy change
ΔG : Gibbs free energy change
ΔP : pressure drop
ΔS : entropy change
ε_i: internal porosity
ε_t : total porosity
ε_e: external porosity
ε_p: intraparticle porosity
η : mobile phase viscosity
λ_i numerical parameter of the structure of the bed particle distribution (multipath dispersion)
λd_p : length of the step of the molecules according to the theory of Giddings
λ_m : ratio of the analyte and pore radius
μ_1 : first moment
μ_2 : second central moment
ν : reduced velocity

ρ : particle density

ρ_s : mobile phase density

σ^2 : peak variance, or contribution to the overall variance

σ_t^2 : temporal variance

σ_V^2 : volumetric variance

σ_z^2 : spatial variance

τ_m : average sojourn time in the mobile phase

τ_s : average sojourn time in the stationary phase

ω : empirical parameter of the Knox equation

ω_i : numerical parameter of the particle distribution (multipath dispersion)

Contents

Chapter 1

Introduction

1.1 Introduction

During the recent years, a number of chromatographic columns with various types of packing materials – such as traditional fully porous and core-shell particles in a wide range of diameters, and monolithic packings – have been introduced. The most frequently used columns dedicated to the recent ultra-high performance liquid chromatography (UHPLC) instrumentation are narrow and short (2.1 mm ID and 50 mm length), and are packed with sub-3-μm or sub-2-μm particles [1–4]. The use of core-shell particles is also wide spread to gain higher efficiency with traditional liquid chromatography systems, or reach the peak performance in fast liquid chromatography. The most frequent particle diameter of the superficially porous packing materials is between 2.5 to 5 μm; the currently available smallest core-shell particles are of 1.3 μm diameter. The performance of the superficially porous particles is typically higher than that of the conventional packings. The efficiency of the columns packed with 2.6 μm core-shell particles is nearly the same as that of columns packed with sub-2-μm fully porous particles, but they can be operated at lower pressures, consequently lesser efficiency loss due to thermal effects is observed [5, 6]. The physical reasons of the increased efficiency lies mostly in the decrease of the mass-transfer contributions to the sample band spreading during the chromatographic analysis. The description of the mass-transfer processes in columns packed with core-shell particles has received great attention [7–13]. Besides the unusually low value of eddy dispersion and thus the reduced longitudinal diffusion caused by the presence of the solid core, the decrease of the intraparticle diffusion is particularly important in core-shell packed columns. The mass-transfer of the solute through the internal network of the mesopores inside the particles is derived from two parallel diffusion mechanisms. One through the mobile phase that fills the pores, and the other along the stationary phase surface. The advantages of the faster mass-transfer to the adsorption sites of the stationary phase surface, i.e. the higher intraparticle diffusion are more expressive during the analysis of macromolecules, such as proteins and other biomolecules, due their smaller diffusion coefficients [14]. Besides the use of the well-known and widely used fully-porous or core-shell packing materials, another potential is in the development of monolithic silica columns, where improved efficiency can be achieved and moderate column

pressures are sufficient to maintain high mobile phase flow owing to the small skeleton size and large (through-pore size)/(skeleton size) ratios [15–19].

The efficiency of a liquid chromatography measurement is determined by a number of additive contributions to the sample band spreading in the chromatographic column such as mobile phase dispersion, the external mass-transfer resistance at the particle boundary, the intraparticle-diffusion or the adsorption–desorption process on the surface of the stationary phase [20]. The fluctuation of local packing density provides the crucial part of the sample band dispersion in the mobile phase. In the packed bed, one can identify tightly and loosely packed regions; the velocity fluctuation that arises from that heterogeneity is the interchannel (short or long range) or transcolumn velocity bias [21]. The microstructural disorder of packed beds has been extensively studied with numerical simulation and the resulting eddy dispersion was quantified for columns packed with totally porous or core-shell particles [22,23]. Recent studies show, that in case of the packed columns another band spreading contribution comes from the presence of the frits at the column ends and from the axial heterogeneity of the column originating from the column packing procedure. The above mentioned contributions have the most significant role in case of the separation of early eluting compounds ($k < 2$), where mobile phase dispersion is the most dominant contribution to the band broadening [24].

Better efficiency can be achieved with given column geometry (i.e. with same column length and inner diameter) by decreasing the particle diameter of the column packing material [25,26]. That leads to the simultaneous reduction of the analysis time too. However, the efficiency that can be reached in a column is inversely proportional to the particle size, the operating back pressure is inversely proportional to the square of the particle diameter too. The use of smaller particles leads to elevated operation pressure and optimum mobile phase velocity, which results in thermal dissimilarities in the column, trough the generated frictional heat of the mobile phase [27].

Previous findings show the difference in efficiency loss using different thermostating procedures such as the still air, forced air or water bath thermostating [28]. Some studies that assume that still air thermostating is near adiabatic, significant difference can be observed between the still air thermostated and the near adiabatic measurements [29]. A more recent study characterizes the effect of frictional heat applying high vacuum and using low-emissivity surface material to minimize the heat loss. Nevertheless, the method provides the ability to control heat dissipation trough the column wall, it require quite difficult technical solutions and sufficient instrumentation [30,31].

When the column is thermostated, and the temperature of the column wall is kept constant, a radial temperature gradient can be observed in the mobile phase between the center and the wall of the column. That means that the velocity of the mobile phase will be higher at the middle of the column than near to the wall. Several studies prove that the efficiency loss caused by the thermal effects can be significant in case of very fine packing materials [32,33]. With the insulation of the column the radial temperature gradient can be eliminated. The efficiency loss doe to the thermal dissimilarities in the mobile phase can be evaluated according the general rate model of chromatography, using various methods for the characterisation of the different

mass-transfer contributions to the observed peak variances in the examined columns.

This study covers the evaluation of the kinetic performance of several reversed phase (C_{18}) columns packed with fully porous and core-shell particles with various particle diameters and the performance of a silica-based monolithic column, regarding the contributions of the intraparticle diffusion, the axial heterogeneity of the packed bed, the frictional heat or the mobile phase dispersion.

Due to technical improvement in instrumentation, supercritical fluid chromatography (SFC) has recently gained increased attention in the fields of applications and theoretical investigations too [34–40]. In case of SFC, the mobile phase is kept under supercritical state using pressure and temperature conditions above its supercritical point. Most frequently carbon-dioxide is used as mobile phase, since it is non corrosive, easy to access and it is easy to maintain the supercritical conditions caused by its low critical point. The biggest advantage of the SFC technique is coming from the low viscosity of the supercritical fluid, that allow to use high flow rate in columns packed with very fine particles at negligible pressure drop and intraparticle plate height contributions.

A number of equilibrium and kinetic macroscopic models are used to understand the chromatographic processes in liquid chromatography. The use of the models, however, is complicated due to the fact that in supercritical fluid chromatography the physico-chemical properties of the mobile phase change along the column with the density of the mobile phase. The characterization of the movement of the sample band trough chromatographic column at molecular level gives another possibility for the description and comparison of the mass-transfer in the different chromatographic modes. For this purpose the stochastic model of chromatography introduced by Giddings [25] is widely used. The model describes the separation process as a random migration, and randomly occurring adsorption–desorption of the molecules in the chromatographic column. Since the density of the supercritical fluid is strongly affected by its composition and by the pressure and temperature conditions, the mobile phase dispersion highly varies during the SFC separations. The advantage of the use of the stochastic model is that it simplifies the correction for the mobile phase band spreading.

The study covers the comparison of supercritical SFC and UHPLC techniques. A number of studies investigated the dependence of retention factors in SFC on temperature, pressure, or the density of the mobile phase [41–44]. Since HPLC columns can be installed and used in SFC, a direct comparison of the two modes of operation can be obtained.

1.2 Research objectives

1. Analysis of frictional heat on column efficiency
   (a) The measurement of efficiency with small molecules with the thermostating and the insulation of the examined columns.
   (b) The determination of the geometrical parameters i.e. the porosity values of the chosen columns packed with sub-2μm core-shell and fully porous particles with total pore blocking experiments.
   (c) The determination of the external obstruction of the stationary phases with peak-parking experiments.
   (d) The characterization and subtraction of the different contributions from the experimental plate height, for the determination of the effect of the thermal dissimilarities caused by the frictional heating of the mobile phase.
2. Comparison of the efficiency of vHPLC stationary phases
   (a) The determination and comparison of the efficiency of different (monolithic and slurry packed) columns with a check-out sample containing the series alkylphenones under the same chromatographic conditions.
   (b) The exploration of the efficiency differences between the examined columns.
   (c) The analysis of the local efficiency at the vicinity of the column ends, by applying the column reversal method.
3. Analysis of the intraparticle diffusion of macromolecules
   (a) The measurement of the efficiency of conventional and core-shell HPLC columns with insulin.
   (b) The estimation and subtraction of the different mobile phase dispersion contributions from the observed sample band variance.
   (c) The identification and examination of the band broadening caused by the intraparticle mass-transfer.
4. Comparison of the mass-transfer properties in SFC and UHPLC
   (a) The measurement of the efficiency of the same reverse phased column in the two different chromatographic modes by injecting the series of alkylbenzenes.
   (b) The calculation and the comparison of the mass-transfer coefficients provided by the stochastic model of chromatography applied on the experimentally recorded peaks.

Chapter 2

Background

2.1 Theoretical overview

2.1.1 Classification of the different liquid chromatography columns

The most commonly used columns in liquid chromatography are the packed columns, where mostly fine spherical silica particles are used as stationary phase. The reversed phase separations – where the stationary phases surface is apolar –, cover the 90% of the liquid chromatography measurements. In this case, the surface of the silica packing is covered with apolar ligands through the silanization of the free silanol groups on the silica surface. For this, most commonly octadecyl groups (C18) are used. In reality the C18-reversed phase columns covers the 80% of available silica based columns on the market.

The use of silica or polymer based monoliths as stationary phases gives alternatives to the slurry packed columns. In this case porous rod structures characterized by mesopores and macropores are used as stationary phase, embedded in a plastic – or less often stainless steel – column hardware. The advantage of these packing is coming from the moderate pressure drop due to the high permeability caused by the large number of channels through the macroporous structure of the monolith, from the very short diffusion distances, and the presence of multiple pathways for solute dispersion through high pore connectivity [45–47]. Although, especially the early generations of the silica based monolithic columns provided less efficiency than spherical packings.

The classical HPLC columns are 10 to 25 cm long with 4.6 mm inner diameter, while the diameter of the packed particles can vary from 3 to 10 μm. These columns can be operated usually of the 400 bar pressure drop, which is actually the highest pressure that a common HPLC instrument can provide. Because of the large geometrical sizes, these columns dispose far too much void volume, that leads to elevated analysis time and solvent consumption.

Simultaneous increase in efficiency with the decrease of the void volume of the chromatographic columns and the keeping of sufficient selectivity is only possible with the improvement of the

stationary phase packing materials. To this end, smaller diffusion distances have been pursued by using smaller and more uniform particles, beside decreased column sizes. However, the backpressure (for a given column diameter and a given volumetric flow) increases inversely proportional to the square of the particle diameter, due to the decrease of the interstitial voids in the column.

Parallel to this, more sophisticated monolithic columns appeared on the market, with more dense monolithic structure, and improved column hardware.

The geometrical parameters of the modern Ultra High Performance (UHPLC) columns are usually 2.1 mm inner diameter with 5 cm length, while the diameter of the particles are near to 2 μm or less. To maintain sufficient mobile phase flow in such columns, very high pressure – up to 1000 bar – is needed, what demand new generational UHPLC instrumentation with improved pumps and reduced void volumes.

As an intermediate solution between the HPLC and UHPLC instruments the fast performance liquid chromatographs appeared which can operate up to 600 bar, and has slightly decreased instrument volume. In this study the fast liquid chromatography (vHPLC) name is suggested for the columns that can be operated properly also in such instruments, but provides similar efficiency to the UHPLC columns.

Besides the decrease of the particle diameter, the development of the pellicular particles gives another opportunity to the improve of the efficiency of the columns. The so called core-shell packing materials are evolved by the covering of a non-porous core with porous layers. The presence of the core in the middle of the particle leads to improved effectiveness through the shortening of the diffusion paths in the particles that results in faster mass-transfer in the column bed.

Despite the manufacturers struggle to produce as uniform packings as possible, with the highest order of the particles, the final result always shows some extent of the radial and axial heterogeneity of the packed bed. The biggest unevenness can be observed at the end of the columns where the frits (porous filters with appropriate size) are closing the particles more or less perfectly in the column hardware.

2.1.2 The different plate height contributions

For the description of the efficiency of a liquid chromatography measurement, the height equivalent to a theoretical plate (HETP) or plate height (H) is used most commonly. The plate models assume that the column is divided into a series of identical equilibrium stages, so called theoretical plates, according to the number of the equilibrium that can be achieved between the mobile and the stationary phases. Since the plate models depict a continuous column – with a given length – with a discrete number of well-mixed cells, they are approximate, empirical models absent from the actual physical system. Although these models cannot be related to the first principles of chromatography, they have been successfully used for the physical and mathematical characterization of the operation of chromatographic columns [20].

Empirically, the plate height originates from the sample band variance and it is the dependent of retention time (t_R) or retention volume (V_R) – depends on which unit are used for the expression of the variance – of the analyte, and the column length:

$$H = L\frac{\sigma^2_{\text{total}}}{V_R^2} \tag{2.1}$$

.

σ^2_{total} is the peak variance, and involves all band broadening contributions that occurs during the chromatographic processes. Under strict isocratic conditions V_R can be written as follows:

$$V_R = V_0(1 + k) \tag{2.2}$$

where V_0 is the column hold up volume and is equal to the volume filled by the mobile phase, and k is the retention factor of the analyte:

$$k = \frac{V_R - V_0}{V_0}. \tag{2.3}$$

Note that the exact expression of V_R and V_0 needs the accurate determination and subtraction of the extra column void volume (V_{ext}) from the corresponding volumes. The mentioned volumes can be easily expressed by the multiplication of the corresponding time values with the volumetric flow rate (F_v):

$$V_x = t_x F_v, \tag{2.4}$$

The observable plate height of the chromatographic process is the result of several additive contributions, such as the sample band spreading in the instrument voids :

$$\sigma^2_{\text{total}} = \sigma^2_{\text{ext}} + \sigma^2_{\text{column}}, \tag{2.5}$$

where σ^2_{ext} and σ^2_{column} represent the extra and intra column band broadening, respectively.

The apparent plate height on a given instrument can be expressed as follows:

$$H_{\text{apparent}} = L\frac{(\sigma^2_{\text{ext}} + \sigma^2_{\text{column}})}{V_0^2 + V_{\text{ext}}^2}\frac{1}{(1+k)^2}, \tag{2.6}$$

where σ^2_{column} can be divided into separate contributions. σ^2_{end} is coming from the effect of the column hardware – i.e. from the effect of the distributor and the frits – together with the heterogeneity of the bed at the end of columns that comes from the inequality caused by column packing procedure, while $\sigma^2_{\text{intrinsic}}$ represent the contribution of the mass-transfer processes in the packing. While σ^2_{end} and σ^2_{ext} are constant values in volume, most of the mass-transfer processes depend on the applied mobile phase velocity.

Nevertheless, the above-mentioned correlations are valid regardless of the definition of the peak variance, it can be defined and used in various units and scales. Most commonly the second central moment of the experimentally recorded peaks – i.e. the band variance expressed on time scale – is used for the determination of the zone broadening, which gives the temporal variance. The longitudinal or spatial variance has more physical relation, and characterizes the band broadening in the column. It can be calculated from the temporal variance as follows:

$$\sigma_z^2 = \sigma_t^2 u_z^2 = \left(\frac{\sigma_t u_0}{k+1}\right)^2, \tag{2.7}$$

where σ_t^2 and σ_z^2 are the temporal and longitudinal variance, respectively, u_z the linear velocity of the band, and u_0 the mobile phase linear velocity.

The extra-column contributions are usually characterized with the volumetric variance, which is calculated for a peak as

$$\sigma_V^2 = \sigma_t^2 F_v^2, \tag{2.8}$$

where σ_V^2 is the volumetric peak variance. By knowing the column characteristics and the retention parameters, the relation between the volumetric and longitudinal variances can be given as

$$\sigma_V = \sigma_z A_z \varepsilon_t (k+1), \tag{2.9}$$

where A_z is the column cross-section area and ε_t is the total porosity of the column. Note that σ_V is directly related to the mobile phase volume that passes through the detector while the sample band elutes from the column.

The semi-empirical van Deemter equation [48] – as the simplified form of the solution of the Lapidus and Amundson model [49] – is widely used for the depiction of the velocity dependent column efficiency:

$$H_{\text{intrinsic}} = A + \frac{B}{u_0} + Cu_0 \tag{2.10}$$

where A, B and C are empirical parameters related to the eddy dispersion, longitudinal diffusion and the slow intraparticle mass-transfer of the sample molecules, respectively.

However, the coefficients used in this equation cannot be directly related to the physical description of the mass-transfer mechanism in a chromatographic column, the corresponding physicochemical processes can be described through numerous analysis. The A term of the equation is derived by the contribution of the eddy or multipath dispersion, which comes from the variation of the average velocities of the mobile phase in the different flow paths of the packing. The B/u term accounts for the axial diffusion in the interstitial void of the column, while the Cu term can be related to the sources of the stationary phase mass-transfer resistances, such as the external mass-transfer resistance (k_{ext}); intraparticle diffusion (D_e); and adsorption – desorption on the surface of the stationary phase. Note that u_0 is equal to the linear velocity of the mobile phase and is written as:

$$u_0 = \frac{F_v}{\varepsilon_t \pi r_c^2} \tag{2.11}$$

where r_c refers to the radius of the column.

A more sophisticated equation was later derived by Knox [50, 51] and his co-workers as result of the experimental study of the particle size effect on the efficiency of a column. The equation is based on the reduced plate height (h) and reduced velocity ν terms introduced by Giddings for the comparison of different columns packed with particles of different diameter [21, 52].

The reduced velocity can be given as:

$$\nu = \frac{u_h d_p}{D_m}, \tag{2.12}$$

where u_h the average interstitial velocity of the mobile phase and it is equal to the ratio of u_0 and the external porosity of the column (ε_e), d_p is the particle diameter of the packing material and D_m is the molecular diffusion coefficient of the solute. Notethat ν is dimensionless, and compares the mobile phase velocity to the velocity of the solute diffusion through the pores of the particle. It can be also identified as the Péclet number (Pe) that is – in the context of mass-transfer – equivalent to the product of the Reynolds number (Re) and the Schmidt number (Sc). Re and Sc are defined as follows:

$$Re = \frac{\rho_s u_h d_p}{\eta} \tag{2.13}$$

$$Sc = \frac{\eta}{\rho_s D_m} \tag{2.14}$$

where ρ_s is the mobile phase density and η its viscosity.

The reduced plate height is defined as,

$$h = \frac{H}{d_p}, \tag{2.15}$$

and it measures the normal plate height in units of the particle diameter.

By using the reduced parameters, the Knox equation can be written as:

$$h = \frac{2\gamma_e}{\nu} + \alpha\nu^{1/3} + \omega\nu \tag{2.16}$$

where γ_e is the external obstruction factor (<1) and describes the tortuosity of the flow channels in the packing, while α and ω are empirical parameters. Since the constants of the equation are derived through a fitting procedure, it is fully empirical lacking any connection to the basic diffusion models.

The sum of the previously described contributions leads to the rough description of the overall plate height that is achievable on a given chromatographic system in the following equation:

$$H_{\text{apparent}} = H_A + H_B + H_C + H_{\text{ext}} + (H_{\text{end}} + H_{\text{heat}}) \tag{2.17}$$

where H_A refers the plate height contribution of the multipath dispersion, H_B represents the longitudinal diffusion while H_C is the contribution of the slow mass-transfer in the stationary phase. H_{ext} is originating from the extra column band broadening. The contributions written in parenthesis appears only in special cases. H_{end} originates from the additional band broadening caused by the presence of the frits, and from the inhomogeneity at the column ends due to the slurry packing procedure in case of packed columns. When high pressure is needed to maintain sufficient flow rates, – typically occurs when the particle diameter of the packing is close to 2 μm – the decrease of the efficiency caused by the viscous heating of the mobile phase introduce (H_{heat}). The contributions to the zone broadening, involving the effect of the hardware will be detailed in this section.

Multipath dispersion

The multipath – or commonly named as eddy – dispersion accounts for the source of band broadening related to the flow unevenness in the column. Since the flow pattern in a chromatographic column is strictly laminar the traditional name could be misleading. Since there are not actual turbulences in the packed bed, the formation of stable eddies is ruled out . The early suggestions – as it was introduced in the A term of the van Deemter equation – [48] accounted the contribution of multipath dispersion to band broadening as a constant term, proportional to the particle diameter.

However, Giddings et. al. demonstrated through experimental results that the multipath dispersion is the complex function of the mobile phase velocity [53–55]. According to their studies,

the channels in the porous medium are considered as the irregular cross-connected network of the stream paths, where the velocity along a given streamlet persists only for the length of a particle diameter (d_p, and changes randomly. The migration process is a random walk process, where the molecules steps randomly back and forward within the stream-paths respect to the average stream velocity. The number of the steps in time unit can be explained as follows:

$$n_1 = \frac{\nu}{2\lambda d_p} \tag{2.18}$$

where λd_p is the length of a step, and ν is the average velocity.

Giddings suggested that in case of the radial concentration gradient of the sample, molecules can change their migration velocity by diffusing from the current stream-path to a nearby one. If the migration distance (l) in this direction is

$$l = \beta d_p, \tag{2.19}$$

then the number of the steps can be considered as:

$$n_2 = \frac{2D_m}{\beta^2 d_p^2}, \tag{2.20}$$

where D_m is the diffusion coefficient of the molecule.

In reality, where the streamlines randomly merge and split, eddy dispersion arise from the coupling of the two contributions, and depends on the random distribution of the packing material – whether it is spherical or monolithic – in the column. Thus the apparent dispersion coefficient gives the following equation as the sum of eq. 2.18 and 2.20:

$$D_A = \frac{\nu^2}{\frac{2D_m}{\beta^2 d_p^2} + \frac{\nu}{2\lambda d_p}}. \tag{2.21}$$

Since the molecules are retained, D_A is correspondingly reduced, and the multipath diffusion term becomes:

$$H_A = \frac{2\lambda d_p}{1 + \frac{4\lambda D_m}{u_h \beta^2 d_p}}. \tag{2.22}$$

However, the description of the heterogeneity of the packed beds with such simple model is hardly sufficient, it have been shown that the flow heterogeneities in the interstitial volume can be divided into three different classes. The classes are defined by the length according to which velocity extremes are expected: the trans-channel diffusion takes place in the distance between two adjacent particles, the short-range inter-channel dispersion occurs in a few particle

diameters length, while the trans-column diffusion is affected by the column inner radius [21]. Each individual plate height term should be written as:

$$H_{A,i} = \frac{1}{\frac{1}{2\lambda_i d_p} + \frac{D_m}{\omega_i u_h d_p^2}} \tag{2.23}$$

where λ_i and ω_i are numerical parameters related to the structure of the bed and the particle distribution, and can be written as:

$$\lambda_i = \frac{\omega_{\beta,i}^2 \omega_{\lambda,i}}{2} \tag{2.24}$$

and

$$\omega_i = \frac{\omega_{\beta,i}^2 \omega_{\alpha,i}^2}{2}. \tag{2.25}$$

$\omega_{\beta,i}$, is equal to the ratio of the difference between the extremes values of the velocities in the type of channels considered and the corresponding mean velocity, while $\omega_{\alpha,i}$ is the ratio of the characteristic diffusion length to the particle diameter, and $\omega_{\lambda,i}$ is the flow-persistence length.

The values of each of these parameters could be estimated according to the initial guesses made by Giddings. The validity of the model was lately confirmed by Magnico and Martin for spherical particles, by using columns specially dry packed with large (210 μm) impenetrable particles to focus on the dispersion sources coming from the mobile phase [56]. More recent investigations provided corresponding values by the numerical reconstruction of packed beds and the calculation of flow-dispersion in the interstitial space of the column [57–59]. The parameters of the multipath dispersion can be estimated also from the actual physical reconstruction of the bed structure using confocal laser scanning microscopy in case of monolithic packings too [23, 60, 61]. It has been shown that the flow velocity profile along the bed can also be visualized by X-ray computed tomography [62], or with nuclear magnetic resonance [63].

Longitudinal diffusion

The longitudinal diffusion becomes preponderant in the overall efficiency when the displacement of the molecules lead by the mobile phase convection is comparable, to the movement of the solute molecules with diffusion at the range of the particle or the monolithic domain size.

The longitudinal diffusion term, H_B depends on the column length, originating from the increment of the band variance arising from the sample diffusion during its elution time:

$$H_B = \frac{2 D_{\text{eff}} t_R}{L} \tag{2.26}$$

where D_{eff} is the effective diffusion coefficient of the sample molecules in the bulk mobile phase, and t_R, the retention time can be given as

$$t_R = \frac{(1 + k_1)L}{u_h}, \tag{2.27}$$

where k_1 the zone retention factor represent the fraction of the molecules in the interstitial space of the sample band.

$$k_1 = F\left[\varepsilon_p + K\left(1 - \varepsilon_p\right)\right] \tag{2.28}$$

and

$$F = \frac{1 - \varepsilon_e}{\varepsilon_e}, \tag{2.29}$$

where K is the equilibrium constant of the adsorption or partition, and F is the column phase ratio.

According to Eq. 2.27 and 2.26 H_B can be written as:

$$H_B = \frac{2(1 + k_1)D_{\text{eff}}}{u_h}. \tag{2.30}$$

The calculation of the longitudinal diffusion term requires the knowledge of the effective diffusion coefficient of the analyte in the heterogeneous column bed, that originates from the addition of the diffusion in the particles impregnated by the eluent (volume fraction $1 - \varepsilon_e$) and the bulk mobile phase (volume fraction ε_e).

Estimation of the axial dispersion coefficient

The axial dispersion in the mobile phase is considered as the sum of the multipath dispersion and the longitudinal diffusion contributions as detailed previously. Although the van Deemter plate height simply assumes that axial dispersion is independent from the flow rate, eddy dispersion and therefore axial dispersion does depend indeed on mobile phase velocity. The axial dispersion coefficient (D_L) can be estimated by using different empirical or semi-empirical equations. The Gunn correlation is one of the possibilities and it is widely used to determine the axial dispersion coefficient [64]:

$$D_L = d_p u_h \left(A + B + \frac{\varepsilon_e}{\tau ReSc}\right) \tag{2.31}$$

where $\tau = 1.4$ is the packing tortuosity factor. A and B terms are expressed as:

$$A = \frac{ReSc}{4\alpha_1^2(1 - \varepsilon_e)}(1 - p)^2 \tag{2.32}$$

and

$$B = \frac{(ReSc)^2}{14\alpha_1^4(1-\varepsilon_e)^2} p(1-p)^3 \left[\exp\left(\frac{-4\alpha_1^2(1-\varepsilon_\mathrm{e})}{\mathrm{p(1-p)ReSc}}\right) - 1\right] \tag{2.33}$$

where $\alpha_1 = 2.405$ is the first root of zero-order Bessel function and

$$p = 0.17 + 0.33\exp\left(\frac{-24}{\mathrm{Re}}\right). \tag{2.34}$$

Note that the ratio between the local linear velocity and the average velocity of the eluent over the column cross-section is assumed to a constant number with zero variance.

The Gunn correlation can be written also with the convenient chromatographic terms. By using the appropriate values of the parameters given by Giddings, the two equations gives rather similar results for the value of D_L at the wide range of reduced interstitial velocities [8, 11].

Dispersion at the particle boundary

The external film mass-transfer – represented by the external mass-transfer coefficient (k_ext) – consider the transfer of solute molecules from the stationary to the mobile phase and vice-versa, and so the filling of the pore openings in the stationary phase. The particles (in packed columns) or the skeleton (in monolithic columns) are surrounded by a mobile phase film, where – due to the laminar flow of the eluent – the velocity is equal to zero. The density of the mass-flux (j_s across this barrier is controlled by the concentration difference between the external moving (C_e), and the internal stagnant eluent (C_i):

$$j_s = k_\mathrm{ext}\left[(C_e - C_i)r_p\right], \tag{2.35}$$

where r_p the characteristic radius of the stationary phase particles can be written for packed columns (spherical particles) as:

$$r_p = \frac{3(1-\varepsilon_e)}{A_s}, \tag{2.36}$$

while for monolithic stationary phases (cylindrical packing) as:

$$R_s = \frac{2(1-\varepsilon_e)}{A_s}. \tag{2.37}$$

A_s is the ratio of the external surface area of the stationary phase and the columns geometrical volume.

However, the physico-chemical description of the convective-diffusive mass-transfer at the interface between the percolating and the internal eluent is a more complex process, empirical correlations are available by the definition of the Sherwood number [20]. The most commonly used correlations were derived by Wilson and Geankoplis [65]:

$$\frac{k_{\text{ext}} d_p}{D_m} = \frac{1.09}{\varepsilon_e} \nu^{1/3} \tag{2.38}$$

and by Kataoka [66]:

$$\frac{k_{\text{ext}} d_p}{D_m} = 1.85(1 - \varepsilon_e)^{1/3} \nu^{1/3}. \tag{2.39}$$

Miyabe et al. investigated and proved the validity of the above-mentioned correlations using 18 μm non-porous and 50 μm fully porous silica-C18 particles with moment analysis. They have found 15 % difference at most between the experimental data and the estimations. However, the relation of the external mass-transfer resistance to the reluctance of the molecules to enter the porous particles is still not fully clarified.

Intraparticle mass-transfer

It is usually assumed that intraparticle diffusion can be divided into two parallel contributions [10, 20, 67, 68]:

$$D_e = D_p + \rho_p K D_s, \tag{2.40}$$

where D_p is the pore diffusion coefficient, ρ_p is the particle density and refers to the ratio of the particle weight to the particle volume, K the equilibrium constant, and D_s is the surface diffusion coefficient. The higher equilibrium constant with the elevated retention at high flow rates may cause the dominance of the surface diffusion, which lead to higher apparent pore diffusion coefficients [67, 68].

Pore diffusion

Pore diffusion (D_p) occurs when the solute molecules diffuse across the open mesoporous network of the particles. The diffusion takes place in the mobile phase, but is hindered by the tortuosity and constriction of the mesoporous network. Pore diffusion can be described as the function of the molecular diffusion coefficient (D_m) and the hindrance contributions of the mesopores: [20]

$$D_p = \gamma_p F(\lambda_m) D_m, \tag{2.41}$$

where γ_p is the internal obstruction factor, which is the function of the internal porosity, the tortuosity of the mesopore pathways, their constriction and their connectivity [10]. Usually γ_p is simply written as the ratio of D_p and D_m [69]. $F(\lambda_m)$ is the hindrance factor that represent the restriction of the sample molecules within the narrow pores. According to the studies of

Renkin et. al. it can be originated from the ratio of the size of the analyte molecules and the mesopore size (λ_m) [70]:

$$F(\lambda_m) = (1 - \lambda_m)^2 \left[1 - 2.104\lambda_m + 2.09\lambda_m^3 - 0.95\lambda_m^5\right] \tag{2.42}$$

The internal obstruction factor γ_p can be calculated according to the studies of Klein and Grüneberg from the band spreading of an unretained sample due to the solute permeation into and out of the pores of the packing material [71]:

$$\sigma^2_{\text{perm}} = \frac{K_d V_i d_p^2 F_v}{30\gamma_p D_m}, \tag{2.43}$$

where σ^2_{perm} is the variance of the peak due to the intraparticle mass-transfer, K_d is the solute distribution coefficient, V_i is the internal pore volume, d_p is the particle diameter, and F_v is the volumetric flow rate of the mobile phase.

Surface diffusion

Surface diffusion (D_s) is usually approached as an activated mass-transfer process of the adsorbed molecules along the surface [72]. When adsorbed molecules gain E_s activation energy, they surpass the energy barrier between two adsorption sites, and migrate to a neighboring site. E_s is proportional to the isosteric heat of adsorption (Q_{st}), so the following correlation can be given:

$$E_s = \alpha(-Q_{\text{st}}), \tag{2.44}$$

where α is positive, and smaller than unity.

Based on the previous assumptions, the following Arrhenius-type equation is widely used for the characterization of the temperature, and adsorbed amount dependence of the surface diffusion:

$$D_s = D_{s_0} \exp\left[\frac{\alpha(-Q_{\text{st}})}{RT}\right], \tag{2.45}$$

where D_{s0} is the frequency factor of surface diffusion.

If the change of the molar volume of the solute is significant upon adsorption, next to the concentration of the sample adsorbed to the stationary phase, -Q_{st} is proportional to the applied pressure as well. This is usually the case during the measurement of proteins or ionic compounds that lose they solvation layer upon adsorption to the stationary phase.

Since the pore and surface diffusion fluxes are additive, therefore, using Eqs. 2.41 and 2.40 the following equation can be written [10]:

$$D_e = \epsilon_p \gamma_p F(\lambda_m) D_m + (1 - \epsilon_p) K D_s, \tag{2.46}$$

where ϵ_p is the internal porosity of the column, and represents the volume fraction of the porous media. Note that the use of porosity rather than pore density in the previous equation gives more realistic explanation, since the surface diffusion correlates more likely with the volume of

the silica skeleton than with its density.

Frictional heat

As it is shown in Equation 2.47, the generated heat power depends on the mobile phase velocity and the pressure drop along the column, that leads to important frictional heating at elevated mobile phase flow rates:

$$P_f = F_V \times \frac{\Delta P}{L}, \tag{2.47}$$

where P_f is the frictional power and it is given in W/m, ΔP is the pressure drop and L is the column length.

The generated heat leads to temperature increase inside the column (especially when poorly dissipated) and forms both radial and longitudinal temperature gradients (as shown in Fig. 2.1) that affects retention and the band broadening of the analyte as well [33] [73]. When the column is thermostated, and so the temperature of the column wall is kept constant, a radial temperature gradient can be observed in the mobile phase between the center and the wall of the column. This means that the velocity of the mobile phase will be higher at the middle of the column than near to the wall. Experiments showed that efficiency loss due to the frictional heat takes place when the friction power exceeds about 4 W/m [74].

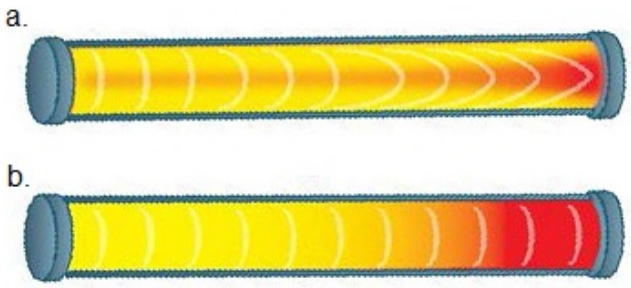

Figure 2.1: The effect of frictional heat in the chromatographic column, a. the presence of axial and gradial thermal gradient, b. the presence of axial thermal gradient next to the insulation of the column.

Under perfectly adiabatic conditions, only axial temperature gradients would exist, resulting only the decrease of the apparent retention factor with the increase of the flow rate. In actual chromatographic systems, a part of the created heat lost is through heat convection of the mobile phase, and thermal diffusion across the column diameter. As the column reached thermal equilibrium, radial temperature gradient will formed, causing radial gradients of eluent viscosity and velocity and also radially changing retention factors of the solutes [75, 76]. The effect of the radial retention gradient is more pronounced in case of well retained compounds, since their migration velocity is larger in the column center where the temperature is higher than close to the column wall [74].

Extra column band broadening

The extra column broadening of the sample band occurs in the instrument parts starting from the injection system including the system drawing the sample into the injection loop, the one ejecting the sample into the needle seat, the needle seat capillary, the injection valve, the tubes connecting the column to the valve and the detector, and the detector cell. The void volume of the different parts depends on the type of the instrument. Note that the injection process itself can be the source of dispersion depending on the type of the injection system which the chromatograph is equipped. Besides these physical sources of dispersion, acquisition rate of the signal need to be taken into account. Table 2.1 shows the void volume and the extra column band broadening of few commercial instruments [1, 77].

Table 2.1: The void volume and the external band broadening of different commercially available instruments

	$V_{\text{extra-column}}$	$\sigma^2_{\text{extra-column}}$
Standard 1290 Infinity	13.8 μL	41.9 μL^2
Optimized 1290 Infinity	10.2 μL	11.1 μL^2
Classic Acquity	7.4 μL	3.0 μL^2
I-Class Acquity	2.1 μL	0.5 μL^2

The easiest method to determine the extent of the extra column band broadening is the injection of a simple sample by the absence of the chromatographic column i.e. by replacing the column with zero dead volume connection . Note that in our experiments the extra column band broadening variance of the Waters I-Class instrument and the Agilent 1290 Infinity was found around 1 and 20 μL^2, respectively.

2.1.3 The general rate model

Several models are utilized to describe the chromatographic process. The chromatographic process involves an intricate combination of complex phenomena of hydrodynamic, thermodynamic, and kinetic origins, which often interact. Since under realistic conditions the band profile is close to Gaussian distribution, the contributions of all independent sources of band broadening to the Gaussian variance can be calculated, and related to the column HETP as the sum of these variances.

The general rate model of chromatography (GR model) is one of the most detailed model, which considers a number of possible sources of mass-transfer resistances. It assumes that diffusion drives the sample molecules from the stream of the mobile phase into the particles and inside the pores of the stationary phase particles. The mobile phase is stagnant in the pores of the particles, and the adsorption-desorption process take place between the stagnant mobile phase and the surface of the pores (see Fig 2.2).

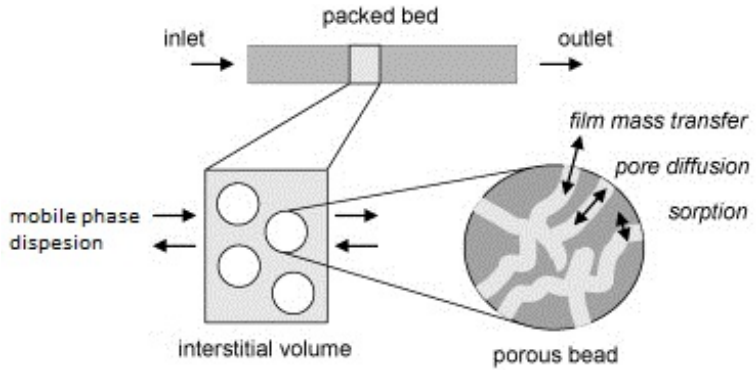

Figure 2.2: The schematic explanation of the general rate model of chromatography (modified from [78])

Since the model considers separately what is taking place inside and outside the particle, it uses several mass balance equations for the description of solute, one for the bulk mobile phase flowing between the particles, and one for stagnant mobile phase inside the particles. It also uses two differential equations for the description of the external film mass-transfer resistance, and for the adsorption-desorption process [20].

A solution of the model in the Laplace domain has been derived by Kućera [79] and Kubin [80]. Although the solution cannot be transformed back into the time domain, it allows the expression of the first five statistical moments. The use of use the Laplace domain solution and moment analysis is frequently used and extensively studied in the literature [81].

The first and second central moments of a chromatographic peak, calculated according to the general rate model allow the derivation of a detailed plate height equation [8, 11].

The retention time, or first moment (μ_1) of a chromatographic peak is obtained as

$$\mu_1 = \frac{\int C(t)tdt}{\int C(t)dt} = \frac{L}{u_h}(1 + k_1) \tag{2.48}$$

where $C(t)$ is the chromatographic band profile. Since the general rate model distinguishes between the percolating mobile phase fraction (in which the analyte is not retained) and the stagnant eluent in the permeable particles (where adsorption-desorption may occur), zone retention factor need to be introduced. The retention time of the solute gives the correspondence between these two factors:

$$t_R = (1 + k)t_0 \tag{2.49}$$

and

$$t_R = (1 + k_1)t_e \tag{2.50}$$

where t_0 the hold-up time is the sum of the time that the molecules spend in the interstitial and stagnant volumes of the eluent, while they spend t_e time in the interstitial volume of the mobile phase [10].

The second central moment calculated via the general rate model is expressed as follows:

$$\mu_2' = \frac{\int C(t)\,(t-\mu_1)^2\,dt}{\int C(t)dt} = \frac{2L}{u_h}\left[\frac{D_L}{u_h^2}\,(1+k_1)^2 + \frac{Fa^2}{u_h}\left(\frac{r_p}{3k_{\text{ext}}} + \frac{r_p^2}{15D_e}\right)\right] \tag{2.51}$$

where – as it was described in the previously – D_L is the axial dispersion coefficient, k_{ext} the external mass-transfer coefficient, D_e the intraparticle diffusion coefficient, $a = \varepsilon_p + K(1-\varepsilon_p)$, while r_p is the average particle radius. The moments calculated from the general rate model allow the derivation of the following plate height equation:

$$H = L\frac{\mu_2'}{\mu_1^2} = \frac{2D_L}{u_h} + \frac{2u_h}{F}\left(\frac{k_1}{k_1+1}\right)^2\left(\frac{r_p}{3k_{\text{ext}}} + \frac{r_p^2}{15D_e}\right) \tag{2.52}$$

The axial dispersion coefficient, must be known to characterize the band broadening in the interstitial volume of the column. The background of the estimation of the longitudinal diffusion and the multipath dispersion was widely studied in the 1960s by Giddings et. al. and other noteworthy authors, such as Gunn or van Deemter [25, 48, 64] (see Section 2.1.2).

As it was previously mentioned in Section 2.1.2 the external mass-transfer coefficient can be calculated using the Wilson-Geankoplis equation (Eq.2.38 [82] as:

$$k_{\text{ext}} = \frac{1.09}{\varepsilon_e}u_h^{1/3}\left(\frac{D_m}{d_p}\right)^{2/3}. \tag{2.53}$$

For this, the molecular diffusion coefficient of the sample need to be known at the corresponding temperature. However, several methods exist for the measurement of D_m – e.g. the use of the arrested flow or peak parking method in open tubular capillary – numerous calculations allow estimation of its value. The most commonly used equation applied for small molecules is the

Wilke–Chang equation [83]:

$$D_m = \frac{8.2 \times 10^{-8} T}{\eta V_a^{1/3}} \left[1 + \left(\frac{3V_b}{V_a} \right)^{2/3} \right] \tag{2.54}$$

where D_m is given in cm^2/s, the viscosity of the mobile phase (η) is given in cP, M_w is the molecular weight of the analyte, T is the absolute temperature and V_a and V_b are the molar volumes (mL/mol) of the solute and the solvent at their normal boiling points.

For the calculation of the molecular diffusion coefficient of macromolecules we can apply the correlation derived by Young et al [84]:

$$D_m = 8.31 \times 10^{-8} \frac{T}{\eta M_w^{1/3}} \tag{2.55}$$

where D_m is given again in cm^2/s, and the viscosity of the mobile phase (η) is similarly given in cP.

Kaczmarski and Guiochon applied the general rate model to superficially porous particles, and studied the influence of an inner solid core on the column efficiency. In case of core-shell particles, the plate height equation (Eq. 2.52) must be corrected, because of the altered geometry of diffusion paths inside the particles. Due to the presence of the solid core, the plate height equation will take the following form [7]:

$$H = L \frac{\mu_2'}{\mu_1^2} = \frac{2D_L}{u_h} + \frac{2u_h}{F} \left(\frac{k_1}{k_1 + 1} \right)^2 \left(\frac{r_p}{3k_{\text{ext}}} + \frac{r_p^2}{15D_e} R \right) \tag{2.56}$$

where R is expressed as follows:

$$R = \frac{r_p^4 + 2r_p^3 r_i + 3r_p^2 r_i^2 - r_p r_i^3 - 5r_i^4}{\left(r_p^2 + r_p r_i + r_i^2 \right)^2}, \tag{2.57}$$

where r_i and r_p are the internal, and the external radii of the porous shell of the superficially particles. For a fully porous particle $R = 1$.

2.1.4 The stochastic model of chromatography

An alternative to the traditional macroscopic models that usually formulates a mass balance equation, e.g. the general rate model, is the microscopic approach by the description of the chromatographic process with the movement of the chromatographic bands at molecular level. The molecular dynamic model of Giddings and Eyring describes the chromatographic process with the random migration of the molecules along the column and with randomly occurring adsorption-desorption events [25]. The average time that a molecule spends in the mobile phase between one adsorption-desorption event is represented by τ_m while τ_s designate the average adsorption time, i.e. the residence time of the molecule on the surface of the stationary phase. The time constants are directly related to the rate constants of the adsorption and desorption kinetics as follows:

$$\tau_m = \frac{1}{k_a} \tag{2.58}$$

$$\tau_s = \frac{1}{k_d}. \tag{2.59}$$

Since the molecules that entered the column at the same time are affected by random influences, they will be found at different positions in a given time. Accordingly, the elution profile is determined as the probability density function of the residence times of the individual molecules in the column. Each molecule spends a constant τ_m time in the mobile phase and random time bound to the stationary phase. The randomly occurring adsorption and desorption – or mass-transfer – steps are characterized by a Poisson distribution, and can be determined using three independent probabilities. One is the probability of r adsorptions during t_0 given as follows:

$$\frac{n^r e^{-n}}{r!}, \tag{2.60}$$

where n, the average number of adsorption steps can be given as

$$n = \frac{t_0}{\tau_m}. \tag{2.61}$$

The probability of $r-1$ desorption steps during t time can be given as the following distribution,

$$\frac{(t/\tau_s)^{r-1} e^{-t/\tau_s}}{(r-1)!}. \tag{2.62}$$

while the probability that one desorption takes place between a given time period can be written as

$$n = \frac{1}{\tau_s} dt. \tag{2.63}$$

The probability density function of the retention times $P(n,t)$ can be obtained from the summation of all the possible values of r:

$$P(n,t) = \sum_{r-1}^{\infty} P_r(n,t) = \sqrt{\frac{n}{t\tau_s}} e^{-n-t/\tau_s} I_1\left(\sqrt{\frac{4nt}{\tau_s}}\right), \tag{2.64}$$

where I_1 is a modified Bessel function of the first kind and first order [85, 86].

The calculations can be made also in the Laplace domain resulting a much simpler solution compared to that can be derived in the time-domain. It allows a very simple determination of the position, the width, and the shape of the peak. The void time (t_0) spent by an unretained compound in the column originates from the average number of mass-transfer steps and the sojourn times of molecules in the mobile phase, while the adjusted retention time (t'_R) is determined by the number of mass-transfer events and the average sojourn times in the stationary phase:

$$t_0 = n\tau_m, \tag{2.65}$$

and

$$t'_R = n\tau_s. \tag{2.66}$$

The variance of the peak can be given as:

$$\sigma^2 = 2n\tau_s^2, \tag{2.67}$$

while the skew that characterizes the peak asymmetry is

$$S = \frac{3}{\sqrt{2n}}. \tag{2.68}$$

On the basis of Eqs. 2.65, 2.66, and 2.67, the number of mass-transfer steps can be calculated from the first absolute and second central moments of the experimentally recorded peaks as follows [87]:

$$n = 2\frac{\mu_1 - \mu_{1_0}}{\mu'_2 - \mu'_{2_0}}, \tag{2.69}$$

where μ_1 and μ'_2 are the first absolute and the second central moments of the sample peak, and μ_{1_0} and μ'_{2_0} are the first absolute and the second central moments of the unretained marker's peak.

The average sojourn time of the molecules in the stationary phase can be expressed as:

$$\tau_s = \frac{\mu_1 - \mu_{1_0}}{n}, \tag{2.70}$$

whereas the average mobile phase sojourn times of the molecules are coming from the ratio of the first moment of an unretained marker (void time) and the number of the mass-transfer

events:

$$\tau_m = \frac{\mu_{1_0}}{n}. \tag{2.71}$$

When we apply the stochastic theory to reversed phase separations, the model will characterize the mass-transfer process – including the external mass-transfer resistance, the diffusion in the pore of the particle and the adsorption kinetics itself – rather than the adsorption process itself.

2.2 Important tools

2.2.1 Total Pore Blocking method

The so-called total pore blocking method (TPB) was introduced by Desmet and his group, for the determination of the porosity of chromatographic columns. The method involves the measuring of the elution time of a non-retained marker after having filled the pores of the stationary phase with hydrophobic solvent that is completely immiscible with the mobile phase [88].

The procedure of the pore blocking method involves the rinsing of the column with isopropanol, the filling up the column with a hydrophobic solvent (octane or dodecane) that gradually replaces isopropanol, and the flushing out of the hydrophobic solvent from the interstitial space by a hydrophilic buffer (ammonium-formate). The hydrophobic solvent block the pores, due to the strong hydrophobic contact with the C18 surface and because it is immiscible with the hydrophilic buffer flowing outside. In result, the originally porous support behaves as a completely non-porous (see at Figure 2.3) media.

The measured elution volume of a polar compound, such as thiourea will correspond exactly to the interstitial volume allow accessed by the hydrophobic liquid.

Applying the pore blocking method, the porosity of the column can be calculated from the elution volume of an unretained peak as follows:

$$V_g = \pi r_c^2 L \tag{2.72}$$

$$V_t = F_v t_0 \tag{2.73}$$

$$V_e == F_v t_e \tag{2.74}$$

where V_g is the volume of the stainless steel tubing, V_t is the total volume of the mobile phase in the column (i.e. the void volume) and V_e is the interstitial volume, L is the length and r_c is radius of the column, t_0 is the elution time of the unretained marker (void time) and t_e is the elution time of the tracer when the pores where blocked with hydrophobic solvent.

The porosity values of the column can calculated by knowing the volume fractions of the column as follows:

$$\varepsilon_t = \frac{V_t}{V_g}, \tag{2.75}$$

$$\varepsilon_e = \frac{V_e}{V_g}, \tag{2.76}$$

$$\varepsilon_p = \frac{\varepsilon_t - \varepsilon_e}{1 - \varepsilon_e}, \tag{2.77}$$

where $\varepsilon_t, \varepsilon_e$ and ε_p refers to the total- external- and internal porosities of the column, respectively.

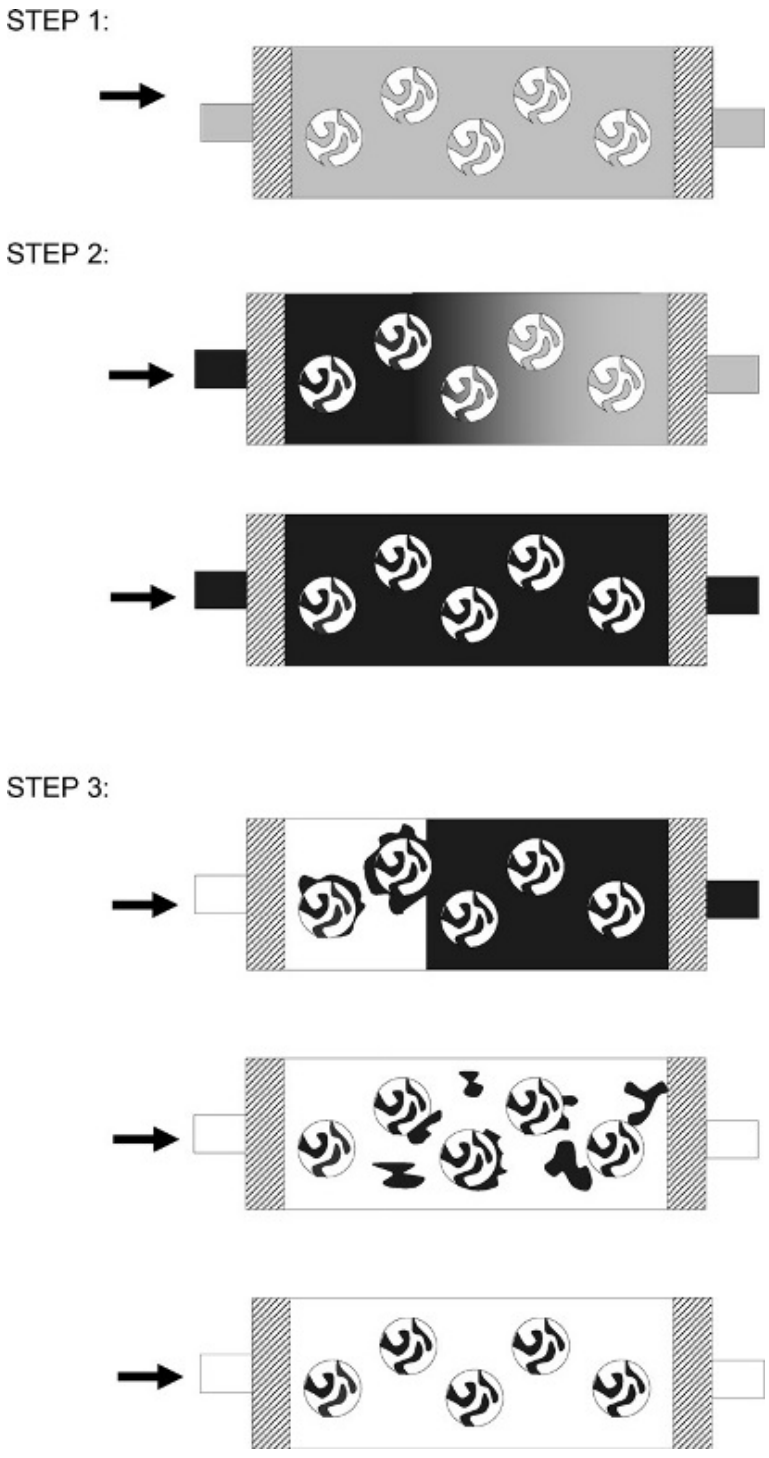

Figure 2.3: Graphical representation of the total pore blocking method: step (1) rinsing of the column with isopropanol (grey), step (2) filling up the column with a hydrophobic solvent (black) that gradually replaces isopropanol, step (3) flushing step in which the hydrophobic solvent (black) is pushed out of the interstitial space by a hydrophilic buffer (white) [88]

2.2.2 Peak Parking method

Knox and McLaren [89] proposed, the peak parking method (PP) (also called the arrested-flow method or stopped-flow method) for the determination of diffusion coefficients and obstructive factors in gas chromatography. Similar method can be used for the determination of the longitudinal diffusion coefficient and so the obstruction factor of the interstitials (γ) in liquid chromatography [10, 73, 90, 91]. The method involves the injection of small volume of non-retained sample onto the column, while continuous mobile phase flow is used. As the band reaches the middle the column, the mobile phase flow is interrupted for a given time - so called peak parking time (t_p)-, during which the band let free to diffuse in the axial direction under stagnant conditions.

As the given parking period elapsed the peak is eluted to the detector. Since the PP experiments needs non retaining conditions, usually a polar unretained marker (thiourea) is used as sample.

The broadening of the sample variance directly proportional with the parking time and depends on the molecular diffusion coefficient and the tortuosity of the packing that hinders the diffusion of the molecules in the mobile phase. The tortuosity of the diffusion channels in the packing is described by the obstruction factor, and can be derived as the ratio of the effective axial diffusion coefficient (D_{eff}) and D_m, while D_{eff} can be calculated from the additional increment of the band variance (σ^2) during t_p according to the following equations:

$$\sigma^2_{\text{PP}} = 2D_{\text{eff}}t_p, \tag{2.78}$$

and

$$\gamma_e = \frac{D_{\text{eff}}}{D_m}, \tag{2.79}$$

where γ_e is external obstruction factor, and refers to the tortuosity of the flow channels in the packed bed.

2.2.3 Flow reversal method

For the evaluation of the band broadening that occurs at the different sections in the chromatographic column the column-reversal method was introduced [92], following the method used by by Soliven et al. [93] for the characterization of the surface modification of monolithic silica. According to the method the columns are installed in a chosen flow direction to the instrument, and an unretained marker (thiourea) is injected. Then the flow is stopped as the sample band reaches the selected region of the column (a given distance from the column inlet or outlet). After the pressure dropped to ambient, the column need to be disconnected and reinstalled in the opposite flow direction. By restarting the mobile phase flow, the sample band can be eluted at the same end as it was entered the column. Practically the flow need to be arrested for the same period of time in each case during the experiments. Since the flow is stopped and the sample band is let free to diffuse for a given time, an additional band variance is introduced,

which can be easily subtracted by the determination of the longitudinal diffusion coefficient with peak parking method.

According to the procedure, the sample band passes through twice (inward and outward) the same column end, the frit, and travels twice through the given column distances. Theoretically if the column is axially homogeneous, and the column inlet and outlet are identical, we can observe similar band broadening in each directions, therefore the plots of the band variance versus the distance that the sample penetrates are linear with the same slope and intercept.

We assume that the frit and the packing material at the vicinity of the frit exhibit a different efficiency than the rest of the packing material. Thus the contributions to the observed band broadening can be written as

$$\sigma^2_{\mathrm{z,total}} = \sigma^2_{\mathrm{system}} + \sigma^2_{\mathrm{park}} + \sigma^2_{\mathrm{end}} + \sigma^2_{\mathrm{bed}}, \tag{2.80}$$

where σ^2_{park} is the band broadening originating from the diffusion during the peak parking period, σ^2_{end} comes from the inhomogeneity and from the mixing effect at the column ends while σ^2_{bed} comes from the broadening of the peak as it passes through the intrinsic column bed.

When the analyte migrates in the column, its band variance increases linearly with the distance traveled:

$$\sigma^2_{\mathrm{bed}} = Hz. \tag{2.81}$$

Accordingly, when the flow is stopped as the sample zone has reached a distance z, and the flow is reversed, the total distance traveled will be $2z$.

The increase of the band variance during the parking period (t_{park}) can be expressed as follows according to Equation 2.78.

With the flow reversal experiments one gets the total band variance as

$$\sigma^2_{\mathrm{z,total}} = \sigma^2_{\mathrm{system}} + 2\sigma^2_{\mathrm{end}} + 2D_{\mathrm{eff}}t_{\mathrm{park}} + 2Hz. \tag{2.82}$$

The moments of the recorded peaks need to be corrected with the extra-column broadening, thus the following relationship can be given

$$\sigma^2_z = \sigma^2_{\mathrm{end}} + 2D_{\mathrm{eff}}t_{\mathrm{park}} + 2Hz. \tag{2.83}$$

When the observed band variance is plotted against the penetration distance, linear correlation can be observed, where the local plate height of the homogeneous packing bed is equal to the slope of the line. The intercept gives the combined contributions of peak parking and column ends.

Chapter 3

Methods and Materials

3.1 Determination of the band variance and elution time of the sample peaks

The shape of the chromatographic band is the result of the contributions of band broadening coming from different sources, and can be used for the estimation of the determinate physical–chemical parameters of the mass-transfer during the chromatographic process. For the determination of the mass-transfer coefficients, and for the calculation of the observable plate height on different columns, the exact sample band variances and elution times must be known. To improve the accuracy, the first, and the second central moments of the sample peaks should be determined by fitting a peak shape model function to the experimental data. The exponentially modified Gaussian (EMG) function is the most frequently used asymmetrical model to describe peak profile in chromatography [94]. The EMG peak profile is written as the following equation:

$$f(t) = \frac{A}{2\tau}\exp\left(\frac{\sigma^2}{2\tau^2} - \frac{\mathrm{t} - \mathrm{t_R}}{\tau}\right)\left[1 - \mathrm{erf}\left(\frac{\sigma}{\sqrt{2}\tau} - \frac{\mathrm{t} - \mathrm{t_R}}{\sqrt{2}\sigma}\right)\right] \tag{3.1}$$

where A is the peak area, t_R the retention time of the peak, σ the standard deviation and τ is a time constant parameter that controls the asymmetry of the peak.

According to that the first moment (μ_1) and the second central moment (μ_2') of a peak can be determined as:

$$\mu_1 = t_R + \tau \tag{3.2}$$

$$\mu_2' = \sigma^2 + \tau^2 \tag{3.3}$$

Note that μ_1 is equal to the elution time, while μ_2' to the variance of the peak. The moments were determined by the fitting of EMG to the experimentally recorded peaks by using PeakFit v4.12 software, except in case of the experiments aiming for the study of the intraparticle mass-transfer, i.e the measurement of the insulin peaks. In this case the first absolute and the second central moments were determined by using the Chemstation software. Note that the method was tested with the comparison to the results obtained by numeric integration and by the fitting of exponentially modified Gaussian (EMG) curve to a set of experimentally recorded peaks, and no significant differences was found.

For the calculation of the plate height values the moments were corrected for the contributions of injection and extra-column band broadening and the corrected moments were used.

3.2 Total pore blocking experiments

The TPB experiments were carried out using octane and dodecane for the fully porous and core-shell packed columns as blocking agent, respectively. The flush solvent was 10mM ammonium-formate. The column was washed at least 20 times of the column volume with isopropanol before the columns were filled with hydrophobic solvent. For completely changing the fluid in the pores, the columns were washed with the blocking agent for 90 minute at 0.2mL/min, than the column was replaced with a dead volume union and the instrument was washed with isopropanol and with the buffer. After that, the column was reinstalled and flushed with buffer until the baseline and the pressure stabilized. The column hold up volumes were measured using thiourea dissolved in buffer.

3.3 Peak parking experiments

The PP measurements were performed using the corresponding mobile phase mixtures, – i.e the same mobile phase that was used during the measurements of the different analytes – and thiourea as sample, while the flow rate was set to 0.2 mL/min. The flow was stopped for t_p= 0, 30, 60, 300, 600, 1200, 2400, 3600 seconds as the half of the void volume passes trough the column after injection. Each measurement was repeated three times.

3.4 Flow reversal method

The flow reversal method is capable for the analysis of the axial heterogeneity of the inner structure of the chromatographic columns, emphasizing the differences at the column ends. During the experiments, the columns were installed in the chosen flow direction, and an unretained marker (thiourea) was injected, while the flow rate was set to 0.2 mL/min. The flow was stopped when the sample band reached the selected region of the column (1, 2, 3 or 4 cm distance from the column inlet or outlet). After the pressure dropped to ambient, the column

was disconnected and reinstalled in the opposite flow direction. Then the flow was restarted and the sample band was eluted from the column at the same end as it entered the column. In each case the flow was arrested for a total of 2 minutes, which was more than enough for the pressure relaxation and for the disconnection and reinstallation of the columns.

Since the flow is stopped and the sample band is let free to diffuse for a given time, an additional band variance is introduced, which can be easily subtracted by the determination of the axial dispersion coefficient with peak parking method [72, 95].

3.5 Measurement of the effect of frictional heating on column efficiency

The homologous series of alkyl-benzenes, containing octyl-, decyl-, dodecyl-, tetradecyl- and octadecyl-benzene in 0.5 mg/mL concentration was injected at flow rates between 0.2 and 0.9 mL/min. Pure methanol was used as mobile phase. The standards were purchased from Sigma-Aldrich (Germany, Schnelldorf) and were dissolved in methanol as sample. Note that since the most retained octadecyl-benzenes peak-intensity was not sufficient in every case to determine the peak variance properly, the results obtained for tetradecyl-benzene was prefered during the calculations. Measurements were carried out on a Waters Aquity I-class UPLC instrument (Waters Corporation, Milford, MA, USA) equipped with diode-array detector.

The examined chromatographic columns were a fully porous Waters BEH (1.7 μm, 50 $\times$ 2.1 mm) column, and a superficially porous Waters Cortecs (1.6 μm, 50 $\times$ 2.1 mm). The measurements next to adiabatic conditions were carried out by the insulation of the columns with polystyrene foam rubber, while the eluent was preheated to 25 °C. The thermostated measurements were carried out at 25 °C.

3.6 Comparison of the efficiency of novel vHPLC stationary phases

The experiments were carried out on a Waters Acquity I-Class UPLC instrument, the mobile phase was the premixed mixture of 65:35 v/v acetonitrile and water (Sigma-Aldrich, Germany, Schnelldorf) for each measurement. All measurements were carried out at constant 40 °C column temperature while the injection volume was 0.2 μL. The system void volume was around 1 μL with the optimization of the tubing. The instrument was controlled by Empower 2 software. Five different reversed phase (C_{18}) chromatographic columns designed for fast liquid chromatography with the same geometrical parameters (2.1 × 50 mm) provided by GL Sciences and Phenomenex were tested during the experiments (see Table 3.1) under the same experimental conditions.

Agilent check-out sample (Agilent Technologies, Palo Alto, CA, USA) containing acetanilide, acetophenone, propiophenone, butyrophenone, benzophenone, valerophenone, hexanophenone, heptanophenone and octanophenone in 100 μg/mL concentration was injected to evaluate the kinetic performance, and thiourea was used to determine the void volumes of the columns. The flow rate was set over the range 0.05–1.0 mL/min.

The instrument void volumes and the effect of the extra-column band broadening were measured by injecting thiourea in the system while the column was replaced with a zero-volume connection. For the calculation of plate heights and peak capacities the first moments – i.e. the retention times of the sample peaks – were corrected with the extra-column voids, that leads to slightly less propitious but more realistic values [10, 24]. In case of the column-reversal method, both the first and second central moments were corrected for the complete elimination of the extra-column effects.

Table 3.1: The characteristics of the columns used for the comparison of the efficiency of novel columns designed for vHPLC, and for the analysis of the axial bed heterogeneity.

	particle diameter (d_p) [μm]	core radii (r_i) [μm]	void volume (V_0) [μL]	total porosity ε_t
InertSustain	2.0	-	86.1	0.49
InertSustainSwift	1.9	-	111.5	0.64
MonoTower	$(1.8)^a$	-	112.2	0.65
Kinetex	2.6	0.95	84.5	0.49
Kinetex EVO	2.6	0.95	84.5	0.49

a: Domain size, or combined size of a through-pore and a skeleton [24].

3.7 Analysis of the intraparticle diffusion of macromolecules

For the analysis of the intraparticle diffusion, solution of human insulin (Sigma-Aldrich, Germany, Schnelldorf) in 1.0 mg/mL concentration dissolved in the eluent was injected as sample, while the column hold-up volumes were determined by the injection of thiourea standard. The injection volume was 1 μL in each measurement. Chromatographic columns were an Agilent Zorbax (100 × 4.6 mm, particle size 3.5 μm) purchased from Agilent, a Waters Xselection (100 × 2.1 mm, particle size 2.5 μm) a Phenomenex Kinetex (100 × 4.6 mm, particle size 2.6 μm) a Phenomenx Aeris Peptide (100 × 4.6 mm, particle size 3.6 μm) and a Phenomenex Aeris Widepore (100 × 4.6 mm, particle size 3.5 μm) (See Table 3.2).

The experiments were carried out on an Agilent 1290 Infinity UHPLC instrument (Agilent Technologies, Palo Alto, CA, USA) equipped with diode-array detector. Agilent Chemstation software was applied on the UHPLC system and used for the determination of the first and second central moments of the samples peak.

Table 3.2: The properties of the columns used for the examination of the intraparticle diffusion of macromolecules.

	geometry (mm)	d_p (μm)	r_i (μm)	r_p ($\AA$)	ε_t	ε_e	ε_p
Xselection	100 × 2.1	2.5	–	48.7	0.642	0.393	0.410
Kinetex	100 × 4.6	2.6	0.95	53.1	0.564	0.431	0.235
Zorbax	100 × 4.6	3.5	–	37.3	0.576	0.424	0.264
Aeris Peptide	100 × 4.6	3.6	1.30	50.0	0.562	0.425	0.238
Aeris Widepore	100 × 4.6	3.6	1.60	121.7	0.508	0.415	0.159

d_p: particle diameter,
r_i: core radius,
ε_t: total porosity,
ε_e: external porosity,
ε_p: intraparticle porosity

The eluent was a mixture of acetonitrile and water, with 0.1% trifluoroacetic acid (Sigma-Aldrich, Germany, Schnelldorf). The mobile phase flow-rate was set over the range 0.05–1.6 mL/min in case of the 4.6-mm ID columns, and 0.02–0.33 mL/min in case of the Waters Xselection column, to obtain the same linear velocities. The acetonitrile content of the eluent was changed between 28 and 29.5% v/v to maintain the same values of the retention factor on each column. The column thermostat was set to 25°C.

The internal and external porosity values determined by Bacskay et al. with a series of ISEC measurements [96] were used for the calculations of the mass-transfer properties of the columns (values shown in Table 3.2).

3.8 Comparison in the efficiency between SFC and UHPLC techniques

The experiments were carried out on an Agilent 1290 Infinity ultra high pressure liquid chromatograph (UHPLC) (Agilent Technologies, Palo Alto, CA, USA) and on a Waters Acquity UPC^2 (Waters Corporation, Milford, MA, USA) supercritical fluid chromatograph (SFC). The instruments were equipped with diode-array detector. The same chromatographic column was installed in the two instruments, an Agilent Zorbax (100 $\times$ 4.6 mm with the particle size of 3.5 μm) purchased from Agilent. Agilent Chemstation software was applied on the UHPLC system while the SFC instrument was controlled by the Empower 3 software. The injection volume was 2 μL, and the flow-rate was set over the range 0.2-2.5 mL/min in each experiment. All measurements were carried out at constant 35°C column temperature.

3.8.1 Liquid chromatography conditions

In case of the UHPLC measurements, the injected sample was a mixture of the homologous series of alkylbenzenes: octylbenzene, decylbenzene, dodecylbenzene, tetradecylbenzene, octadecylbenzene and thiourea. The sample was prepared in 0.2 mg/mL concentration dissolved in methanol. The standards were purchased from Sigma-Aldrich, (Germany, Schnelldorf). The mobile phase was mixture of methanol and water (Sigma-Aldrich, Germany, Schnelldorf). Two mobile phase compositions were used during the experiments: one was a mixture of methanol and water 97.5:2.5% v/v and the other was pure methanol. The retention factor (k) of the most retained compound (octadecylbenzene) was found around 14 and 7.2 at the different mobile phase compositions, respectively (see Table 3.3).

Table 3.3: The conditions used for the UHPLC experiments, and the corresponding retention factors.

HPLC conditions

	eluent composition	ABPR	k
1.	100% methanol	–	7.3–6.9
2.	97.5%methanol:2.5% water	–	14.6–13.5

3.8.2 Supercritical fluid chromatography conditions

The same mixture of octylbenzene, decylbenzene, dodecylbenzene, tetradecylbenzene, octadecylbenzene, in 1 mg/mL concentration, dissolved in heptane was injected during SFC experiments. The standards were purchased from Sigma-Aldrich, (Germany, Schnelldorf). The SFC measurements were carried out under three different conditions. In the first two cases the eluent was pure CO_2, while the ambient back pressure regulator (ABPR) was set to 105 and 150 bar (hereinafter low- and high pressure conditions), respectively. In the third case 9% of methanol was added to the mobile phase, and the ABPR was set to 105 bar, to obtain subcritical conditions. The different settings and the corresponding retention factors are shown in Table 3.4.

Table 3.4: The conditions used for the SFC experiments, and the corresponding retention factors.

SFC conditions

	eluent composition	ABPR	k
1.	100% CO_2	105 bar	12.4–4.8
2.	100% CO_2	150 bar	6.1–3.6
3.	91% CO_2 and 9% methanol	100 bar	3.1–2.8

Chapter 4

Results and Discussion

4.1 The effect of frictional heat on column efficiency

For the analysis of the efficiency loss due to the frictional heat in UHPLC columns, the efficiency of two column with the same geometrical parameters packed with fully porous (BEH) and a core-shell (Cortecs) particles with sub-2-μm diameter were probed. The examination was based on the series of experiments where a solution of the homologous series of alkyl-benzenes was injected onto the columns under thermostated and insulated conditions at different flow rates. According to the general rate model, the different additional band broadening contributions can be separated as a result of Eq. 2.51 and 2.17, and can be expressed in reduced plate height as follows:

$$h = h_A + h_B + h_e + h_p + h_{\text{heat}}, \tag{4.1}$$

$$h_A = \frac{2\lambda\omega\nu/F}{2\lambda + \omega\nu/F}, \tag{4.2}$$

$$h_B = \frac{2\gamma}{\nu}, \tag{4.3}$$

$$h_{\text{ext}} = \left(\frac{k_1}{k_1+1}^2\right)\frac{u_h}{3Fk_{\text{ext}}}, \tag{4.4}$$

$$h_p = \left(\frac{k_1}{k_1+1}^2\right)\frac{\nu}{30F}\frac{D_m}{D_e}R \tag{4.5}$$

where h_B, h_A, h_p, h_p, h_{heat} are the contributions of the longitudinal diffusion, the multipath dispersion, the external mass-transfer, the intraparticle diffusion and the frictional heating to the reduced plate height, respectively. Note that the terms h_B and h_A originate from the axial dispersion coefficient D_L, i.e. from the band broadening in the interstitial volume of the column.

As it was mentioned in Section 2.1.2, the Gunn's correlation [64] is widely used to estimate the axial dispersion coefficient. A simplified form of the Gunn correlation written with convenient

chromatographic terms are resulting in the following equation [8, 11]:

$$\frac{2D_L}{u_h d_p} = \frac{2\gamma}{\nu} + \frac{2\lambda\omega\nu/F}{2\lambda + \omega\nu/F} \tag{4.6}$$

where γ was determined via peak parking and was found 0.67 and 0.84 for the Cortecs and the BEH column, respectively $\lambda = 2.586$, $\omega = 0.0712$, ν is the reduced interstitial velocity and F is the phase ratio (defined in Eq. 2.29). The numerical values of the parameters were determined by the fitting Eq. 4.6 to the Gunn correlation over a wide range of reduced interstitial velocities [8]. Note that the axial dispersion calculated by Eq. 4.6 resulted in values rather similar to those that can be obtained by the protocol suggested by Gritti and Guiochon [97].

The geometrical parameters of the examined columns were determined via TPB and PP method, and are summarized in Table 4.1. The values of the longitudinal dispersion coefficients – calculated as the sum of the axial dispersion (resulting from the PP experiments) and the eddy dispersion (originating from the Gunn correlation) – the external mass transfer coefficients, and the intraparticle diffusion coefficients of the columns at the optimal mobile phase velocity are also shown at Table 4.1. Since the same mobile phase compositions and analytes were used during the experiments, and the geometrical parameters of the columns are quite similar, the examined mass-transfer coefficients are close to each other.

Table 4.1: The parameters of the examined columns in the study of the effect of the frictional heat, and the observed mass-transfer coefficients of tetradecylbenzene around the optimal mobile phase velocity.

	d_p [μm]	d_i [μm]	ε_e	D_L [cm^2/s]	D_p [cm^2/s]	k_{ext}
BEH	1.7	-	0,34	1.62×10^{-5}	7.91×10^{-7}	0.37
Cortecs	1.6	1.1	0.38	1.48×10^{-5}	7.02×10^{-7}	0.32

d_p: particle diameter
d_i: core diameter
ε_e: external porosity
D_L: longitudinal dispersion
D_p: intraparticle diffusion
k_{ext}: external mass-transfer coefficient

It has been found that in case of the superficially porous Cortecs column, around 45% of the observed plate heights are attributable to the intraparticle processes, while in case of the BEH column, 60-65% of the column efficiency can be explained by the same phenomenon. As it was already shown in a number of papers, the contribution of the intraparticle mass-transfer is moderate in case of superficially porous packings, where the diffusion paths are shortened by the presence of the solid core in the center of the particles [7, 11, 98]. This leads to smaller C-term contribution to the HETP, and so smaller observable plate height values for the core-shell packed Cortecs column, especially at elevated mobile phase velocities.

The insulation of the columns cause 20-25% decrease in the reduced plate height values of

tetradecylbenzene at the highest flow rates (see Fig. 4.1). The efficiency decrease is present regardless to the retention of the molecules.

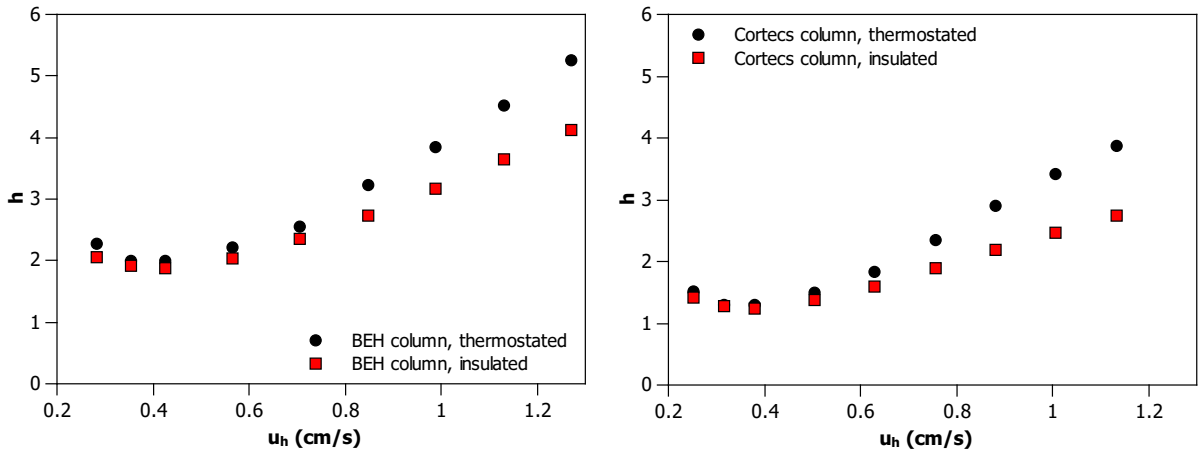

Figure 4.1: The observed reduced plate heights of tetradecylbenzene with the thermostation and the insulation of the columns,(left: BEH column, right: Cortecs column).

Since the frictional heat introduce mostly at elevated flow velocities, the effect of the thermal heterogeneities on the efficiency appears above 0.6 cm/s interstitial mobile phase velocity.

As it was already mentioned, the established radial temperature gradient forms a radial temperature gradient too that affects the highly retained compounds more expressively. This suggest, that the efficiency loss caused by the thermal heterogeneities are increasing with the increase of the retention, particularly at elevated flow rates. Although in case of the fully porous packing this exact behavior was observed, the superficially porous packing showed less conspicuous difference in the efficiency loss for the analytes with different retention (see at Fig. 4.2). The controversial results obtained for the Cortecs column may originates from measurement error occurred during the thermostated experiments. Note that the presence of a tiny extra void in the system connectors can cause significant difference in the observed plate heights of the slightly retained compounds. Because of this, the results of the most retained compound, (tetradecylbenzene) can be considered relevant.

Insulation also causes a slight decrease (around 5%) of the retention factors, since the columns reach the equilibrium at higher temperature. With the increase of the flow rate, the concomitant effects of pressure and frictional heating can be observed. Elevated pressures tend to increase the retention through the change of the molar volume of the analytes, while the effect of the heating leads to the decrease of retention due to the temperature gradient along the column [33]. Since the change of the molar volume of small molecules upon adsorption is almost negligible, the effect of the frictional heating will be dominant and it leads to the decrease of retention with the increase of the flow rate. However, the retention factor decreases in the same extent, whether the column was insulated or thermostated (see Fig. 4.3), caused by the presence of a longitudinal temperature gradient in the column in both cases.

Figures 4.4 and 4.5 show the different contributions to the reduced plate height of tetradecylben-

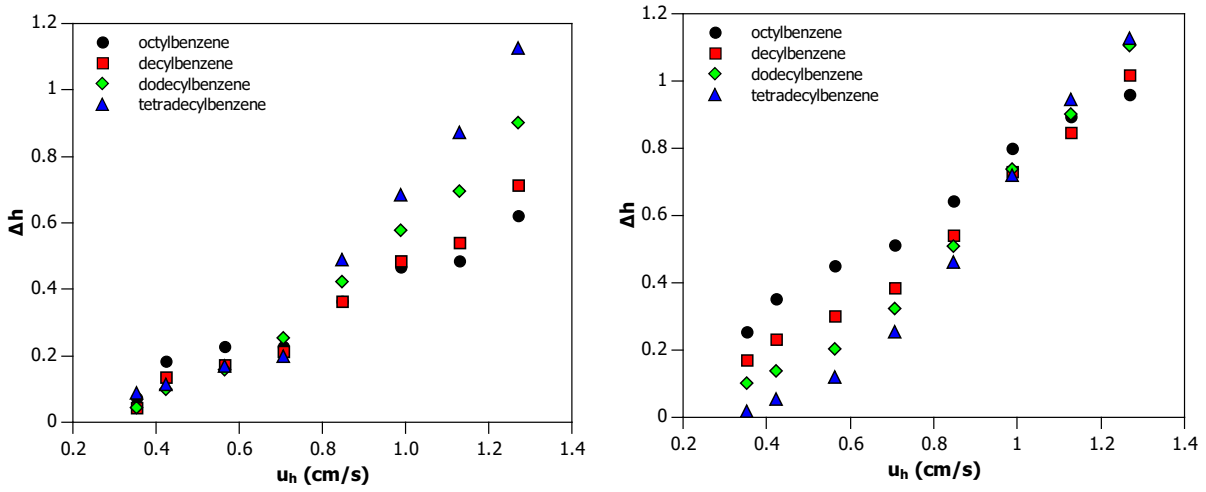

Figure 4.2: The difference in the reduced plate heights of the alkylbenzenes between the thermostated and insulated measurements,(left: BEH column, right: Cortecs column).

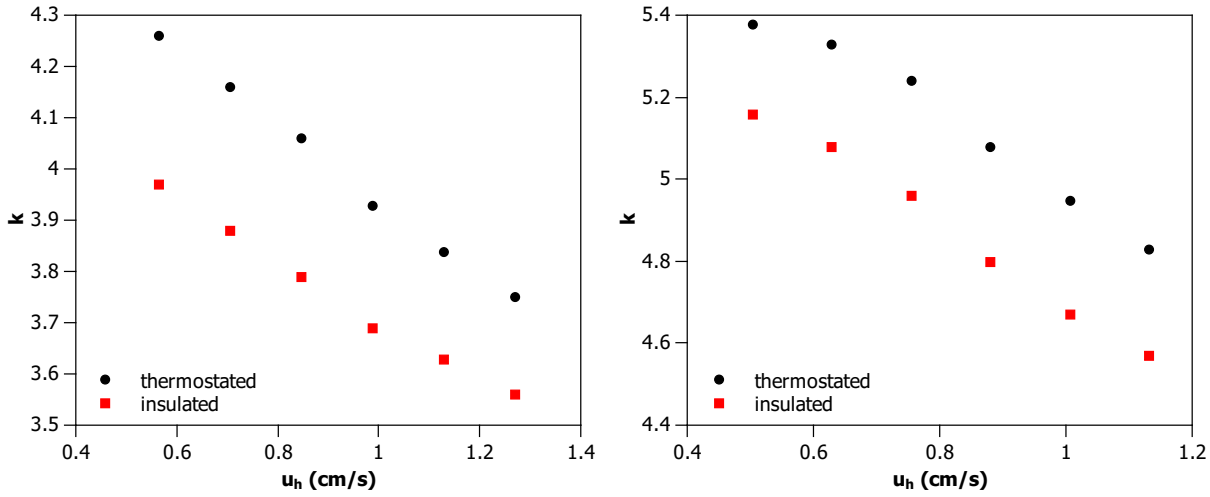

Figure 4.3: The observed retention factors of tetradecylbenzene with the thermostating and the insulation of the columns at the different mobile phase velocities, (left: BEH column, right: Cortecs column).

zene and decylbenzene at the examined mobile phase velocities. According to the estimations, the dispersion of the sample band in the mobile phase is in the same magnitude for the examined columns. The mean contribution to the overall plate height comes from the intraparticle mass-transfer regardless of the applied mobile phase velocity. Better efficiency can be reached with the core-shell Cortecs column, hence in this case the most determinative process, the intraparticle diffusion has lesser impact attributed to the shortened diffusion paths in the solid phase.

When significant frictional heat occurs at elevated flow rates, the evolving radial temperature gradient causes velocity biases in the mobile phase flow. The band dispersion coming from this effect is in the same magnitude as the sum of the another mobile phase dispersion effects (i.e longitudinal diffusion and multipath dispersion together). However, according to our findings, it is only present at high flow rates i.e. near the optimal mobile phase velocity the role of this

effect is almost negligible.

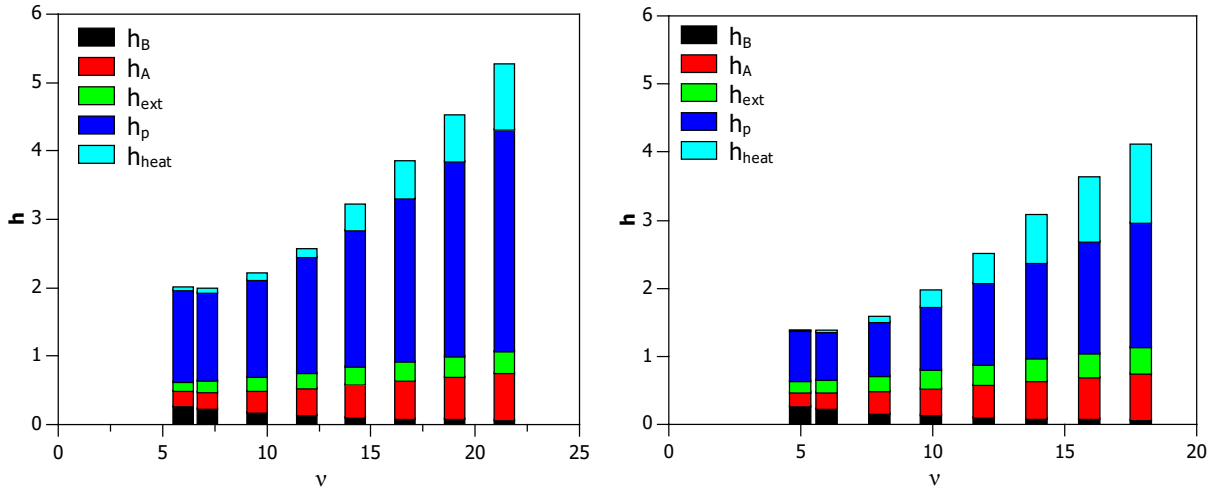

Figure 4.4: The different contributions to the reduced plate height of the tetradecylbenzene at the examined mobile phase velocities,(left: BEH column, right: Cortecs column).

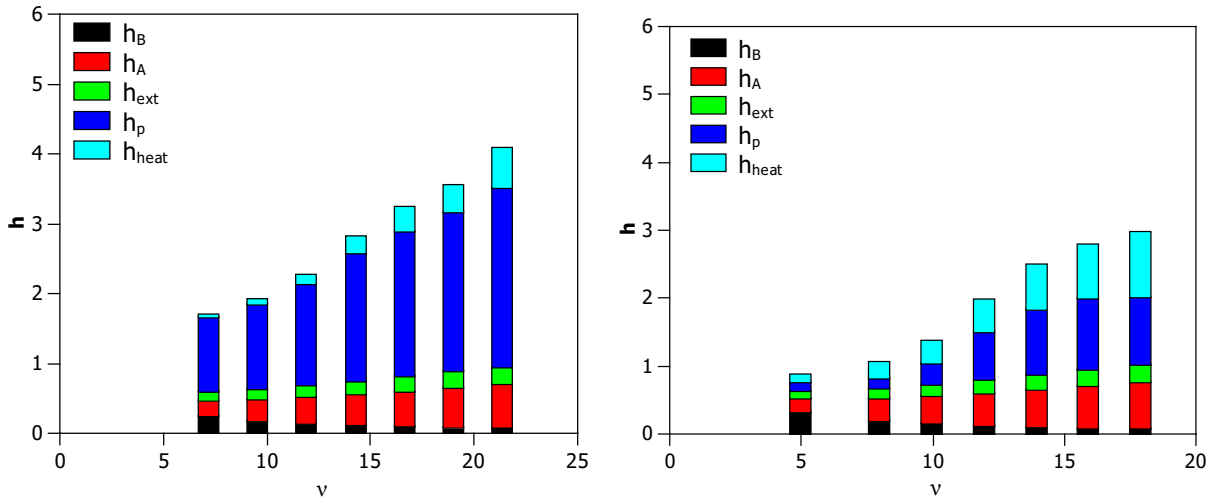

Figure 4.5: The different contributions to the reduced plate height of the decylbenzene at the examined mobile phase velocities,(left: BEH column, right: Cortecs column).

The efficiency loss caused by the frictional heat seems to be slightly moderated in case of the BEH column, especially when the retention of the analyte is small, as it is observable in case of decylbenzene (see at Fig. 4.5). However, it could be said that the thermal heterogeneities are present in the same extent in both of the columns, suggesting that there are no significant differences in the heat conduction between the two type of packings. It can be concluded, that the efficiency loss originating from the frictional heating of the mobile phase at elevated flow rates must taken into account, since it cause comparable band broadening to the particular mass-transfer processes in the column.

4.2 Comparison of the efficiency of novel vHPLC stationary phases

4.2.1 Kinetic performance measurements

The efficiency of five different reversed phase (C_{18}) chromatographic columns, including an InertSustain and an InertSustainSwift (GL-Sciences) column packed with fully porous particles, a new generation monolithic column (MonoTower) provided by GL Sciences, and two core-shell Kinetex columns with the same geometrical parameters (2.1 × 50 mm) were tested during the experiments (shown in Table 3.1) under the same experimental conditions.

The tested columns show rather similar column efficiency, i.e. similar plate height values between 3.5–5.5 μm at the optimum mobile phase velocities, with similar values that can be found in earlier studies [24, 99, 100]. We found that the highest plate number (N = 11 800) can be obtained with the MonoTower column for heptanophenone at 0.3 mL/min flow rate. However, this column shows notable change in efficiency with the mobile phase velocity, similarly to the InertSustaineSwift column, that shows the decrease of efficiency with the increase of the mobile phase velocity in the same magnitude. Since the total porosity of these columns are close to each other, similar contribution of the mobile phase effects to the band broadening can be suggested. As it could been expected, the flattest H–u curves were provided by the core-shell Kinetex columns. The observed column performance specifics are summarized in Table 4.2.

Table 4.2: The observed kinetic performance parameters of the vHPLC columns. The results shown were obtained for heptanophenone peaks at optimal mobile phase velocity.

	N (optimal)	plate height [μm]	$k_{\text{heptanophenone}}$
InertSustain	10 900	4.5	5.9
InertSustainSwift	9500	5.2	3.2
MonoTower	11 800	4.3	5.4
Kinetex	11 300	5.1	4.4
Kinetex EVO	9600	5.2	4.0

The columns with core-shell packing material provide efficiencies similar to the InertSustain and SustainSwift columns, which were packed with much smaller particles (Figure 4.6).

The dependence of efficiency on the retention factor highlight the dissimilarities of the mass-transfer contributions from a rather interesting aspect. The bandwidth of a peak eluted at larger retention factor (k) is accompanied with a relatively smaller contribution of the extra-column band broadening and in smaller mobile phase dispersion to the total peak variance or experimentally observed plate height.

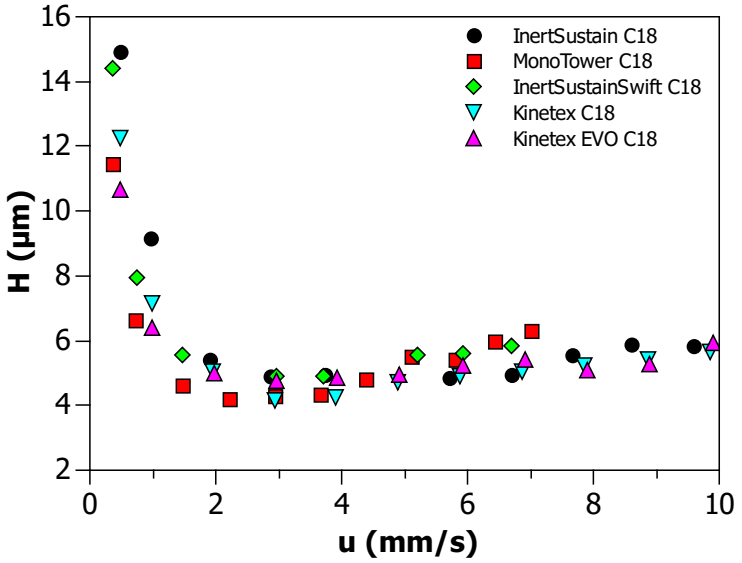

Figure 4.6: The observed plate height values of heptanophenone on the vHPLC columns using acetonitrile:water 65:35% (v/v) as mobile phase

Figure 4.7 shows, that the monolithic column provide significantly better efficiency for early eluting compounds than the packed columns, where the efficiency of the measurements originate mostly from mobile phase dispersion. Note that the plate heights plotted against the retention factor was observed at F_v=0.4 mL/min flow rate, – close to the optimal mobile phase velocity – for each column.

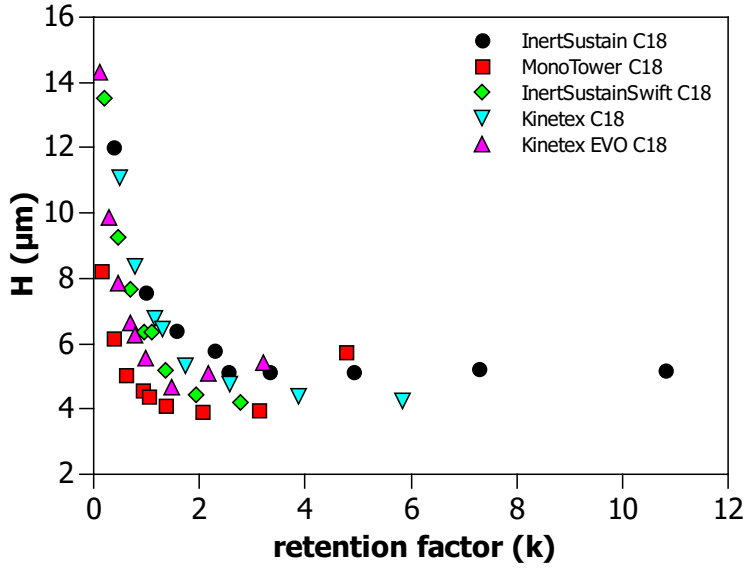

Figure 4.7: The observed plate height values against the retention factor on the examined vHPLC columns using acetonitrile:water 65:35% (v/v) as mobile phase at F_v=0.4 mL/min.

Another additional contribution to the band broadening is expected in case of the packed columns, attributed to the dispersion in the column voids i.e. the frits and the column hard-

ware, or may originate from the axial heterogeneity of the packing. Assuming that the best performing tested column (MonoTower) has ideal connections between the column hardware and the stationary phase – which of course cannot be the real case – different σ^2 values have to be subtracted from the peak variances measured on the packed columns to get similar efficiency that was provided by the monolithic column. The difference in the variance is a different value for each column and is independent from the retention factor of the analyte. According to this a column-specific band broadening is suspected in the hardware of the examined packed columns [24, 101].

In case of the MonoTower column, the monolith is fixed in a glass tube that is embedded in epoxy resin and covered with a stainless steel tube. The tube can be mounted in a stainless steel cartridge that allows the attachment to the commonly used UHPLC instruments. A precise PEEK gasket is used to provide zero dead volume connection between the monolith and the hardware without any leakage (see at Fig.4.8).

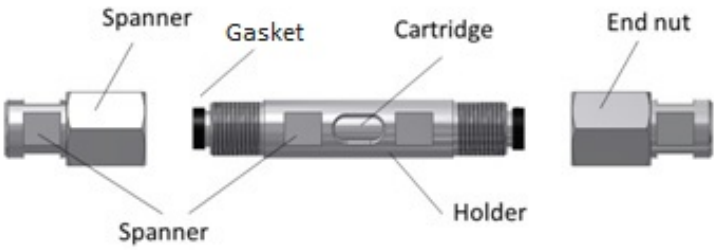

Figure 4.8: Schematic illustration of the structure of the monolithic MonoTower columns mountable hardware (provided by GL-Sciences).

The effect of the frits on efficiency was evaluated by attaching commercially available frits to the hardware of the MonoTower column. It was found, that the efficiency of the monolithic column with the frits attached is similar to the packed columns with the poorest efficiency, and shows similar behaviour with the change of the retention factor as the packed columns (see Figure 4.9). Accordingly, the frits add a nearly constant variance to the band broadening similarly to a mixer with a constant void volume. Note that since according to the manufacturers guide the porosity value of each 1-mm-long frit with 2.2 mm diameter is around ε=0.2 each frit has volume around 0.76 μL. However, the additional band broadening introduced by the two frits during the experiment was estimated as $\sigma_V^2 = 3.75\ \mu\mathrm{L}^2$. Considering that the frits operate as ideal mixers standard deviation increment induced should be. $\sigma_V^2 = 1.15\ \mu\mathrm{L}^2$.

In a similar manner, the contribution of the frits and the terminal bed heterogeneity to the band variance was estimated as $\sigma_V^2 = 1.75\ \mu\mathrm{L}^2$ for the Kinetex column. Note that these variances are larger than the extra-column variance of the instrument used ($\sigma^2_{\mathrm{system}} = 1.06\ \mu\mathrm{L}^2$). These controversial results highlight, that a more sophisticated method is needed to describe the effect of the column hardware on efficiency.

The experiments were repeated with three MonoTower columns produced with the same geometrical and chemical parameters, but in case of MonoTower 1, the column was mounted to the

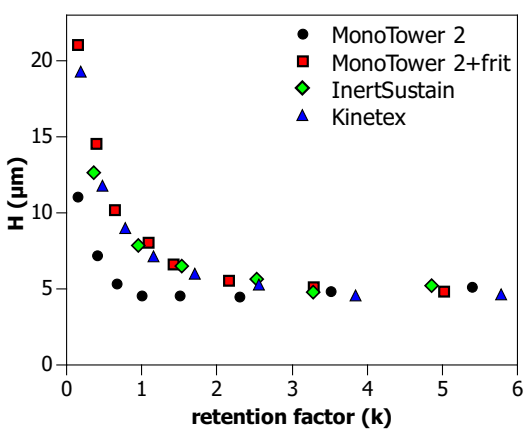

Figure 4.9: The comparison of the observed plate height values when commercial frits was installed on the MonoTower column. Note, that H measured at F_v=0.4 mL/min is plotted against the retention factor

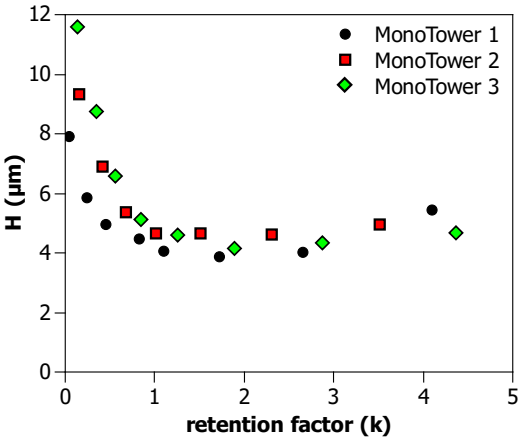

Figure 4.10: The observed plate height values observed at at F_v=0.4 mL/min against the retention factor on three same type MonoTower columns. Note that Monotower 1 was mounted by the manufacturer.

cartridge by the manufacturer, while MonoTower 2 and 3 were installed by the user following the manufacturer's instructions. As it is shown in Figure 4.10, a slight, but obvious difference can be observed in efficiency between the reproductions, which can originate from the differences in the goodness of the monolithic silica or in the column mounting. The repeatability of the mounting was tested by repeating the experiments after disassembling and remounting the column in the cartridge, and close to the same results were obtained.

4.2.2 Analysis of the effect of the frits and the bed heterogeneity at the column ends on efficiency

The efficiency near to the two ends of the examined columns was probed with flow reversal studies. Following the procedure detailed in Section 2.2.3, an unretained marker (thiourea) was injected, and the flow of the mobile phase was stopped when the sample band penetrated a given distance into the column. When the pressure has relaxed, the column was rotated during a 2 minute arrested flow period, and the unretained marker was eluted at the same end of the column where it was entered.

An interesting band compression effect of the flow reversal was observed during the experiments. The peaks observed with reversed flow are always narrower and more symmetrical than the peaks obtained without reversing the flow (see Figure 4.11). Assuming that the molecules mostly travel through the same interstitial channels inward and outward the column, the compensation of the multipath dispersion effects can be an acceptable explanation for this behaviour.

The spreading of chromatographic peaks is described by the different velocities of the individual solute molecules at microscopic level. As it was mentioned in Section 2.1.2, the coupling of the mobile phase broadening terms are determinant. There are a number of ways in which velocity

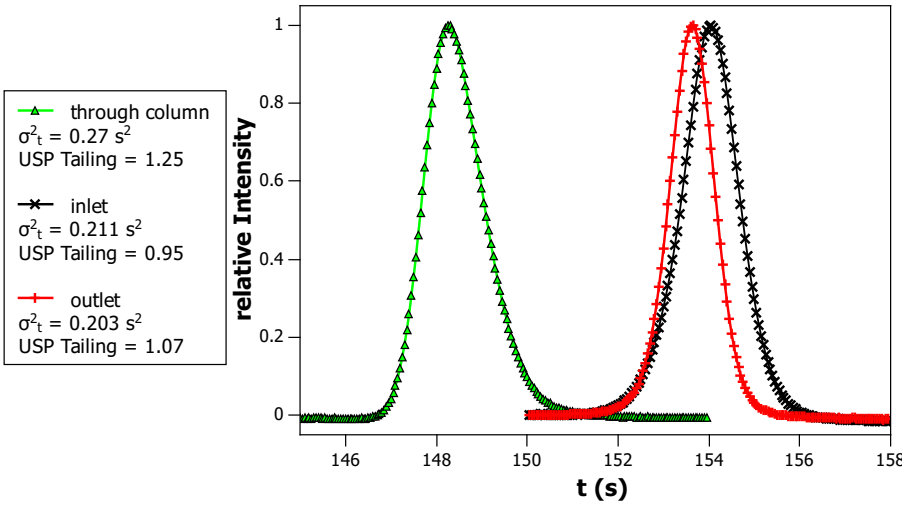

Figure 4.11: The peak shapes of thiourea observed with the elution in the standard flow direction, and with the reversal of the column including 2 minutes arrested flow in each cases on the InertSustain column using acetonitrile:water 65:35% (v/v) as mobile phase with 0.2 mL/min flow rate.

differences can arise in the complicated structure of a packed or monolithic bed. For the interpretation of the flow reversal experiments, the short-range interchannel effect [21] has to be emphasized. According to the definition of Giddings, molecules travel faster in some channels than in other neighboring ones. The velocity bias of the molecules can be relaxed by either flow (a molecule migrating in a fast channel will slow down as the geometry of the channel changes due to the heterogeneity of the interstitial space) or diffusion (a molecule diffuse from a fast channel to a slow one, and vice versa).

More recent studies identified three distinguishable coaxial zones in the bed with differing average flow velocities, by imaging the spatial distribution of particles in a consolidated bed [102]. According to this, a thin (1.4 particle diameter wide) layer neighboring the column wall with a loose, and orderly packed region is followed by a thicker, more dense, and randomly packed intermediate region. In the center of the column is a bulk randomly packed region located [103,104]. The studies show, that the local flow velocity close to the wall is significantly higher (1.5 times higher), while the intermediate layer shows slightly slower mobile phase flow compared to the velocity in the bulk region of the column. Assuming that molecules can travel through the same channel forward and backward, some of the short-range interchannel and trans-column effects will cancel resulting narrower and more symmetrical peaks compared those were recorded without flow reversal.

Due to the nature of the column packing procedure, the inlet and the outlet ends of the columns exhibit a different structure and efficiency, thus experiments were carried out to test either the column inlet or the outlet, and the σ^2_{end} variance was determined respectively (σ^2_{inlet} or σ^2_{outlet}).

In order to characterize the band broadening due to peak parking – i.e the band broadening occurring during the 2 minutes period when the flow was stopped – a series of experiments

were executed with 1, 2, 5, and 10 minutes arrested flow when the column was reversed. Those experiments were executed on a monolithic column in one flow direction, and with one of the core-shell packed columns (Kinetex) in both flow directions. The results are presented in Figures 4.12 to 4.14.

When $z = 0$, the intercepts of the straight lines give the band variance due to the contributions of column ends and parking time:

$$\sigma_z^2 = \sigma_{z,\text{end}}^2 + 2D_{\text{eff}}t_{\text{park}} \tag{4.7}$$

The respective band broadening contributions due to peak parking and terminal column heterogeneity can be separated, since if we plot the intercept values – i.e. the variance at $z = 0$ – against the parking time, a linear correlation should be observed, where the slope of the equation is $2D_{\text{eff}}$.

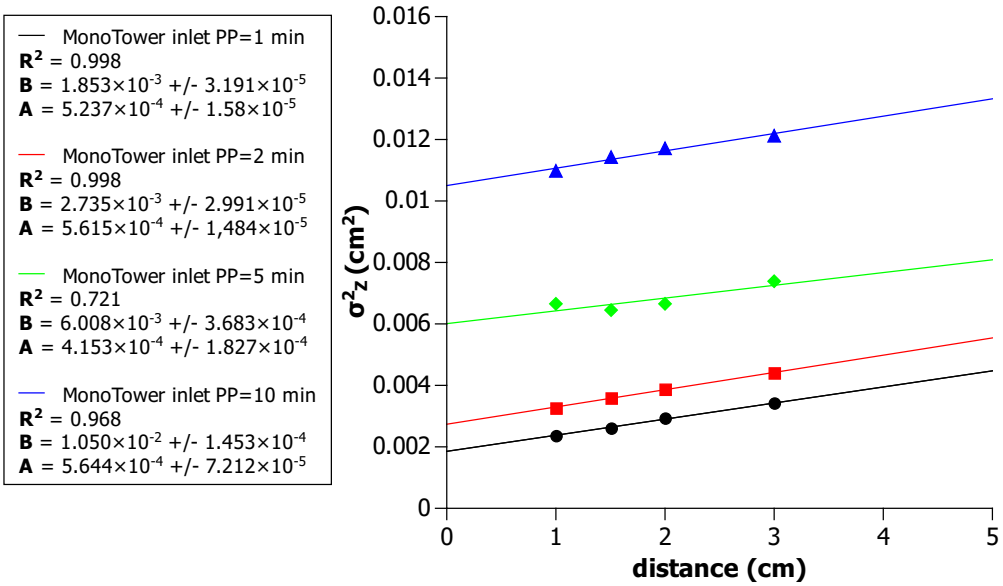

Figure 4.12: Band variance obtained for the MonoTower column with flow reversal. The flow was arrested for 1, 2, 5, and 10 minutes respectively. The column inlet was probed. The fitted parameters are given $A = 2H$ in cm, and $B = 2\sigma_{z,\text{end}}^2$ in cm^2/s units.

Those measurements were carried out at a flow-rate $F_v = 0.2$ mL/min, where the volumetric variance (σ_V^2) of the extra-column broadening is $\sigma_{V,\text{system}}^2 = 1.059\ \mu\text{L}^2$. Note, that the relation between the volumetric, and the longitudinal variance was given in Equation 2.9

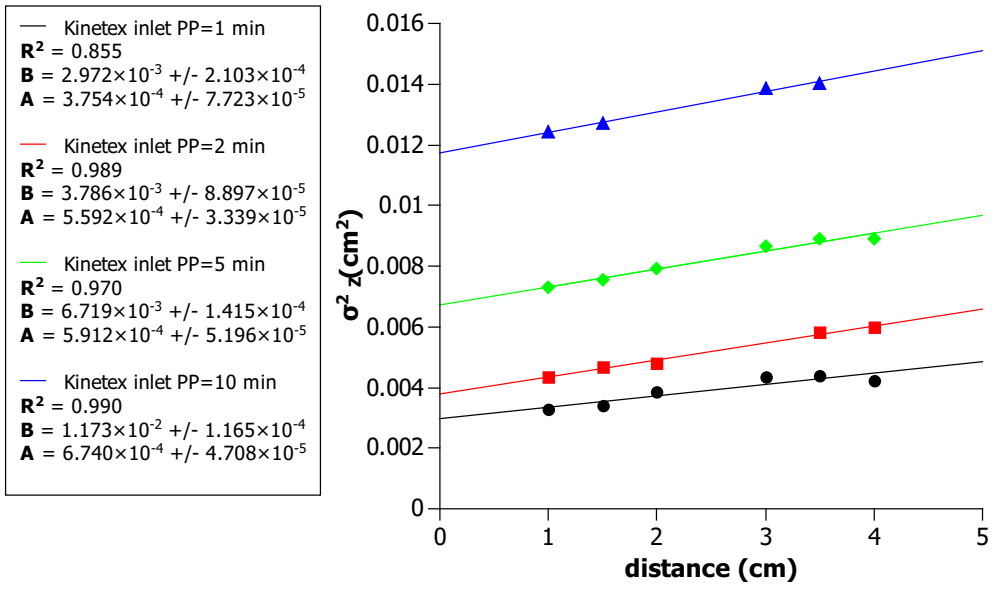

Figure 4.13: Band variance obtained for the Kinetex column with flow reversal. The flow was arrested for 1, 2, 5, and 10 minutes, respectively. The column inlet was probed.The fitted parameters are given $A = 2H$ in cm, and $B = 2\sigma^2_{z,\text{end}}$ in cm^2/s units.

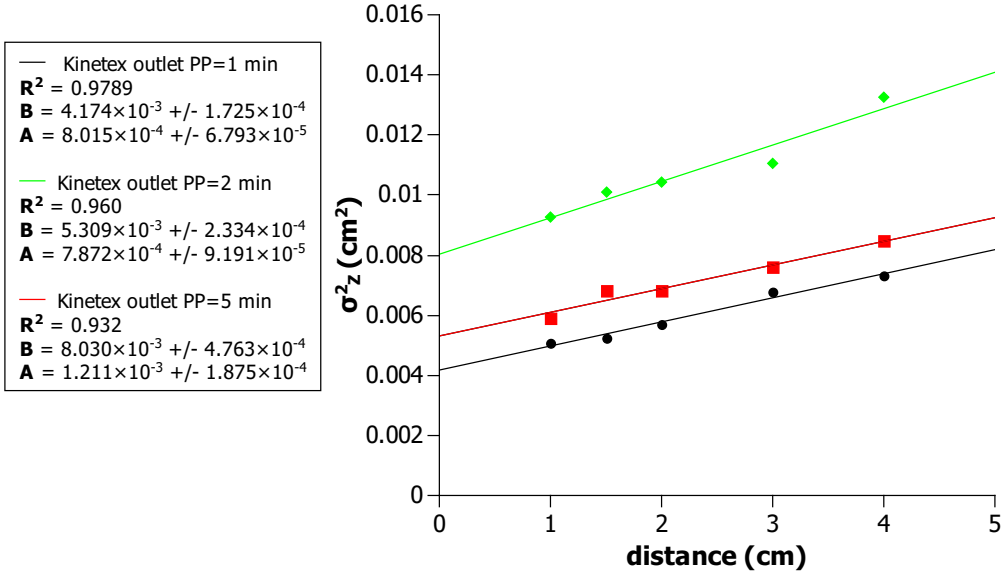

Figure 4.14: : Band variance obtained for the Kinetex column with flow reversal. The flow was arrested for 1, 2, and 5 minutes, respectively. The column outlet was probed. The fitted parameters are given $A = 2H$ in cm, and $B = 2\sigma^2_{z,end}$ in cm^2/s units.

Figure 4.15, shows the band variances extrapolated to $z = 0$ – i.e. the intercept values in Figures 4.12 to 4.14 – against the parking times. Since all the slopes in Figure 4.15 are nearly identical, – they are around 1.6×10^{-5} cm^2/s, for the packed and monolithic columns as well – similar band broadening contribution related to the peak parking were suggested for each column.

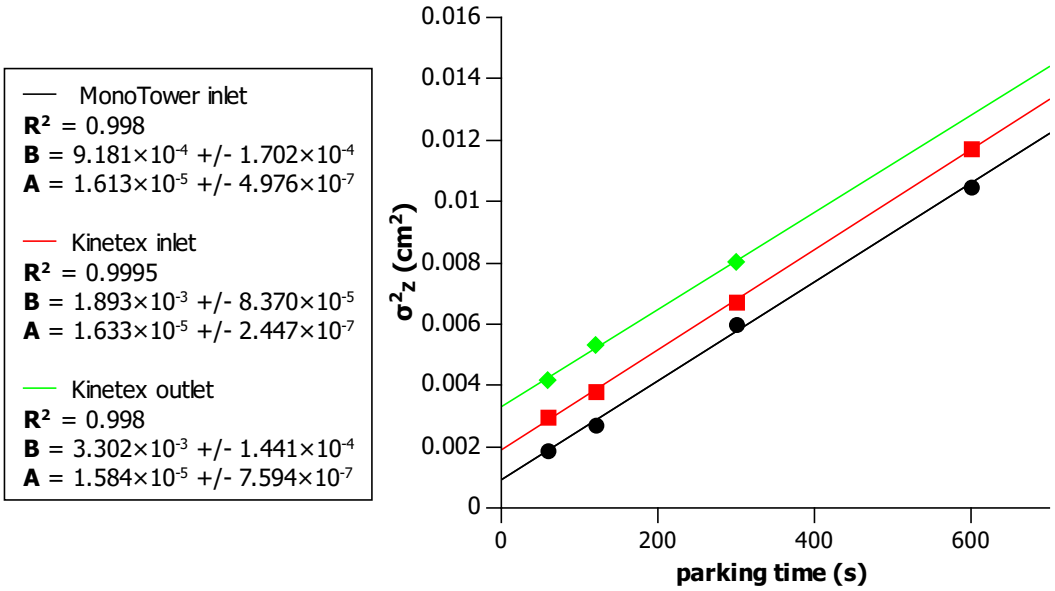

Figure 4.15: Band variance extrapolated to $z = 0$ for the MonoTower and Kinetex columns with flow reversal. Note that in this case A=$2D_{eff}$ [cm^2/s] while B is equal to the variance of the injected peak without PP.

The intercepts in Figure 4.15 give the variance due to the column ends (see Eq. 4.7). It was found the smallest for the inlet of the MonoTower column: $2\sigma^2_{z,\mathrm{end}} = 9.18 \times 10^{-4}$ cm^2. For the inlet of the Kinetex column one gets $2\sigma^2_{z,\mathrm{end}} = 1.89 \times 10^{-3}$ cm^2, which value is about twice as large as for the MonoTower column. For the outlet of the Kinetex column one gets a still larger terminal variance: $2\sigma^2_{z,\mathrm{end}} = 3.30 \times 10^{-3}$ cm^2.

In the following flow reversal experiments thiourea was injected on each column and the flow was stopped for 2 minutes when the sample band penetrated 1, 1.5, 2, 2.5, 3, 3.5 or 4 cm into the column, respectively. Then the column was disconnected, reinstalled in the opposite flow direction and the sample band was eluted. The results obtained for the various tested columns are presented in Figures 4.16 to 4.18. The contribution of peak parking to the total variance during the 2-minutes of arrested flow is equal to $\sigma^2_{z,\mathrm{park}} = 2D_{\mathrm{eff}}t_{\mathrm{park}} = 1.6\times10^{-5}$ cm^2/s$\times$120 s = 1.92×10^{-3} cm^2.

The intercepts of the fitted lines – when corrected for the contribution of peak parking – give the variance due to the column inlets or outlets. From the slopes of the fitted lines, the intrinsic, local plate height of the columns can be determined by means of Eq. 2.83. Those variance and plate height values are summarized in Table 4.3.

As it is shown in Figure 4.16 in case of the monolithic column the inlet or outlet variances are rather similar, thus the direction of the flow makes no difference. The peak variances run together, regardless of the flow direction.

Each of the packed columns shows an observable difference between the inlet or outlet variance. For the InertSustain, Kinetex, and Kinetex Evo columns (Figures 4.17, and 4.18,) the inlet variance is smaller than the outlet variance, it is between 0.75 and 1.5 μL^2 after correction with

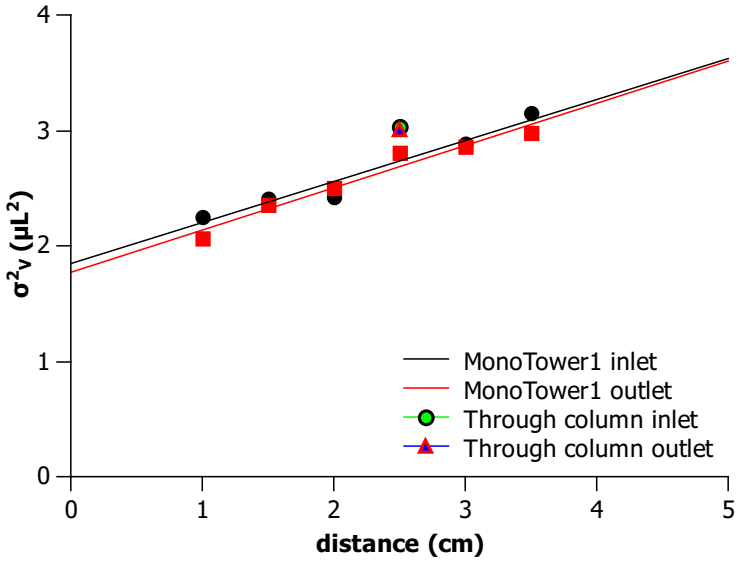

Figure 4.16: Band variance obtained for the MonoTower column with flow reversal, including 2-minute arrested flow. The symbols at 2.5 cm indicate the variance obtained without flow reversal but also including 2-minute arrested flow.

$\sigma^2_{V,\text{park}}$. For the InertSustain Swift column, the outlet variance is smaller, and shows slightly higher values (around 1.5 μL^2) than the ones we observed for the other columns.

The slopes of the fitted lines give the local plate height in the homogeneous column bed. One may expect that for a given column, those lines run parallel regardless of the flow direction. We always observed, however, more pronounced differences for the local plate height in case of the packed columns, depending on the flow direction. The difference is more conspicuous in case of the InertSustainSwift and Kinetex columns (Figures 4.17 and 4.18) although the columns show rather similar behavior in normal elution mode. Nevertheless, the column manufacturers handle the slurry packing procedure as a factory secret, different techniques are known, such as the use of constant flow rate, or constant pressure with different slurry densities to optimize the bed homogeneity in the columns. There is no agreement between the manufacturers even in that if the columns are packed from the inlet or the outlet direction. The distinct procedures may explain the observed differences found in the local efficiency of the examined columns.

Note that the local plate height values obtained with flow reversal are always smaller than the ones measured for the whole column without reversing the flow. The band variance obtained for thiourea with the flow arrested for 2 minutes without reversing the column are represented for each column with symbols plotted at 2.5 cm distance at Figures 4.16 to 4.18. These results agree with the chromatograms plotted in Figure 4.11 and with the discussion in Section 4.2.2.

The effect of the frits was studied on a MonoTower monolithic column – which does not require a frit – by installing the same commercial frits to the column ends that are present in the examined packed columns . The band variances obtained with flow reversal are plotted in Figure 4.19. Similarly to the previous ascertainments, the variances were found nearly independent from the flow direction, the two column ends show rather similar performance. When the

Table 4.3: The results of the flow reversal experiments. H is the intrinsic plate height calculated from the slopes of the straight lines plotted in Figures 4.16 to 4.18 by probing the column from either end. $\sigma^2_{V,\text{park}}$ is the band broadening induced by the 2-minute peak parking. $\sigma^2_{V,\text{end,in}}$ and $\sigma^2_{V,\text{end,out}}$ are the variances due to the column inlet and outlet, respectively. F_v was set to 0.2mL/min.

	H (forward) [μm]	H (backward) [μm]	$\sigma^2_{V,\text{park}}$ [μL^2]	$\sigma^2_{V,\text{end,in}}$ [μL^2]	$\sigma^2_{V,\text{end,out}}$ [μL^2]
InertSustain	5.56	4.21	0.76	0.82	1.18
InertSustainSwift	11.94	4.35	1.21	1.65	1.48
MonoTower 1	4.74	4.89	1.21	0.64	0.56
MonoTower 2	4.41	6.67	1.21	0.69	0.28
MonoTower 3	6.81	5.30	1.21	0.48	0.83
Kinetex	3.25	4.84	0.72	0.78	1.15
Kinetex EVO	2.47	3.22	0.72	0.97	1.29

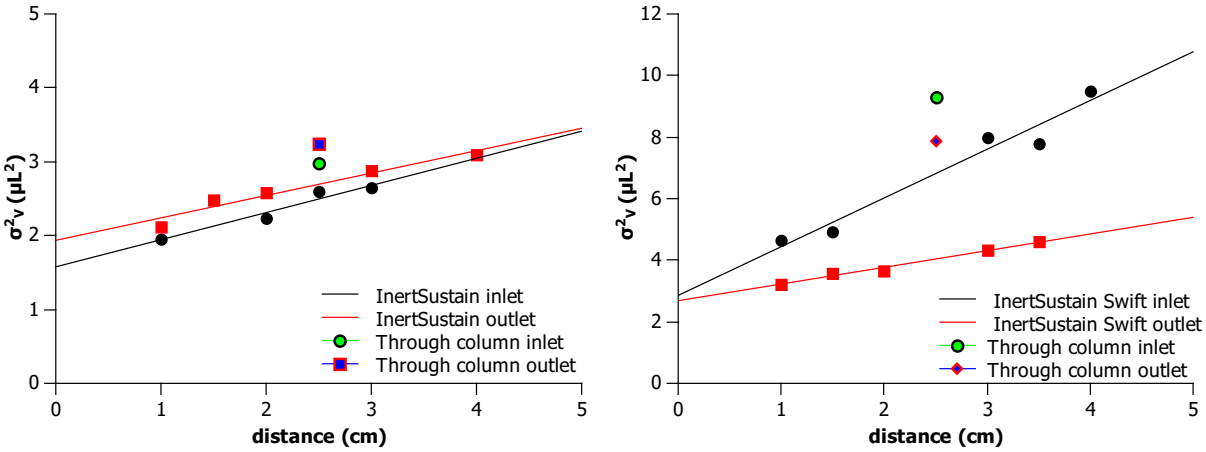

Figure 4.17: Band variance obtained for the InertSustain (left) and for the InertSustainSwift column (right) with flow reversal, including 2-minute arrested flow. The symbols at 2.5 cm indicate the variance obtained without flow reversal but also including 2-minute arrested flow.

frits are installed, however, the volumetric variance is increased roughly by 1.5 μL^2. It can be concluded, that the band broadening that introduce by the presence of frits at the column ends are comparable with the extra column dispersion in the instrument voids, and are close to the zone broadening in the packed bed.

As the conclusion of Section 4.2, the outstanding performance of the monolithic MonoTower column can be stated, especially for early eluting compounds due to the low band broadening in the column hardware. The efficiency loss due to band broadening in the frits and near to the column ends seems to be determinate in case of the slurry packed columns, while observable difference exist between the performance of the distinct column ends. It can be concluded that

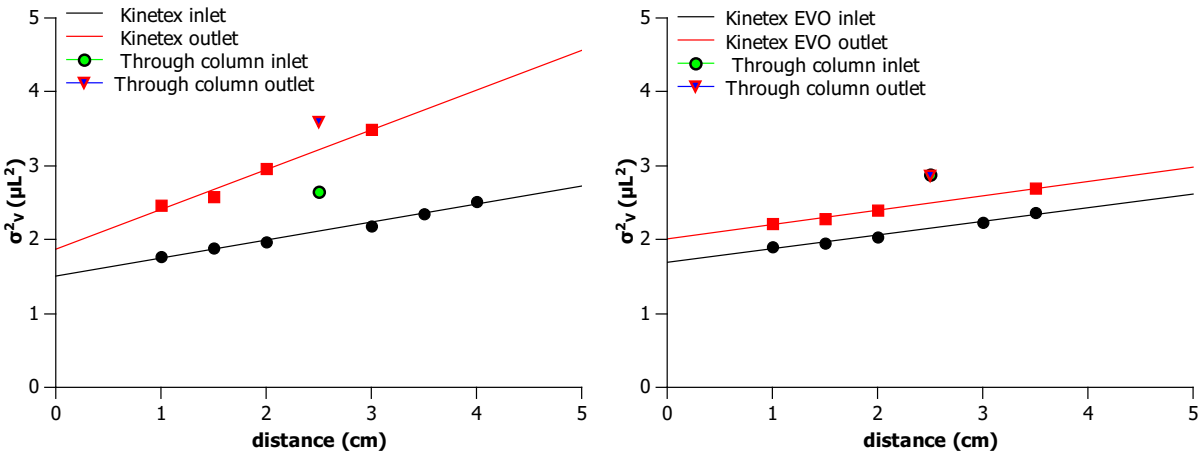

Figure 4.18: Band variance obtained for the Kinetex (left) and for the Kinetex Evo column (right) with flow reversal, including 2-minute arrested flow. The symbols at 2.5 cm indicate the variance obtained without flow reversal but also including 2-minute arrested flow.

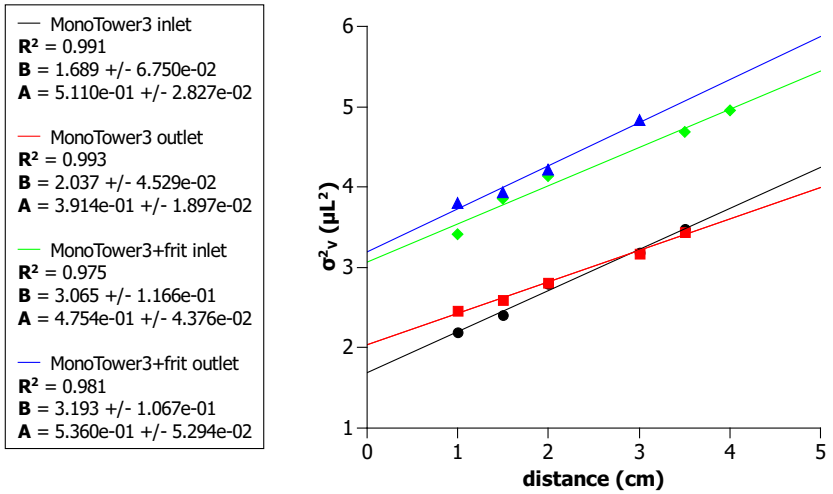

Figure 4.19: Band variance obtained with flow reversal including 2-minute arrested flow for the MonoTower 3 column with and without frits installed.

the third of the total peak variance obtained for an unretained peak, originates from the band broadening at column ends, while the rest comes from the extra column dispersion, and from the mass-transfer in the packed bed in an equal extent.

4.3 Analysis of the intraparticle diffusion of macromolecules in different stationary phases

The intraparticle mass transfer process in five different columns was investigated by injecting insulin at eleven different linear velocities set between 0.01 and 0.16 cm/s. The list of the examined columns are shown in Table 3.2. Note, that the packing of the columns differs in particle diameter and the particle structure as well. Three different core-shell like column was probed together with columns packed comparable fully porous particles. It is a well known phenomena that the retention factor of peptides changes with the alteration of the flow rate, due to the change of the average column pressure. Figure 4.20 shows the pressure dependence of the retention factor of insulin on the examined columns. For proteins and other macromolecules or ionic molecules with significant hydration layer, the retention factor strongly increases with the average pressure on the column, what cause the variation of the retention with the applied flow rate. This is due to the decrease of the partial molar volume of the analyte, caused by the loss of the hydration layer of the solute molecules upon adsorption on the hydrophobic stationary phase. For proteins, the conformational changes (unfolding or spreading) lead to the exposure of their hydrophobic core, by which the molar volume decrease is more pronounced [105, 106]. Figure 4.21 shows the plot of the reduced plate height values (h) of the columns versus the interstitial velocity (u_h).

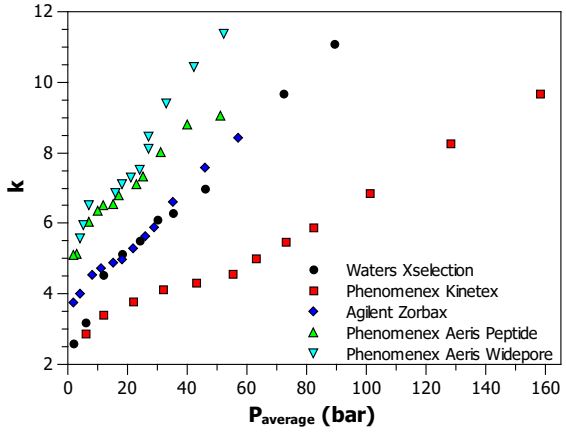

Figure 4.20: The plot of the retention factor of insulin against the average back pressure applied on the different columns.

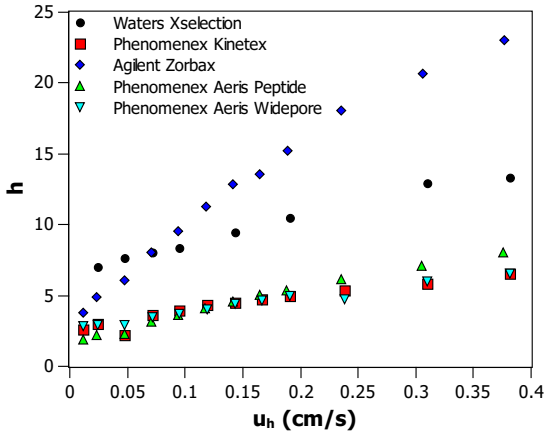

Figure 4.21: The reduced plate height values determined for the examined columns at different interstitial velocities .

Especially at higher flow rates, we observed significantly lower reduced plate heights for the Kinetex and Aeris columns than for the columns packed with fully porous particles. Since the retention factor is strongly affected by the mobile phase velocity, the fitting of plate height equation to the experimental data for the calculation of the mass-transfer coefficients, will be prone to error.

4.3.1 The pressure dependence of the retention of insulin

The decrease of the partial molar volume upon adsorption on a hydrophobic surface is substantial in case of proteins and peptides. The retention parameters can be related to the following thermodynamic quantities:

$$\Delta G = -RT \ln K = \Delta H - T\Delta S = \Delta E + p\Delta V_m - T\Delta S, \tag{4.8}$$

where ΔG, ΔH, ΔE, and ΔS are the change of the Gibbs free energy, enthalpy, internal energy, and entropy of the system, respectively, R is the universal gas constant, T is the absolute temperature, K is the equilibrium constant of adsorption, p is the pressure, and ΔV_m is the difference between the partial molar volume of the solute when it is adsorbed or it is in the mobile phase.

Equation 4.8 can be reformulated as:

$$\ln K = \ln k\phi = \frac{\Delta E}{RT} - p\frac{\Delta V_m}{RT} + \frac{\Delta S}{R}. \tag{4.9}$$

Assuming that the volumetric phase ratio (ϕ) remains constant regardless of the pressure change, and the temperature is constant, the first derivative of $\ln k$ with respect to pressure becomes:

$$\frac{\partial \ln k}{\partial p} = -\frac{\Delta V_m}{RT} \tag{4.10}$$

According to Eq. 4.10, the pressure dependence of the retention is more pronounced at high ΔV_m values [11].

4.3.2 The estimation of the mobile phase dispersion and the external mass transfer coefficients.

The axial dispersion (D_L) and the external mass transfer coefficients (k_{ext}) were calculated for each mobile phase velocities by using the simplified form of the Gunn correlation (Eq. 4.6) and the Wilson–Geankoplis equation (Eq. 2.53), respectively. As it is shown in Fig. 4.22 and 4.23, D_L and k_{ext} depends on the flow rate. According to Eqs. 4.6 and 2.53, the differences of the values of D_L and k_{ext} for the different columns at the same mobile phase velocities, are coming from the different column geometries, notedly from the different particle sizes and porosities of the columns. The observed values are similar to the columns with similar particle geometry and correspond to the values found in the literature [107, 108].

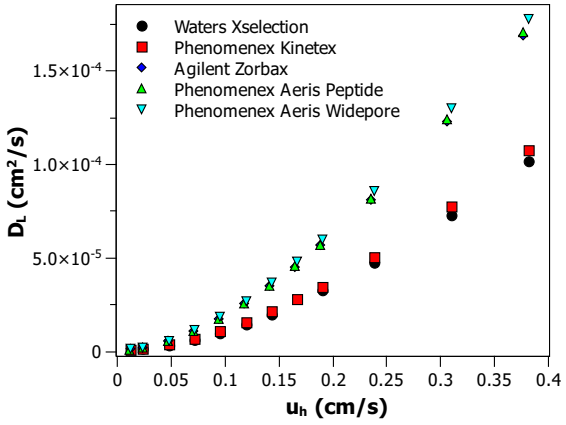

Figure 4.22: The calculated axial dispersion on the examined columns at different interstitial velocities.

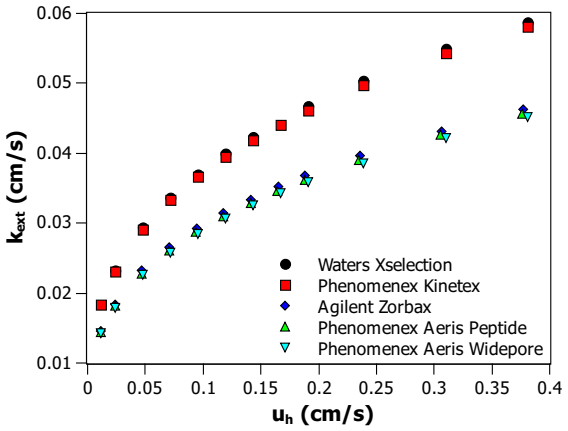

Figure 4.23: The calculated external mass transfer coefficients on the examined columns at different interstitial velocities.

4.3.3 The intraparticle diffusion

Once the molecules reach the entry of the stationary phase pores, the slow intraparticle diffusion will be the dominating process that drives the molecules to the adsorption sites of the surface from the pore entry and vice-versa. By knowing D_L and k_{ext}, the intraparticle diffusion coefficient (D_e) can be calculated according to Eq. 2.56, using the experimentally determined plate height values. D_e slightly varies with the mobile phase velocities as shown in Fig. 4.24. The flow-rate dependence of D_e can be attributed to the fact, that the retention factor of the analyte increases with the increase of the pressure at higher flow rates. The mass-transfer coefficients determined according to the GR model are summarized in Table 4.4.

Though the values of the calculated mass-transfer coefficients are in the same range for each column, we can observe that the intraparticle diffusion coefficients are slightly higher in case of the columns packed with superficially porous particles (see Table 4.4). However, it was found that the change of the pore diameter and core-to-particle diameter ratio has no significant effect on D_e. The Aeris Peptide and the Kinetex columns are packed with particles that have different particle diameters (3.6 μm and 2.7 μm respectively), but similar core-to-particle ratios ($R = 0.451$ and 0.438) and pore size diameters (100 $\AA$), whereas the Aeris Widepore column was packed with significantly larger core relative to the particle diameter ($R = 0.184$) and has three times larger average pore diameter. Even so, the observable intraparticle diffusion coefficients are slightly lower for the Aeris Widepore column than for the Kinetex or Aeris Peptide columns

As it was already mentioned at Section 2.1.2 intraparticle diffusion originates from the sum of two parallel contributions. One is the diffusion of the molecules in the pores filled with the mobile phase, and the another is the surface diffusion that occurs when analyte is adsorbed to the surface of the pores. The effect of these two process will be detailed in the following sections.

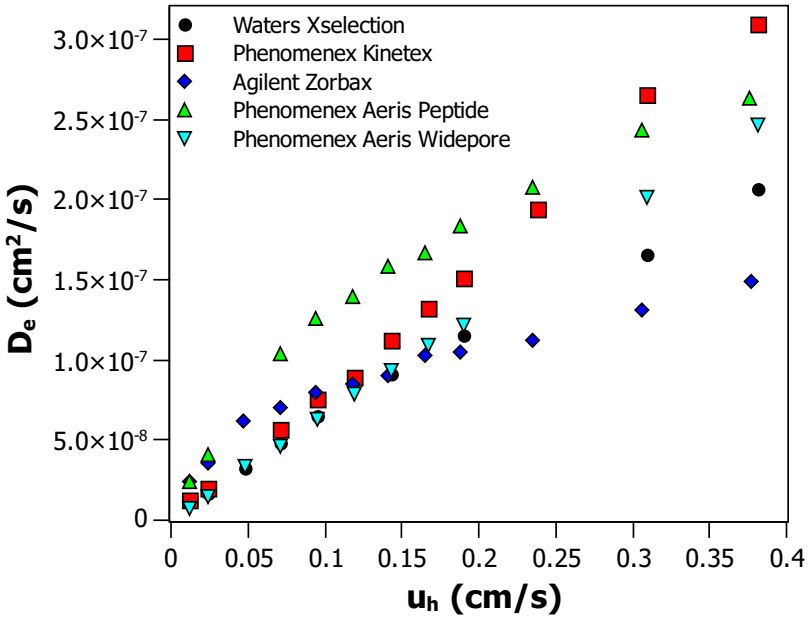

Figure 4.24: Plot of the estimated intraparticle diffusion coefficients (D_e) obtained on the different columns at different interstitial velocities.

Table 4.4: The mass-transfer coefficients of insulin on the different HPLC columns calculated by the general rate model of chromatography. D_L represent the axial dispersion coefficient, k_{ext} is the external mass transfer coefficient and D_e represents the intraparticle diffusion coefficient.

	D_L (cm^2/s)	k_{ext} (cm/s)	D_e (cm^2/s)
Xselection	1.64×10^{-6} – 1.06×10^{-4}	0.0256 – 0.0644	1.66×10^{-8} – 1.88×10^{-7}
Kinetex	1.21×10^{-6} – 1.05×10^{-4}	0.0187 – 0.0593	1.27×10^{-8} – 2.99×10^{-7}
Zorbax	1.31×10^{-6} – 1.69×10^{-4}	0.0146 – 0.0463	2.43×10^{-8} – 1.49×10^{-7}
Aeris Peptide	1.25×10^{-6} – 1.93×10^{-4}	0.0151 – 0.0479	3.04×10^{-8} – 3.50×10^{-7}
Aeris Widepore	1.32×10^{-6} – 1.78×10^{-4}	0.0145 – 0.0461	7.04×10^{-8} – 2.47×10^{-7}

Table 4.5: The calculated values of the intraparticle obstruction (γ_p) and hindrance parameter ($F(\lambda_m)$), and the observed pore (D_p) and surface diffusion (D_s) coefficients on the examined columns

	γ_p	$F(\lambda_m)$	D_p (cm^2/s)	D_s (cm^2/s)
Xselection	4.71×10^{-5}	0.0343	9.18×10^{-13}	4.16×10^{-9} – 1.59×10^{-8}
Kinetex	1.34×10^{-3}	0.0504	2.50×10^{-10}	4.47×10^{-9} – 3.10×10^{-8}
Zorbax	1.52×10^{-3}	0.0081	4.72×10^{-12}	6.57×10^{-9} – 1.72×10^{-8}
Aeris Peptide	3.20×10^{-3}	0.0388	4.48×10^{-11}	6.22×10^{-9} – 3.98×10^{-8}
Aeris Widepore	5.02×10^{-3}	0.3553	6.28×10^{-10}	1.10×10^{-9} – 2.18×10^{-8}

Pore Diffusion

The diffusion a of the molecules in the stationary phase is roughly restrained by the internal tortuosity of the pores. According to the studies of Klein and Grüneberg, the internal obstruction factor (γ_p) can be calculated by using Eq. 2.43 by knowing the internal pore volume and the particle diameter of the columns, the solute distribution coefficient, and the band variance originating from the intraparticle mass transfer (σ^2_{perm}). For the calculation of γ_p, experimental results of ISEC measurements provided by Bacskay et al. were used [96], by applying the same columns that were examined in this study. σ^2_{perm} were determined by the subtraction of the contributions of the axial dispersion and the external mass transfer resistance from the total broadening.

The values of D_p according to Eq. 2.41 are at least three orders of magnitude lower than the total intraparticle diffusion coefficients, which means that D_s is dominating in the movement of the molecules in the stationary phase. Note, that the average pore diameter of the Aeris Widepore column is around three times larger than the another columns, causing that D_p is significantly higher attributed to the lower hindrance of the large pores of the insulin molecules (see also in Table 4.5). The presence of an internal core seems to cause larger intraparticle obstruction factor, caused by the reduction of the rambling of the molecules in the stationary phase. The extraordinary low value of γ_p for the Waters Xselection column may be caused by the narrow or shrinking channels in the porous media.

Surface diffusion

As already discussed, pore and surface diffusion fluxes are additive, therefore, by using Eqs. 2.40 and 2.41 the following equation can be written [10]:

$$D_e = \epsilon_p \gamma_p F(\lambda_m) D_m + (1 - \epsilon_p) K D_s, \tag{4.11}$$

where ϵ_p is the internal porosity of the column, and represents the volume fraction of the porous media.

The easiest way for the determination of D_s is the subtraction of D_p from the D_e according to the previous equation. The calculated values of D_s slightly varies with the flow rate, consequently with the applied pressure on the column (see Fig. 4.25). According to the plots, D_s has a maximum value on each column at elevated average column pressures.

As it was explained in Section 2.1.2 surface diffusion is approached as the activated mass-transfer process of the adsorbed molecules (See in Eqs.2.44 and 2.45). The activation energy that is required for the migration of the molecules along the surface, is dependent from the isosteric heat of adsorption (Q_{st}). Besides the concentration of the sample adsorbed to the stationary phase, $-Q_{st}$ is proportional to the applied pressure as well. The pressure dependence is due to the mentioned change of the molar volume of the insulin molecules upon adsorption. According to Eqs. 4.8, 4.9 and 4.10, the enthalpy change of the proteins upon adsorption is more pronounced at elevated pressures. Another contradictory effect is that the increase of the amount adsorbed, which is pronounced toward high k values, decreases $-Q_{st}$ and causes the increase of the surface diffusion. These two phenomena may explain the change of D_s with the flow rate.

In conclusion, the crucial role of the surface diffusion regarding to the overall intraparticle mass-transfer can be stated in case of proteins. The retention factor of insulin along with the surface and so the intraparticle diffusion coefficients varies with the pressure drop on the column, and so with the applied mobile phase flow. The superficially porous packings provided better efficiency than the fully porous particles, due to the higher pore diffusion coefficients and so the faster intraparticle mass-transfer.

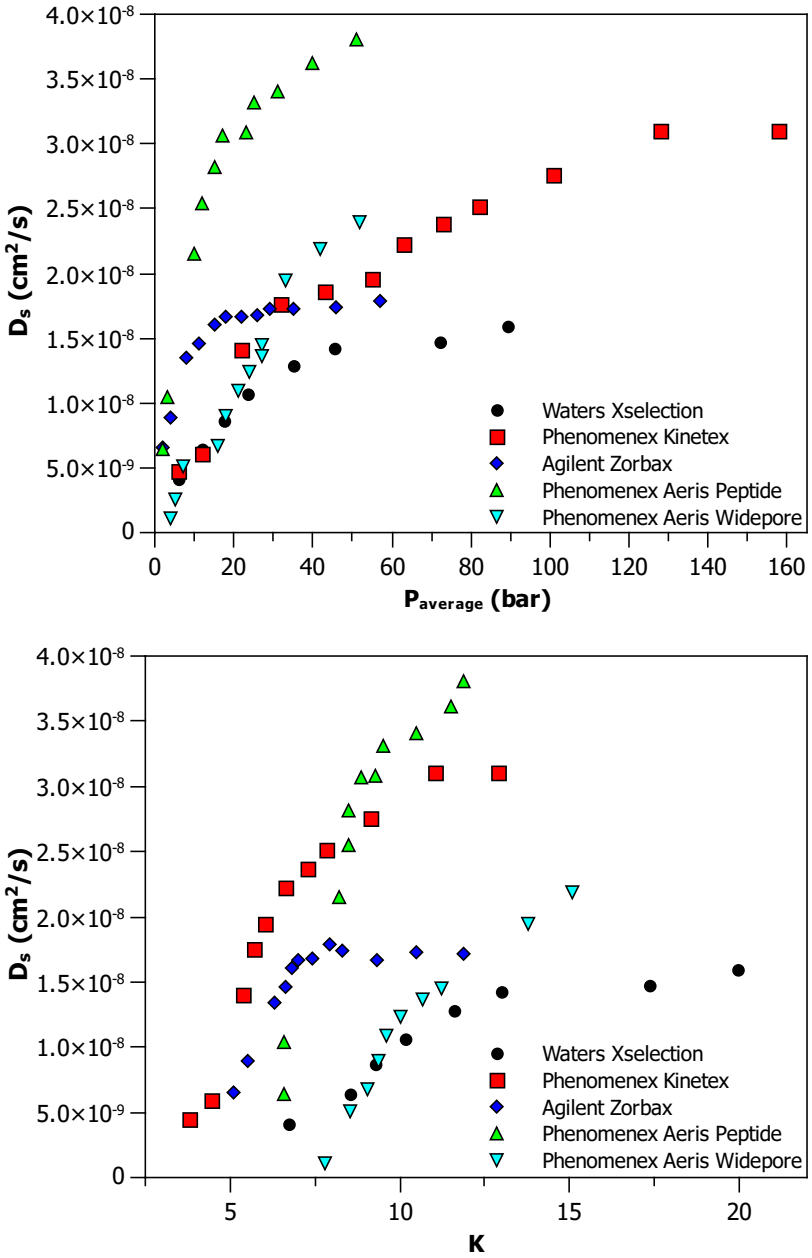

Figure 4.25: The change of the surface diffusion coefficient with the average pressure drop on the columns (top) and with the equilibrium constant of adsorption (bottom).

4.4 Comparison of the efficiency of SFC and UHPLC techniques

In this section the comparison of the mass-transfer properties of two chromatographic techniques, supercritical fluid chromatography and liquid chromatography will be detailed according to the stochastic model of chromatography. For this, the injection of the series of alkyl-benzenes was performed on the same HPLC column in the two chromatographic modes at different experimental conditions (detailed in Section 3.8). As it was already explained in Section 2.1.4, to apply the stochastic model of chromatography the mobile phase dispersion and the extra column effects on the band spreading have to be eliminated by the subtraction of the corresponding moments of an unretained compound from the moments of the sample peaks. However, the correct determination of the μ_2' of an unretained compound can be difficult, especially in case of SFC where the less retained compounds typically provides asymmetric or tailing peak shapes.

Therefore an alternate calculation was suggested and used. The moments of the measured peaks were corrected with the moments of the unretained compounds peak. According to Eqs. 2.65, 2.66 and 2.67, the following correlations can be given:

$$\Delta\mu_1 = t_R - t_0 = \mu_1 - \mu_{1,0} \tag{4.12}$$

$$\Delta\mu_2' = \sigma^2 - \sigma_0^2 = \mu_2' - \mu_{2,0}' \tag{4.13}$$

$$\Delta\mu_1 = n\tau_s \tag{4.14}$$

$$\Delta\mu_2' = 2n\tau_s^2 \tag{4.15}$$

where $\Delta\mu_1$ is the corrected first moment of a peak and it is equal to the adjusted retention time; $\Delta\mu_2'$ is the corrected second central moment of the peak and represents the variance of the peak due to the stationary phase process.

Assuming that the members of a homologous series elute with identical plate heights, the above written equations can be rearranged to give a linear relationship between the square of $\Delta\mu_1$ and $\Delta\mu_2'$ for the members of a homologous series of alkylbenzenes (see Fig. 4.26):

$$\mu_2' = \mu_{2,0}' + 2n\tau_s^2 = \frac{2}{n}\Delta\mu_1^2 + \mu_{2,0}' \tag{4.16}$$

The slope of the linear equation gives information about the number of the mass-transfer events, while the intercept is equal to the band spreading of an unretained compound in the mobile phase.

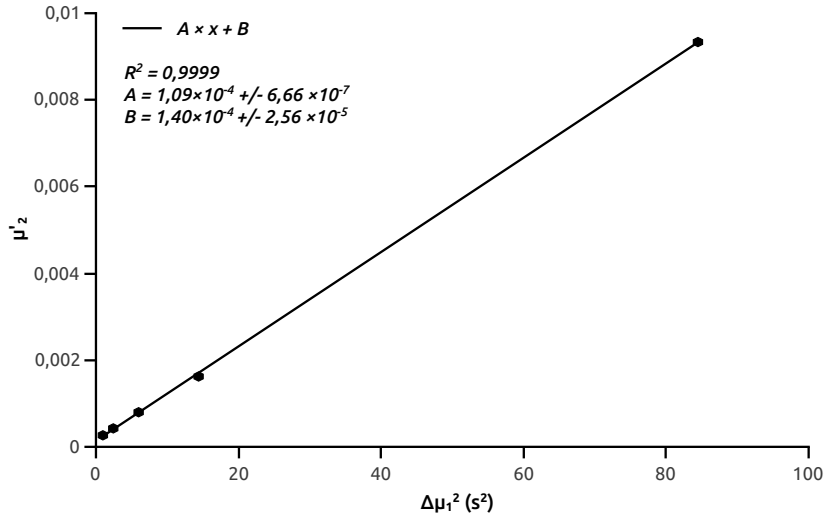

Figure 4.26: The plot of μ_2' against the square of $\Delta\mu_1$ for the series of alkylbenzenes measured in the UHPLC experiments.

The intersticial velocities were calculated using the porosity values determined for the column in use by Bacskay et al. [96], and from the void time determined using a non-retained compound. The first and the second moments of the sample peaks were used for the calculation of the plate height values.

4.4.1 Liquid chromatography measurements

The homologous series of alkylbenzenes (octylbenzene, decylbenzene, dodecylbenzene, tetradecylbenzene, octadecylbenzene) and thiourea were injected at flow-rates between 0.2 and 2.5 mL/min, using two different chromatographic conditions as described in section 3.8 on a fully porous Agilent column. Figure 4.27 shows the observed reduced plate height values during the measurements using 97.5% v/v methanol and water as eluent. We found that the optimum interstitial velocity is around 0.15 cm/s regardless of the retention factor, and above that velocity a significant efficiency loss can be observed due to the slow mass-transfer in the stationary phase.

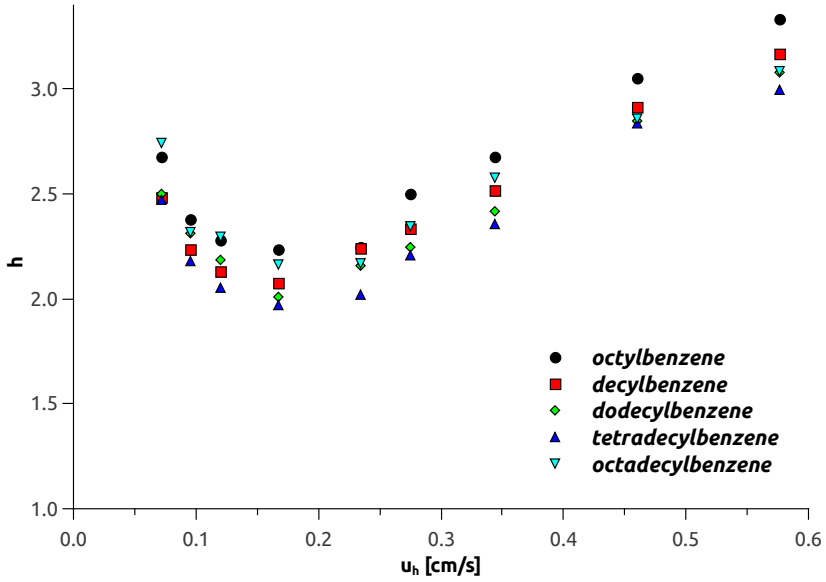

Figure 4.27: The observed plate height values of the alkylbenzene standards during the UHPLC experiment using a methanol:water 97.5:2.5% (v/v) mobile phase

Stochastic analysis

As it was mentioned previously, the stochastic model considers the stationary phase processes only and so the effect of the mobile phase dispersion was eliminated. Table 4.6 summarizes the results of the stochastic analysis of the LC experiments. The number of mass transfer events is between 14 000 and 24 000 in the examined range of flow-rate. The number of the events, however, slightly varies with the change of the mobile phase velocity. As shown in Figure 4.28 the parameters change at low flow-rates but they stabilize at high flow-rates.

Table 4.6: The measured plate heights and the calculated residence times of the octadecylbenzene molecules at the various UHPLC conditions

	h	n	τ_m [ms]	τ_s [ms]
100 % methanol	4.1–2.5	13 908–23 727	20.8–1.6	151.9–10.7
methanol and 2.5 % water	3.1–2.4	15 125–23 580	13.4–1.6	194.5–21.1

The average sojourn times of the molecules in the stationary phase increase with the retention, i.e. with the size of the side chain of the alkylbenzene molecules, as the interaction with the stationary phase becomes stronger. The observed residence times are decreasing with the increase of the interstitial velocity of the mobile phase and tends to a minimum value (see at Fig. 4.29).

There is an almost two-fold difference in the retention factors at the two employed mobile phase compositions (shown in Table 3.4) that causes the doubling of the residence time values too (see Fig. 4.30). For the most retained compound, the value of the sojourn time in the stationary phase is about 27 ms close to the optimum mobile phase velocity when pure methanol was used,

while its value was found around 55 ms when the eluent composition allows higher retention.

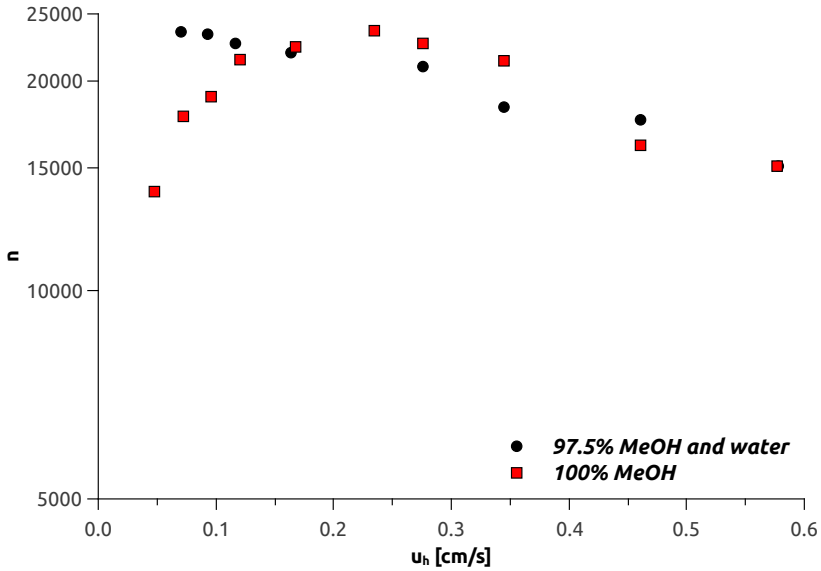

Figure 4.28: The number of the mass-transfer events calculated from the UHPLC experiments with the stochastic model of chromatography.

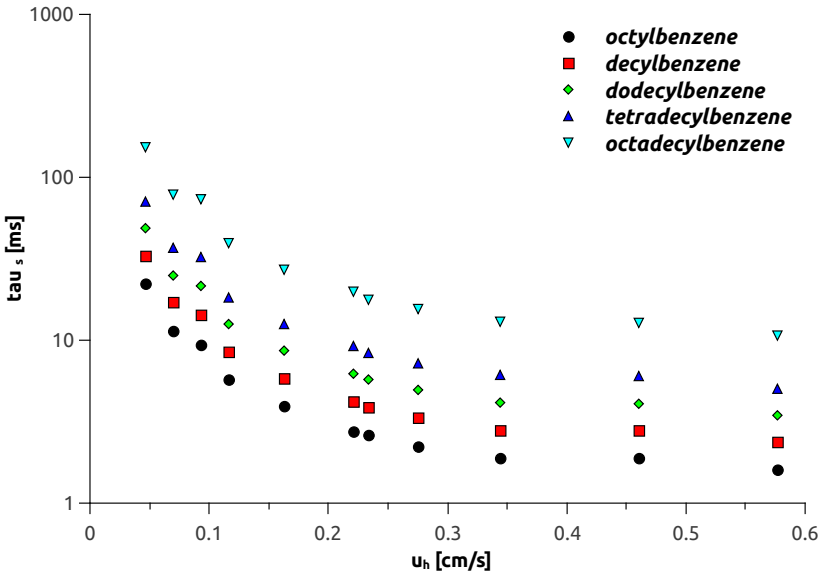

Figure 4.29: The average sojourn time of the alkylbenzene molecules in the stationary phase calculated from the UHPLC experiments using pure methanol as eluent.

The residence times of the molecules in the mobile phase are independent from the retention strength, but again they depend on the mobile phase velocity (see Fig. 4.30). Accordingly, the mobile phase residence times are around 4 ms at the optimum velocity, and they vary between 1.6 to 14 ms and 1.6 to 21 ms in the examined flow-rate range (as shown in Table 4.6) at the various conditions. Note that the results of the stochastic analysis are in good agreement with earlier findings [8, 85].

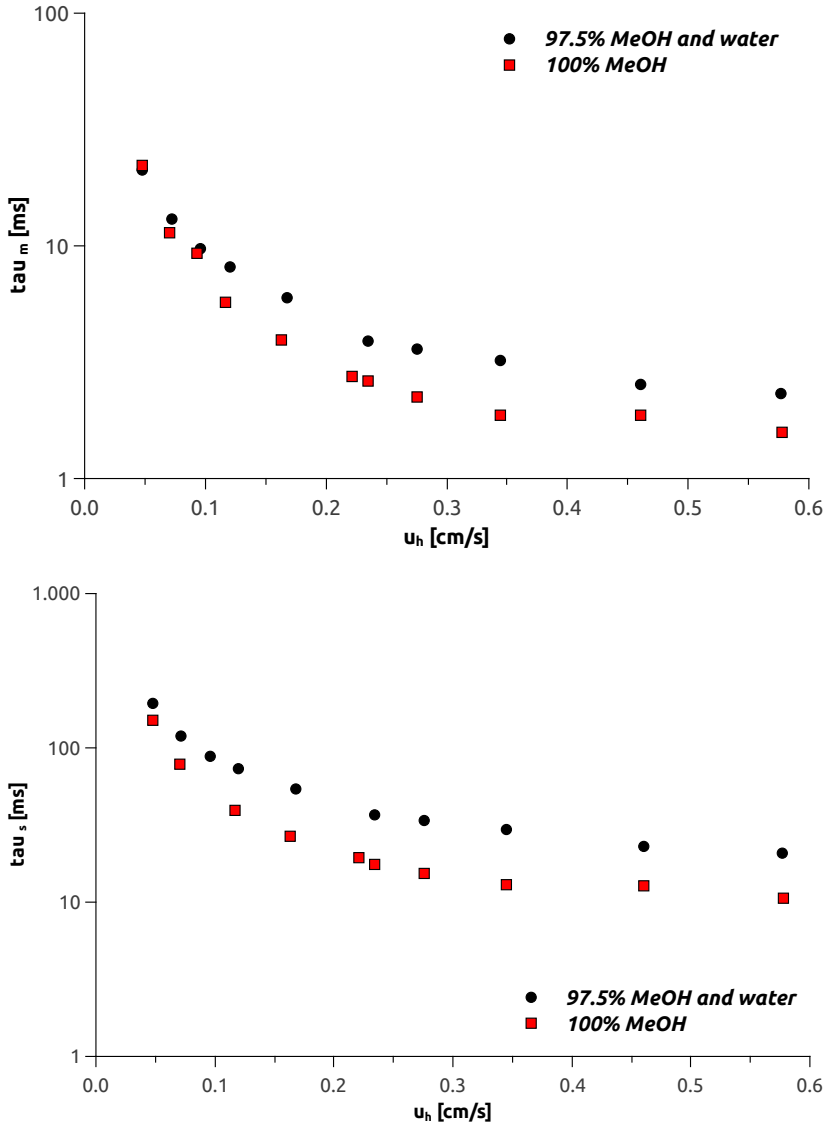

Figure 4.30: The average sojourn time of the octadecylbenzene molecules in the mobile (upper) and the stationary (lower) phases calculated from the UHPLC experiments at different conditions.

4.4.2 Supercritical fluid chromatography measurements

In case of supercritical fluid chromatography, most frequently carbon-dioxide is used as mobile phase, due to its low supercritical point. Fluids in supercritical state has very low viscosity, which results in orders of magnitudes higher molecular diffusion coefficients in supercritical carbon-dioxide compared to conventional liquid mobile phases [109]. The high molecular diffusivity of the sample cause significant dissimilarities in the mass-transfer properties compared to the liquid chromatographic measurements.

Supercritical carbon-dioxide is a highly non-polar solvent, its polarity is close to that of n-heptane. Usually, SFC is used for normal phase separations where the most common polar modifier is methanol.

Figure 4.31 shows the reduced plate height values of the alkylbenzenes observed under the low pressure conditions. Since the molecular diffusivity of the analytes is much larger in SFC than in UHPLC, the optimum mobile phase velocity shifts to higher linear velocities compared to the liquid chromatographic experiments. The benefit of the fast intraparticle mass-transfer is striking trough the phenomenon that no significant efficiency decrease can be observed with the elevation of the mobile phase velocity.

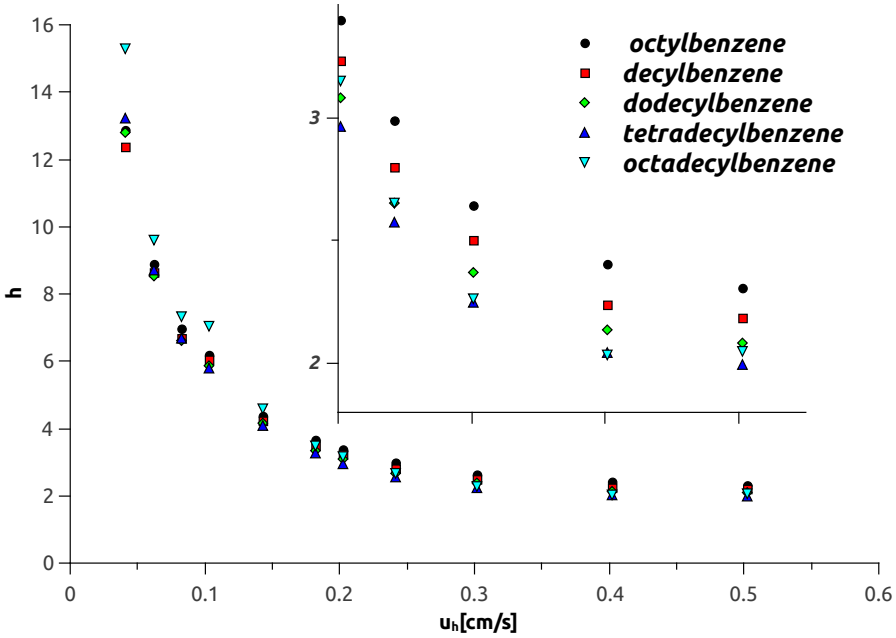

Figure 4.31: The reduced plate height values of the alkylbenzenes observed under low pressure conditions(i.e. eluent was pure CO_2 and the ABPR was set to 105 bar).

For the demonstration of the role of the axial dispersion and the stationary phase mass-transfer the fitting of van Deemter curve to the experimental data (see in Fig. 4.32) was carried out. The contribution of the B term to the plate height was found an order of magnitude larger, while the C term contributions were almost an order of magnitude smaller in the SFC measurement compared to the LC experiments.

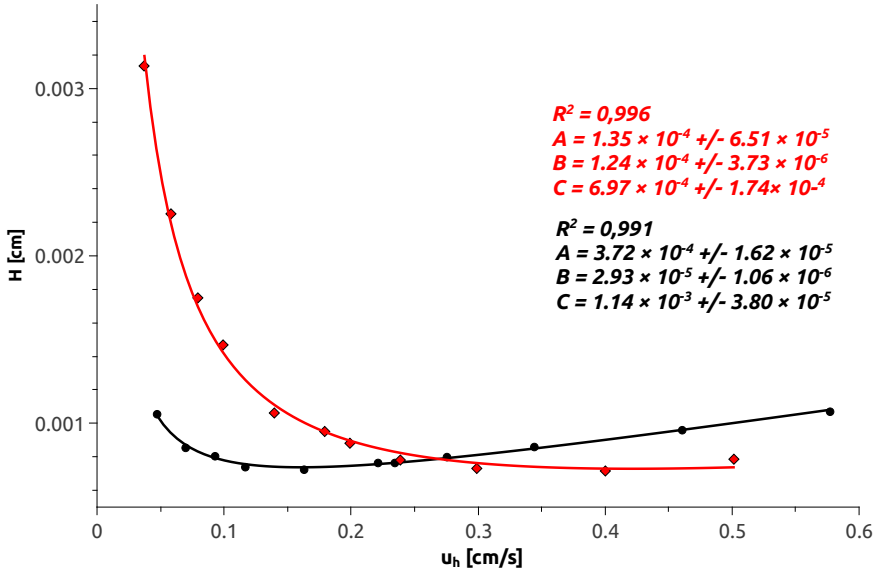

Figure 4.32: The van Deemter plots of the octadecylbenzene standard. Red dots refer to the experimental data observed in SFC measurements under high pressure conditions (i.e. eluent was pure CO_2 and the ABPR was set to 150 bar) conditions, while black dots result from the UHPLC measurements carried out with pure methanol as eluent. Lines are the fitting of the van Deemter equation to the experimental data.

The density of the supercritical fluid varies strongly with the change of the pressure or temperature even more close to its supercritical point [44, 110]. By changing the flow-rate, i.e. the pressure drop on the column, the density of the mobile phase, and also the apparent phase ratio of the given column will change as well. The increase of the density of the eluent leads to the increase of the elution strength, what will lead to flow-rate dependent retention factors especially when the mobile phase conditions are close to the supercritical point. However, using higher back pressures, or with the use of a small amount of methanol as mobile phase modifier, this effect can be moderated [111, 112]. The use of methanol push the conditions close to subcritical that will lead again to higher mobile phase density. Note that the density varies continuously with the local pressure along the column, thus the observed retention factors are apparent values originating from the sum of the local retention contributions along the column.

Another source of the uncertainty comes from the compressibility of the supercritical fluid that cause that the volumetric flow rate varies along the column with the density. Note that the emerging average flow rate is usually less than it is provided by the movements of the pump pistons. Since the pressure drop along the column was relatively small at the examined mobile phase velocities, the set volumetric flow rate compliance well to the real average volumetric flow rate of the mobile phase [44, 113–115].

The column used for this work was a conventional silica based reversed phase (C_{18}) column, modified with octadecyl chains and end-capped with methyl groups. Although neat carbon-dioxide was used as eluent, the retention order of the alkylbenzene standards in SFC is the same as in reversed phase liquid chromatography. As it is shown in Fig. 4.33, the retention factor decreases with the increase of mobile phase density i.e. with the increase of back pressure

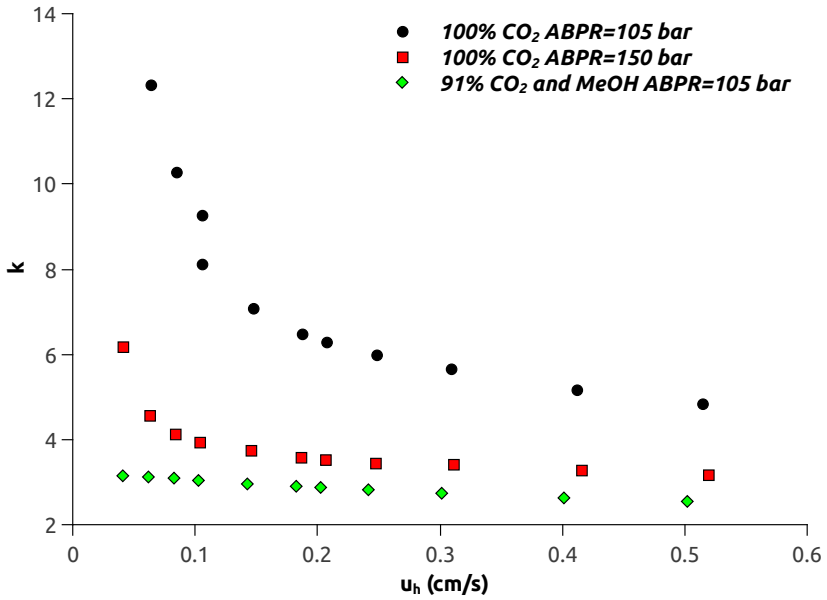

Figure 4.33: The change of the retention factor with the average linear velocity at different SFC conditions

on the column, but it also decreases with the addition of methanol to the eluent.

Besides, adding organic solvent to carbon dioxide will increase the density of the mobile phase above that of pure carbon dioxide, there is a strong interaction between the modifier and the adsorbent surface. Depending on the chemical structure of the column packing, significant adsorption of methanol occurs, that can affect the accessibility of the adsorption sites of the analyte molecules on the surface [39, 41, 116] . Steric hindrance may occur when the modifier adsorbs significantly on the apolar surface, which can inhibit the adsorption of the analyte molecules more or less depending on the thickness of the adsorbed modifier layer.

Stochastic Analysis

As it was mentioned in the previous section, a slight retention gradient will be formed, depending on the pressure drop along the column. Although, the stochastic model of chromatography is only valid under strictly isocratic conditions, the obtained results can be considered sufficient due to the low pressure drop applied during the experiments. Table 4.7 summarizes the results of the stochastic analysis for the SFC experiments. The number of the mass transfer events is between 3200 and 22 000 in the examined flow-rate range. Particularly in the cases when the mobile phase density is strongly affected by the pressure drop on the column, the dependence of the number of the mass-transfer events on the mobile phase velocity is obvious. However, even under subcritical conditions when the retention factor is almost independent of from flow-rate, the number of the events varies strongly with the mobile phase velocity (Fig. 4.34).

Similarly to the LC experiments, the average sojourn times of the molecules in the stationary

Table 4.7: The measured plate heights and the calculated residence times of octadecylbenzene at the different SFC conditions

	h	n	τ_m [ms]	τ_s [ms]
low pressure	l7.6–2.7	3241–21 303	65.3–1.2	804.9–6.0
high pressure	13.5–2.9	4207–20 062	79.6–1.4	488.7–4.3
subcritical	13.1–3.5	4308–16 095	76.8–1.7	241.3–4.3

phase increase with the retention, and tends toward a minimum value with the interstitial velocity of the mobile phase (Fig. 4.35). Under low-pressure conditions i.e. when the ABPR regulator was set to 105 bar, the retention factor varies strongly with the flow-rate, consequently we can observe the highest differences in the stationary phase sojourn times in that case, too. The observed residence times are closer to each other under the high pressure and the subcritical conditions at the corresponding mobile phase velocities. However, the differences between the three conditions are more pronounced at low flow-rates, and they diminish as the densities of the mobile phases become more similar with the elevation of the pressure drop on the column.

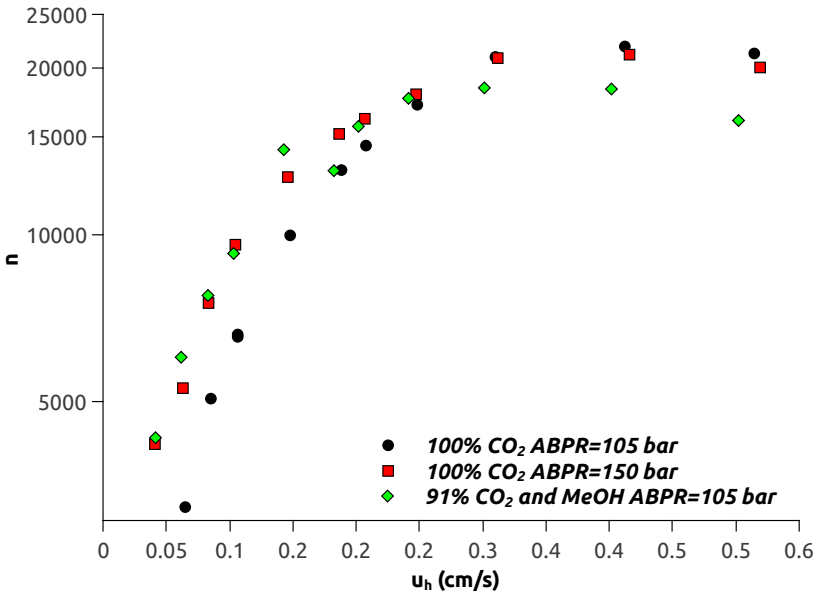

Figure 4.34: The number of mass-transfer events calculated from the SFC experiments with the stochastic model of chromatography.

At the highest mobile phase velocities – which can be identified as the optimum velocity for the SFC measurements – the stationary phase sojourn times are only about one-half, while the number of the events is in similar range compared to the liquid chromatographic measurements. Although the average residence times in the mobile phase are similar at each conditions and they vary more than in the case of liquid chromatography, at high mobile phase velocities their values are similar to those in LC.

It appears from the results of the stochastic analysis that mass-transfer in supercritical fluid chromatography is highly affected by the mobile phase velocity. However, the extraordinarily high molecular diffusion in the supercritical fluid can introduce errors at low velocities, where the mobile phase dispersion is the most dominating effect in the mass-transfer of the molecules.

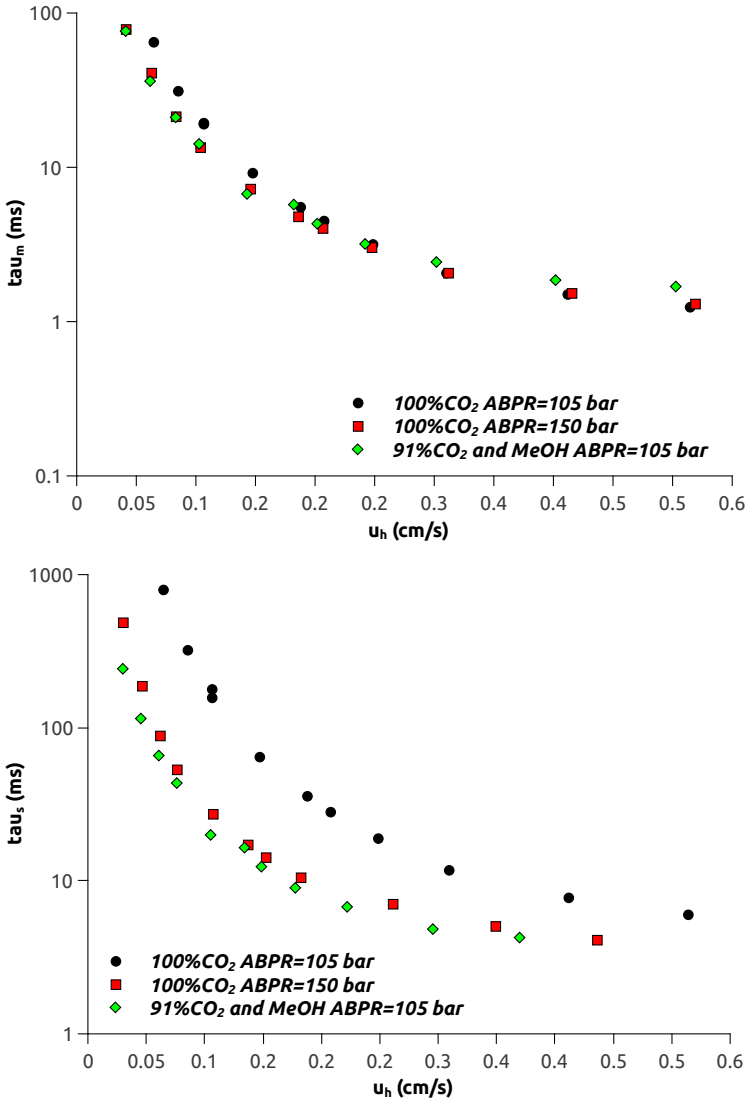

Figure 4.35: The average sojourn time of the molecules in the mobile (upper) and the stationary (lower) phases calculated from the SFC experiments with the stochastic model of chromatography.

It can be concluded, that although the mass-transfer properties in SFC shows broader variation with the change of the mobile phase flow compared to the LC experiments, the observed mobile phase residence times, and the – most characteristic – number of adsorption events are in the same range. The LC experiments was more effected by the mobile phase conditions regarding to the mobile phase sojourn times, while the applied back-pressure and mobile phase settings influence more the stationary phase sojourn times in case of SFC.

Chapter 5

Conclusion

5.1 Summary

5.1.1 Effect of the frictional heat on efficiency in columns packed with sub-2μm particles

This work has demonstrated from experimental viewpoint that the mobile phase dispersion in columns packed with sub-2μm packings are significantly affected by the heat loss through their walls. This heat flux originates from frictional heating of the mobile phase against the stationary packed bed and a cause crucial efficiency loss, – h decrease with value between 0.4 and 1.2 – at elevated flow rates.

The efficiency loss do to the temperature heterogeneities in the column is in the same range as the loss that originates from the external mass-transfer resistance and axial dispersion contributions altogether.

Thermal heterogeneities are present in the same extent in the core-shell type and in the fully porous packing materials. There was no significant difference observed in the behaviour of the core-shell like or fully porous packings regarding to the frictional heating effects.

5.1.2 Comparison of the efficiency of novel vHPLC stationary phases

The kinetic performance of a series of 2.1 × 50 mm packed and monolithic columns was tested and compared. The observed columns show rather similar plate height values close to $H = 5$ μm at the optimal mobile phase velocities.

Outstanding performance was ascertained for the monolithic MonoTower column, that provides sufficient efficiency next to significantly less pressure drop. Striking performance was found for early eluting compounds, what can be attributed to the moderate mobile phase dispersion caused by the simple column hardware by the absence of frits. The attachment of commercial

frits to the ends of the monolithic column cause similar measurable properties to the packed columns for the entire range of retention factor, what proves the above mentioned phenomenon.

The Kinetex and Kinetex EVO columns packed with 2.6-μm core-shell particles show similar efficiency as the columns packed with smaller particles. The Kinetex EVO colum perform slightly better than its predecessor.

The sample band broadening in the immediate vicinity of the column ends was characterized by the column reversal method. It was demonstrated that the local efficiency at the two respective column ends differ from each other in every case, however the difference is negligible for the monolithic column. It seem to be the dependent of the manufacturer, whether the inlet or the outlet of the columns perform better, no clear statement can be given. The contribution of the column ends to the overall band variance was found between 0.78 μL and 1.65 μL for the different packed columns, and around 0.6 μL^2 in average on the monolith column.

Unique peak compression effect of the flow reversal was found, - i.e the peaks observed with reversed flow are always narrower and more symmetrical than the peaks obtained without reversing the flow, that can be attributed to the self compensation effect of the interchannel multipath dispersion. Accordingly, the local plate height was found smaller in every case than the one we get for the unretained thiourea after a simple injection without arrested and reversed flow.

5.1.3 Analysis of the intraparticle diffusion of macromolecules in different stationary phases

According to the results of the experiments made with insulin on different HPLC columns, there is no significant difference in respect of the intraparticle diffusion coefficients, although the fully porous particles shows slightly slower intraparticle mass-transfer.

Mobile phase velocity dependent intraparticle diffusion coefficients, and so, surface diffusion coefficients were found, due to the pressure dependent retention of the insulin sample. As an example, the intraparticle diffusion coefficients observed in case of the Xselection fully porous column increase from 1.66 $\times$ 10^{-8} cm^2/s to 1.88 $\times$ 10^{-7} cm^2/s, as the linear mobile phase changes from 0.012 (cm/s) to 0.38 (cm/s).

The analysis of the intraparticle mass-transfer highlight that the surface diffusion has a crucial role in the intraparticle movement of the macromolecules. The values of the pore diffusion coefficients are at least one order of magnitude lower than the values of the surface diffusion coefficients that are between 1.59 – 3.98 $\times$ 10^{-8} cm^2/s at the highest flow rate used for the examined columns.

Significant differences were obtained in the pore diffusion between the fully porous columns and the core-shell packed columns caused by the dissimilarities of the intraparticle obstruction and of the hindrance factors. The value of D_p=4.72 $\times$ 10^{-12} cm^2/s was found for the fully porous

Zorbax column, while the coreshell packed Kinetex Aeris Peptide column with corresponding particle and pore diameters provided D_p=4.48 $\times$ 10^{-11} cm^2/s.

5.1.4 Comparison of the efficiency of SFC and UHPLC techniques

The study of the chromatographic behaviour of small molecules in supercritical fluid chromatography and in reversed phase liquid chromatography with the stochastic model of chromatography shows the broader variation of the mass-transfer properties in SFC than in liquid chromatography. This is mostly due to the varying of the mobile phase density with the flow-rate in SFC mode.

The residence times in the stationary and in the mobile phases depend on the flow-rate in both chromatographic method, however the dependence is much more pronounced in SFC. The mobile phase sojourn time decrease from 65.3 ms to 1.2 ms under low pressure conditions as the applied flow rate increase, while the stationary phase residence times varies between 804.9 ms and 6.0 ms.

It was found that the stationary phase sojourn times in SFC are about one-half of those in UHPLC, at the optimum mobile phase velocities, while the number of the mass transfer events is in the same range. The mobile phase residence times take similar values at high flow-rates as the mobile phase density and thus the apparent phase ratio of the column becomes more similar in the two chromatographic modes.

The mobile phase sojourn times are less dependent from the mobile phase conditions in case of the SFC measurements, oppositely the sojourn times in the stationary phase depend strongly on the pressure and mobile phase settings.

The number of mass transfers events was found as the most characteristic property in the determination of the efficiency of the measurements. The value of the events was found to be in the range of n = 15 000–20 000 at high flow-rates in SFC and also in HPLC.

By and large, at high linear velocities the mass-transfer properties of SFC and HPLC are rather similar; both the number of mass transfers and the sojourn times are in the same range.

5.2 Thesis statements

1. I have identified the different sources of sample band spreading occurring at the separation of small molecules in ultra high performance liquid chromatography columns, and used that information for the characterization of the effect of frictional heating on efficiency. I have demonstrated that the emerging temperature heterogeneities in the mobile phase provide band spreading comparable to the sum of the external mass-transfer and axial dispersion contributions.

2. I have tested the kinetic performance of a series of 2.1 × 50 mm monolithic and packed columns with different type of particles, emphasizing the sample band broadening in the vicinity of the column ends using the column reversal method. According to this, I have concluded that the local efficiency at the two respective column ends differ from each other in case of the columns packed with slurry packing procedure.

   I found that the monolithic MonoTower column provides outstanding performance in case of early eluting compounds, which can be attributed to the moderate mobile phase dispersion caused by the lack of frits in the simple column hardware.

3. I have made the comparison of the intraparticle mass-transfer in superficially porous and fully porous columns with the subtraction of the band broadening contributions of the mobile phase dispersion and the external mass-transfer resistance from experimentally recorded peaks of insulin. I have identified intraparticle diffusion as the additional effect of the pore and surface diffusions, and have demonstrated that surface diffusion is the dominant in the overall intraparticle diffusion.

4. I have studied the chromatographic behaviour of small molecules in supercritical fluid chromatography (SFC) and in reversed phase liquid chromatography (RPLC) using the stochastic model of chromatography. I have observed similar mass-transfer properties at high linear velocities regarding the number of mass transfer events and sojourn times in both cases. I have demonstrated that the change of the mobile phase density with the applied flow rate causes broader variation in the mass-transfer coefficients, especially when the conditions are set close to the supercritical point of the carbon-dioxide mobile phase.

5.3 Publications related to the thesis

Nándor Lambert, Miyazaki Shota, Ohira Masayoshi, Tanaka Nobuo, Attila Felinger
Comparison of the kinetic performance of different columns for fast liquid chromatography, emphasizing the contributions of column end structure
Journal of Chromatography A 1473: pp. 99-108. (2016) IF=3.981

Nándor Lambert, Attila Felinger
Performance of the same column in supercritical fluid chromatography and in liquid chromatography
Journal of Chromatography A 1409: pp. 234-240. (2015) IF=3.926

Nándor Lambert, Ibolya Kiss, Attila Felinger
Mass-transfer properties of insulin on coreshell and fullyporous stationary phases
Journal of Chromatography A 1366: pp. 84-91. (2014) IF=4.169

5.3.1 Related conference presentations

Poster presentations

HPLC 2011
36th Internatiomal Symposium on High Performance Liquid Phase Separations and Related Techniques, Budapest, Hungary, June 19-23, 2011
Nándor Lambert, Attila Felinger
Study of Axial Dispersion with Peak Parking in Different Columns

ISSSB 2011
11th International Symposium and Summer School on Bioanalysis, Austria, Graz, September 18-28, 2011
Nándor Lambert, Attila Felinger
Study of axial dispesion with peak parking

ISSSB 2012
12th Inernational Symposium and Summer School on Bioanalysis, Cluj-Napoca July 4-14, 2012
Nándor Lambert, Attila Felinger
Mass-transfer kinetics of biomolecules in chromatographic columns with porous or coreshell packing materials

MSB 2012
27th International Symposium on MicroScale Bioseparations and Analyses, Geneva, Switzerland, February 12–15, 2012
Nándor Lambert, Attila Felinger
Study of the effective diffusion in coreshell packed columns under stagnant conditions

HPLC 2013
39th International Symposium on High-Performance-Liquid-Phase Separations and Related Techniques, Amsterdam, The Netherlands, June 16-20, 2013
Nándor Lambert, Attila Felinger
Stochastic analysis of mass-transfer properties in Supercritical Fluid Chromatography and in Liquid Chromatography

MSB 2014
30th International Symposium on MicroScale Bioseparations and Analyses, Pécs, Hungary, April 27 - May 1, 2014
Nándor Lambert, Attila Felinger
Evaluation of the mass-transfer properties in chromatographic columns packed with sub-2-*mu*m particles

ISC 2014
30th International Symposium on Chromatography, Salzburg, Austria, September 14-18, 2014,
Nándor Lambert, Attila Felinger
The effect of the frictional heat in chromatographic columns packed with sub-2-*mu*m particles

BS 2015
11th Balaton Symposium on High-Performance Separation Methods, Siófok, Hungary, September 2-4, 2015,
Nándor Lambert, Attila Felinger, Shota Miyazaki, Masayoshi Ohira, Nobuo Tanaka
Comparison of the kinetic performance of different packing materials for fast liquid chromatography

HPLC 2017
45th International Symposium on High Performance Liquid Phase Separations and Related Techniques, Prague, Czech Republic June 18-22, 2017
Nándor Lambert, Attila Felinger.
Analysis of the mass-transfer properties in chromatographic columns using total pore blocking method

Oral presentations

CECE 2013
10th International Interdisciplinary Meeting on Bioanalysis, Pécs, Hungary, April 25-27, 2013
Nándor Lambert, Attila Felinger
Comparison of overall mass-transfer coefficients of Supercritical Fluid Chromatography and Liquid Chromatography

IDK 2013
9th János Szentágothai Interdisciplinary Conference 2013, Pécs Hungary, May 3-4, 2013
Nándor Lambert, Attila Felinger
Determination of overall mass-transfer coefficients in Supercritical Fluid Chromatography and in Liquid Chromatography

IDC 2014
Interdisciplinary Doctoral Conference 2014, Pécs, Hungary, April 15-17, 2014
Nándor Lambert, Attila Felinger
Evaluation of the mass-transfer properties in liquid chromatographic columns

BS 2017
12th Balaton Symposium on High-Performance Separation Methods, Siófok, Hungary, September 6-8 , 2017 Nándor Lambert , Dóra Zelenyánszki, Attila Felinger
Characterization of Stationary Phases for Fast Liquid Chromatography

Acknowledgements

I would like to express my sincere gratitude to my supervisor Prof. Attila Felinger for the continuous support of my Ph.D study and related research, for his patience, motivation, and immense knowledge.

My sincere thanks also goes to Prof. Ferenc Kilár who provided me the opportunity to join to the work of the department and gave access to the laboratory and research facilities.

I thank my fellow labmates and co-workers the help and patience during the everyday research work, and for all the good advices they supported my work.

Last but not the least, I would like to thank my family: my parents my brother and sister for supporting me spiritually throughout writing this thesis and my life in general.

Köszönetnyílvánítás

Köszönetemet szeretném kifejezni témavezetőmnek Dr. Felinger Attila tanszékvezető egyetemi tanárnak, aki tudományos pályafutásomat figyelemmel kísérte, munkámat szakmai tapasztalatával,tanácsaival segítette.

Köszönöm Dr. Kilár Ferencnek, hogy lehetővé tette, hogy munkámat a tanszéken megkezdjem, biztosítva a kutatómunkámhoz szükséges feltételeket.

Köszönöm a tanszék minden dolgozójának a mindennapi kutatómunkám során nyújtott türelmet, segítséget és a jó tanácsokat.

Köszönöm családomnak, szüleimnek és testvéreimnek valamint barátaimnak a motívációt valamint a támogatást és a türelmet melyet munkám és tanulmányaim során nyújtottak.

Bibliography

[1] K. J. Fountain, U. D. Neue, E. S. Grumbach, D. M. Diehl, Effects of extra-column band spreading, liquid chromatography system operating pressure, and column temperature on the performance of sub-2-μ m porous particles, Journal of Chromatography A 1216 (32) (2009) 5979–5988.

[2] J. Mazzeo, U. Neue, M. Kele, R. Plumb, A new separation technique takes advantage of sub-2-μm porous particles, Analytical Chemistry 77 (23) (2005) 460–467.

[3] T. H. Walter, R. W. Andrews, Recent innovations in uhplc columns and instrumentation, TrAC Trends in Analytical Chemistry 63 (2014) 14–20.

[4] J. De Vos, K. Broeckhoven, S. Eeltink, Advances in ultrahigh-pressure liquid chromatography technology and system design, Analytical Chemistry 88 (2016) 262–278.

[5] F. Gritti, G. Guiochon, Comparison of heat friction effects in narrow-bore columns packed with core–shell and totally porous particles, Chemical Engineering Science 65 (2010) 6310–6319.

[6] F. Gritti, G. Guiochon, Performance of columns packed with the new shell kinetex-c18 particles in gradient elution chromatography, Journal Chromatography A 1217 (2010) 1604–1615.

[7] K. Kaczmarski, G. Guiochon, Modeling of the mass-transfer kinetics in chromatographic columns packed with shell and pellicular particles, Analytical Chemistry 79 (2007) 4648–4656.

[8] I. Bacskay, A. Felinger, Macroscopic and microscopic analysis of mass transfer in reversed phase liquid chromatography, Journal Chromatography A 1216 (2009) 1253–1262.

[9] A. Felinger, Diffusion time in core–shell packing materials, Journal Chromatography A 1218 (2011) 1939–1941.

[10] F. Gritti, G. Guiochon, Mass transfer kinetics, band broadening and column efficiency, Journal Chromatography A 1221 (2012) 2–40.

[11] I. Kiss, I. Bacskay, F. Kilar, A. Felinger, Comparison of the mass transfer in totally porous and superficially porous stationary phases in liquid chromatography, Analytical and Bioanalytical Chemistry 397 (2010) 1307–1314.

[12] F. Gritti, K. Horvath, G. Guiochon, How changing the particle structure can speed up protein mass transfer kinetics in liquid chromatography, Journal Chromatography A 1263 (2012) 84–98.

[13] S. Fekete, E. Oláh, J. Fekete, Fast liquid chromatography: The domination of core–shell and very fine particles, Journal Chromatography A 1228 (2012) 57–71.

[14] F. Gritti, I. Leonardis, J. Abia, G. Guiochon, Physical properties and structure of fine core–shell particles used as packing materials for chromatography: Relationships between particle characteristics and column performance, Journal Chromatography A 1217 (2010) 3819–3843.

[15] H. Minakuchi, K. Nakanishi, N. Soga, N. Ishizuka, N. Tanaka, Effect of domain size on the performance of octadecylsilylated continuous porous silica columns in reversed-phase liquid chromatography, Journal of Chromatography A 797 (1–2) (1998) 121–131.

[16] H. Minakuchi, K. Nakanishi, N. Soga, N. Ishizuka, N. Tanaka, Effect of skeleton size on the performance of octadecylsilylated continuous porous silica columns in reversed-phase liquid chromatography, Journal of Chromatography A 762 (1–2) (1997) 135–146.

[17] F. Gritti, W. Piatkowski, G. Guiochon, Study of the mass transfer kinetics in a monolithic column, Journal of Chromatography A 983 (1–2) (2003) 51–71.

[18] G. Guiochon, Monolithic columns in high-performance liquid chromatography, Journal of Chromatography A 1168 (1–2) (2007) 101–168.

[19] N. Tanaka, D. V. McCalley, Core–shell, ultrasmall particles, monoliths, and other support materials in high-performance liquid chromatography, Analytical Chemistry 88 (2016) 279–298.

[20] G. Guiochon, A. Felinger, D. G. Shirazi, A. M. Katti, Fundamentals of Preparative and Nonlinear Chromatography, Academic Press, Amsterdam, The Netherlands, 2006.

[21] J. Giddings, Dynamics of Chromatography, Part I: Principles and Theory, Marcel Dekker, New York, 1965.

[22] S. Khirevich, A. Höltzel, A. Seidel-Morgenstern, U. Tallarek, Time and length scales of eddy dispersion in chromatographic beds, Analytical Chemistry 81 (2009) 7057–7066.

[23] A. Daneyko, D. Hlushkou, V. Baranau, S. Khirevich, A. Seidel-Morgenstern, U. Tallarek, Computational investigation of longitudinal diffusion, eddy dispersion, and trans-particle mass transfer in bulk, random packings of core–shell particles with varied shell thickness and shell diffusion coefficient, Journal Chromatography A 1407 (2015) 139–156.

[24] Y. Ma, A. W. Chassy, S. Miyazaki, M. Motokawa, K. Morisato, H. Uzu, M. Ohira, M. Furuno, K. Nakanishi, H. Minakuchi, K. Mriziq, T. Farkas, O. Fiehn, N. Tanaka, Efficiency of short, small-diameter columns for reversed-phase liquid chromatography under practical operating conditions, Journal of Chromatography A 1383 (2015) 47–57.

[25] C. J. Giddings, H. Eyring., Molecular dynamic theory of chromatography, Journal of Physical Chemistry. 59 (1955) 416–421.

[26] G. Kennedy, J. Knox, Performance of Packings in high performance liquid chromatographyY (HPLC) .1. porous and surface layered supports, Journal of Chromatographic Science 10 (9) (1972) 549.

[27] G. Mayr, T. Welsch, Influence of viscous heat dissipation on efficiency in high-speed high-performance liquid chromatography, Journal of Chromatography A 845 (1–2) (1999) 155–163.

[28] M. M. Fallas, M. R. Hadley, D. V. McCalley, Practical assessment of frictional heating effects and thermostat design on the performance of conventional (3 μm and 5 μm) columns in reversed-phase high-performance liquid chromatography, Journal of Chromatography A 1216 (18) (2009) 3961–3969.

[29] F. Gritti, G. Guiochon, Measurement of the axial and radial temperature profiles of a chromatographic column: Influence of thermal insulation on column efficiency, Journal of Chromatography A 1138 (1–2) (2007) 141–157.

[30] F. Gritti, M. Gilar, J. A. Jarrell, Achieving quasi-adiabatic thermal environment to maximize resolution power in very high-pressure liquid chromatography: Theory, models, and experiments, Journal of Chromatography A 1444 (2016) 86–98.

[31] F. Gritti, M. Gilar, J. A. Jarrell, Quasi-adiabatic vacuum-based column housing for very high-pressure liquid chromatography, Journal of Chromatography A 1456 (Supplement C) (2016) 226 – 234.

[32] K. Broeckhoven, J. Billen, M. Verstraeten, K. Choikhet, M. Dittmann, G. Rozing, G. Desmet, Towards a solution for viscous heating in ultra-high pressure liquid chromatography using intermediate cooling, Journal of Chromatography A 1217 (13) (2010) 2022–2031.

[33] S. Fekete, J. Fekete, D. Guillarme, Estimation of the effects of longitudinal temperature gradients caused by frictional heating on the solute retention using fully porous and superficially porous sub-2 μm materials, Journal of Chromatography A 1359 (2014) 124–130.

[34] M. Saito, History of supercritical fluid chromatography: Instrumental development, Journal of Bioscience and Bioengineering 115 (2013) 590–599.

[35] F. Gritti, G. Guiochon, Effect of methanol concentration on the speed-resolution properties in adiabatic supercritical fluid chromatography, Journal of Chromatography A 1314 (2013) 255–265.

[36] K. Kaczmarski, D. P. Poe, A. Tarafder, G. Guiochon, Pressure, temperature and density drops along supercritical fluid chromatography columns. II. theoretical simulation for neat carbon dioxide and columns packed with 3-μm particles, Journal of Chromatography A 1250 (2012) 115–123.

[37] A. G.-G. Perrenoud, J.-L. Veuthey, D. Guillarme, The use of columns packed with sub-2-μm particles in supercritical fluid chromatography, TrAC Trends Analalytical Chemistry 63 (2014) 44–54.

[38] P. Vajda, G. Guiochon, Determination of the column hold-up volume in supercritical fluid chromatography using nitrous-oxide, Journal of Chromatography A 1309 (2013) 96–100.

[39] P. Vajda, G. Guiochon, Modifier adsorption in supercritical fluid chromatography onto silica surface, Journal of Chromatography A 1305 (2013) 293–299.

[40] A. Tarafder, P. Vajda, G. Guiochon, Accurate on-line mass flow measurements in supercritical fluid chromatography, Journal of Chromatography A 1320 (2013) 130–137.

[41] E. Lesellier, Retention mechanisms in super/subcritical fluid chromatography on packed columns, Journal of Chromatography A 1216 (2009) 1881–1890.

[42] K. Kaczmarski, D. P. Poe, A. Tarafder, G. Guiochon, Efficiency of supercritical fluid chromatography columns in different thermal environments, Journal of Chromatography A 1291 (2013) 155–173.

[43] M. Le′ko, D. P. Poe, K. Kaczmarski, Modelling of retention in analytical supercritical fluid chromatography for co_2—methanol mobile phase, Journal of Chromatography A 1305 (2013) 285–292.

[44] A. Tarafder, K. Kaczmarski, M. Ranger, D. P. Poe, G. Guiochon, Use of the isopycnic plots in designing operations of supercritical fluid chromatography: IV. pressure and density drops along columns, Journal of Chromatography A 1238 (2012) 132–145.

[45] T. T. M. Etzel, F. Svec, Monolithic materials, Elsevier, Amsterdam, 2003.

[46] R. Hahn, M. Panzer, E. Hansen, J. Mollerup, A. Jungbauer, Mass transfer properties of monoliths, Separation Science and Technology 37 (7) (2002) 1545–1565.

[47] A. Jungbauer, Chromatographic media for bioseparation, Journal of Chromatography A 1065 (1) (2005) 3–12.

[48] J. van Deemter, F. Zuiderweg, A. Klinkenberg, Longitudinal diffusion and resistance to mass transfer as causes of nonideality in chromatography, Chemical Engineering Science 5 (6) (1956) 271 – 289.

[49] L. Lapidus, N. Amundson, Mathematics of adsorption in beds, The effect of longitudinal diffusion in ion exchange and chromatographic columns, Journal of Physical Chemistry 56 (8) (1952) 984–988.

[50] J. Knox, Practical Aspects of LC Theory, Journal of Chromatographic Science 15 (9) (1977) 352–364.

[51] J. Done, J. Knox, Performance of packings in high speed liquid chromatography, the effect of particle size, Journal of Chromatographic Science 10 (10) (1972) 606.

[52] J. Giddings, Evidence on the Nature of Eddy Diffusion in Gas Chromatography from Inert (Nonsorbing) Column Data, Analytical Chemistry 35 (10) (1963) 1338.

[53] J. Giddings, Eddy Diffusion In Chromatography, Nature 184 (4683) (1959) 357–358.

[54] J. Giddings, R. Robinson, Failure Of Eddy Diffusion Concept Of Gas Chromatography, Analytical Chemistry 34 (8) (1962) 885.

[55] J. C. Giddings, Nature Of Gas Phase Mass Transfer In Gas Chromatography, Analytical Chemistry 34 (10) (1962) 1186.

[56] P. Magnico, M. Martin, Dispersion in the interstital space of packed-columns, Journal of Chromatography 517 (1990) 31–49.

[57] S. Khirevich, A. Holtzel, D. Hlushkou, U. Tallarek, Impact of conduit geometry and bed porosity on flow and dispersion in noncylindrical sphere packings, Analytical Chemistry 79 (24) (2007) 9340–9349.

[58] S. Khirevich, A. Hoeltzel, A. Seidel-Morgenstern, U. Tallarek, Time and Length Scales of Eddy Dispersion in Chromatographic Beds, Analytical Chemistry 81 (16) (2009) 7057–7066.

[59] S. Khirevich, A. Daneyko, A. Hoeltzel, A. Seidel-Morgenstern, U. Tallarek, Statistical analysis of packed beds, the origin of short-range disorder, and its impact on eddy dispersion, Journal of Chromatography A 1217 (28) (2010) 4713–4722.

[60] D. Hlushkou, S. Bruns, U. Tallarek, High-performance computing of flow and transport in physically reconstructed silica monoliths, Journal of Chromatography A 1217 (23) (2010) 3674–3682.

[61] D. Hlushkou, K. Hormann, A. Hoeltzel, S. Khirevich, A. Seidel-Morgenstern, U. Tallarek, Comparison of first and second generation analytical silica monoliths by pore-scale simulations of eddy dispersion in the bulk region, Journal of Chromatography A 1303 (2013) 28–38.

[62] T. Laiblin, W. Arlt, R. Kaiser, R. Kirsch, Measurement possibility of speed in a preparative HPLC-column with help of magnetic-resonance-Tomography, Chemie Ingenieur Technik 79 (8) (2007) 1213–1216.

[63] J. Gotz, K. Zick, C. Heinen, T. Konig, Visualisation of flow processes in packed beds with NMR imaging: determination of the local porosity, velocity vector and local dispersion coefficients, Chemical Engineering and Processing 41 (7) (2002) 611–629.

[64] D. J. Gunn, Axial and radial dispersion in fixed-beds, Chemical Engineering Science 42 (1987) 363–373.

[65] E. Wilson, C. Geankoplis, Liquid mass transfer at very low Reynolds numbers in packed beds, Industrial and Engineering Chemistry Fundamentals 5 (1) (1966) 9.

[66] K. U. T. Kataoka, H. Yoshida, Mass tramsfer in laminar region between liquid and packing material surface in the packed bed, Journal of Chemical Engineering of Japan 5 (2) (1972) 132–136.

[67] K. Miyabe, G. Guiochon, Surface diffusion in reversed-phase liquid chromatography, Journal Chromatography A 1217 (2010) 1713–1734.

[68] K. Miyabe, G. Guiochon, New model of surface diffusion in reversed-phase liquid chromatography, Journal Chromatography A 961 (2002) 23–33.

[69] J. R. Dustin, A. M. Striegel, The obstruction factor in size-exclusion chromatography. 1. the intraparticle obstruction factor, Journal Chromatography A 1217 (2010) 7131–7137.

[70] E. Renkin, Filtration, diffusion, and molecular sieving through porous cellulose membranes, Journal of General Physiology 38 (1954) 225–243.

[71] J. Klein, M. Gruneberg, Mass transfer of macromolecules in steric exclusion chromatography. 1. diffusional transport in the pores of steric exclusion chromatography materials, Macromolecules 14 (1981) 1411–1475.

[72] K. Miyabe, G. Guiochon, Correlation between surface diffusion and molecular diffusion in reversed-phase liquid chromatography, Journal Physical Chemistry B 105 (2001) 9202–9209.

[73] F. Gritti, G. Guiochon, A protocol for the measurement of all the parameters of the mass transfer kinetics in columns used in liquid chromatography, Journal of Chromatography A 1217 (32) (2010) 5137–5151.

[74] K. Kaczmarski, F. Gritti, J. Kostka, G. Guiochon, Modeling of thermal processes in high pressure liquid chromatography: Ii. thermal heterogeneity at very high pressures, Journal of Chromatography A 1216 (38) (2009) 6575–6586.

[75] U. D. Neue, M. Kele, Performance of idealized column structures under high pressure, Journal of Chromatography A 1149 (2) (2007) 236–244.

[76] F. Gritti, G. Guiochon, Optimization of the thermal environment of columns packed with very fine particles, Journal of Chromatography A 1216 (9) (2009) 1353–1362.

[77] F. Gritti, G. Guiochon, Accurate measurements of the true column efficiency and of the instrument band broadening contributions in the presence of a chromatographic column, Journal of Chromatography A 1327 (2014) 49–56.

[78] E. von Lieres, J. Andersson, A fast and accurate solver for the general rate model of column liquid chromatography, Computers and Chemical Engineering 34 (8) (2010) 1180–1191.

[79] E. Kučera, Contribution to the theory of chromatography : Linear non-equilibrium elution chromatography, Journal Chromatography A 19 (1965) 237–248.

[80] M. Kubin, Beitrag zur theorie der chromatographie, Collection of Czechslovak Chemical Communications 30 (4) (1965) 1104–1118.

[81] H. W. Haynes, P. N. Sarma, A model for the application of gas chromatography to measurements of diffusion in bidisperse structured catalysts, AIChE Journal 19 (5) (1973) 1043–1046.

[82] E. Wilson, C. Geankoplis, Liquid mass transfer at very low reynolds numbers in packed beds, Industrial and Engineering Chemistry Fundamentals 5 (1966) 9–14.

[83] C. R. Wilke, P. Chang, Correlation of diffusion coefficients in dilute solutions, AIChE Journal 1 (2) (1955) 264–270.

[84] M. Young, P. Carroad, R. Bell, Estimation of diffusion-coefficients of proteins, Biotechnology and Bioengineering 22 (1980) 947–955.

[85] A. Felinger, Molecular movement in an HPLC column: A stochastic analysis, LC–GC North America 22 (2004) 642.

[86] A. Felinger, Molecular dynamic theories in chromatography, Journal of Chromatography A 1184 (1-2) (2008) 20–41.

[87] I. Bacskay, A. Felinger, Rapid estimation of overall mass-transfer coefficients in liquid chromatography, Analytical Methods 2 (2010) 1989–1993.

[88] D. Cabooter, F. Lynen, P. Sandra, G. Desmet, Total pore blocking as an alternative method for the on-column determination of the external porosity of packed and monolithic reversed-phase columns, Journal of Chromatography A 1157 (1–2) (2007) 131–141.

[89] J. H. Knox, L. McLaren, A new gas chromatographic method for measuring gaseous diffusion coefficients and obstructive factors., Analytical Chemistry 36 (8) (1964) 1477–1482.

[90] K. Miyabe, N. Ando, G. Guiochon, Peak parking method for measurement of molecular diffusivity in liquid phase systems, Journal of Chromatography A 1216 (20) (2009) 4377–4382.

[91] K. Miyabe, Y. Kawaguchi, G. Guiochon, Kinetic study on external mass transfer in high performance liquid chromatography system, Journal of Chromatography A 1217 (18) (2010) 3053–3062.

[92] N. Lambert, S. Miyazaki, M. Ohira, N. Tanaka, A. Felinger, Comparison of the kinetic performance of different columns for fast liquid chromatography, emphasizing the contributions of column end structure, Journal of Chromatography A 1473 (2016) 99 – 108.

[93] A. Soliven, G. Dennis, E. Hilder, R. Andrew Shalliker, P. Stevenson, The development of the in situ modification of 1st generation analytical scale silica monoliths, Chromatographia 77 (2014) 663–671.

[94] A. Felinger, Data Analysis and Signal Processing in Chromatography, Elsevier, Amsterdam, 1998.

[95] K. Miyabe, Surface diffusion in reversed-phase liquid chromatography using silica gel stationary phases of different {C1} and {C18} ligand densities, Journal Chromatography A 1167 (2) (2007) 161–170.

[96] I. Bacskay, A. Sepsey, A. Felinger, Determination of the pore size distribution of high-performance liquid chromatography stationary phases via inverse size exclusion chromatographt, Journal Chromatography A 1339 (2014) 110–117.

[97] F. Gritti, G. Guiochon, A protocol for the measurement of all the parameters of the mass transfer kinetics in columns used in liquid chromatography, Journal Chromatography A 1217 (32) (2010) 5137–5151.

[98] N. Lambert, I. Kiss, A. Felinger, Mass-transfer properties of insulin on core–shell and fully porous stationary phases, Journal Chromatography A 1366 (2014) 84–91.

[99] E. Oláh, S. Fekete, J. Fekete, K. Ganzler, Comparative study of new shell-type, sub-2-μm fully porous and monolith stationary phases, focusing on mass-transfer resistance, Journal Chromatography A 1217 (2010) 3642–3653.

[100] F. Gritti, C. A. Sanchez, T. Farkas, G. Guiochon, Achieving the full performance of highly efficient columns by optimizing conventional benchmark high-performance liquid chromatography instruments, Journal Chromatography A 1217 (2010) 3000–3012.

[101] J. Billen, P. Gzil, N. Vervoort, G. Baron, G. Desmet, Influence of the packing heterogeneity on the performance of liquid chromatography supports, Journal Chromatography A 1073 (2005) 53–61.

[102] A. E. Reising, S. Schlabach, V. Baranau, D. Stoeckel, U. Tallarek, Analysis of packing microstructure and wall effects in a narrow-bore ultrahigh pressure liquid chromatography column using focused ion-beam scanning electron microscopy, Journal of Chromatography A 1513 (2017) 172 – 182.

[103] F. Gritti, A stochastic view on column efficiency, Journal of Chromatography A 1540 (2018) 55 – 67.

[104] F. Gritti, On the relationship between radial structure heterogeneities and efficiency of chromatographic columns, Journal of Chromatography A 1533 (2018) 112 – 126.

[105] A. Felinger, B. Boros, R. Ohmacht, Effect of pressure on retention factors in HPLC using a non-porous stationary phase, Chromatographia 56 (2002) 61–64.

[106] X. Liu, P. Szabelski, K. Kaczmarski, D. Zhou, G. Guiochon, Influence of pressure on the chromatographic behavior of insulin variants under nonlinear conditions, Journal Chromatography A 988 (2003) 205–218.

[107] L. Hong, A. Felinger, K. Kaczmarski, G. Guiochon, Measurement of intraparticle diffusion in reversed phase liquid chromatography, Chemical Engineering Science 59 (2004) 3399–3412.

[108] P. Szabelski, X. Liu, G. Guiochon, Pressure-induced effects in the heterogeneous adsorption of insulin on chromatographic surfaces, Journal Chromatography A 1015 (2003) 43–52.

[109] A. Tarafder, G. Guiochon, Use of isopycnic plots in designing operations of supercritical fluid chromatography: I. the critical role of density in determining the characteristics of the mobile phase in supercritical fluid chromatography, Journal of Chromatography A 1218 (2011) 4569–4575.

[110] A. Tarafder, G. Guiochon, Use of isopycnic plots in designing operations of supercritical fluid chromatography: II. the isopycnic plots and the selection of the operating pressure–temperature zone in supercritical fluid chromatography, Journal of Chromatography A 1218 (2011) 4576–4585.

[111] D. P. Poe, D. Veit, M. Ranger, K. Kaczmarski, A. Tarafder, G. Guiochon, Pressure, temperature and density drops along supercritical fluid chromatography columns. I. experimental results for neat carbon dioxide and columns packed with 3- and 5-micron particles, Journal of Chromatography A 1250 (2012) 105–114.

[112] A. Tarafder, K. Kaczmarski, D. P. Poe, G. Guiochon, Use of the isopycnic plots in designing operations of supercritical fluid chromatography. V. pressure and density drops using mixtures of carbon dioxide and methanol as the mobile phase, Journal of Chromatography A 1258 (2012) 136–151.

[113] P. Vajda, J. J. Stankovich, G. Guiochon, Determination of the average volumetric flow rate in supercritical fluid chromatography, Journal of Chromatography A 1339 (2014) 168–173.

[114] G. Guiochon, A. Tarafder, Fundamental challenges and opportunities for preparative supercritical fluid chromatography, Journal of Chromatography A 1218 (2011) 1037–1114.

[115] K. Kaczmarski, D. P. Poe, A. Tarafder, G. Guiochon, Pressure, temperature and density drops along supercritical fluid chromatography columns. II . theoretical simulation for neat carbon dioxide and columns packed with 3-μm particles, Journal of Chromatography A 1250 (2012) 115–123.

[116] J. R. Strubinger, H. Song, J. F. Parcher, High-pressure phase distribution isotherms for supercritical fluid chromatographic systems. 2. binary isotherms of carbon dioxide and methanol, Analitycal Chemistry 63 (1991) 104–108.